Control of neuronal input-output coupling by recurrent inhibition in the hippocampus

Dissertation
zur
Erlangung
des
Doktorgrades (Dr. rer. nat.)
der
Mathematisch-Naturwissenschaftlichen Fakultät
der
Rheinischen Friedrich-Wilhelms Universität Bonn

Vorgelegt von:
Christina Müller aus Trier

Bonn 2011

Angefertigt mit Genehmigung der
Mathematisch-Naturwissenschaftlichen Fakultät
der Rheinischen Friedrich-Wilhelms Universität Bonn

1. Gutachter: Jun. -Prof. Dr. Stefan Remy
2. Gutachter: Prof. Dr. Horst Bleckmann

Tag der Promotion: 1. Juni 2012
Erscheinungsjahr: 2012

Erklärung

Hiermit erkläre ich, daß ich die vorliegende Dissertation selbständig angefertigt habe. Es wurden nur die in der Arbeit ausdrücklich benannten Quellen und Hilfsmittel benutzt. Wörtlich oder sinngemäß übernommenes Gedankengut habe ich als solches kenntlich gemacht.

Ort, Datum Unterschrift

Ich danke herzlichst:

Meinem Betreuer und Doktorvater Jun.-Prof. Dr. Stefan Remy, für seine stete und kompetente Unterstützung und seine Fähigkeit Begeisterung für Wissenschaft zu wecken.
Prof. Dr. Horst Bleckmann und PD. Dr. Joachim Mogdans für einen gelungen Einstieg in das wissenschaftliche Arbeiten während meiner Diplomarbeit am Institut für Zoologie in Bonn.
Prof. Dr. Heinz Beck für seine Unterstützung und guten Rat und dafür, dass ich so lange Zeit Teil seines Labors sein durfte mit all seinen Möglichkeiten.
Prof. Dr. Ivan Soltesz und Prof. Dr. Douglas Coulter für die Gelegenheit neue Techniken in ihren Labors erlernen zu dürfen.
Den AGs Remy und Beck für die großartige Zeit!
Meinem Freund Roland danke ich dafür, dass er immer für mich da war und ist und für all die lebhaften Diskussionen, die ab und zu sogar fachlicher Natur waren.
Und nicht zuletzt danke ich meiner Familie dafür, dass sie immer bedingungslos hinter mir gestanden hat!

Vielen Dank!

Abstract

During different states of hippocampal network activity neurons receive excitatory synaptic input on dendritic compartments and transform it into axonal action potential output. The ensemble output of pyramidal neurons activates local inhibitory microcircuits, which provide recurrent compartment-specific inhibition. In the present study it was observed that neuronal activity patterns that are likely to be present during sharp-waves recruit recurrent inhibition differently than repetitive activity at theta frequency. The observed results suggest that this could adapt the efficacy of input-output conversion to the network-state. In the present study dendritic spikes and their activity-dependent plasticity were identified as specialized signals, which endow correlated excitatory branch input with the ability to withstand recurrent inhibition and to generate precisely timed action potential output independent of the previous activity. These findings suggest that dendritic spikes may provide a cellular correlate for reliable and temporally precise reactivation of behaviorally relevant neuronal assemblies during both exploration and sleep.

Contents

1 Introduction 1
- 1.1 Anatomy of the hippocampus . . . 1
- 1.2 Hippocampal function . . . 3
  - 1.2.1 The hippocampus in disease . . . 4
- 1.3 Extrinsic inputs to the CA1 subfield . . . 4
- 1.4 Interneurons and local microcircuits in CA1 . . . 5
- 1.5 Dendritic integration in CA1 pyramidal neurons . . . 8
  - 1.5.1 Dendritic spikes . . . 11
- 1.6 Oscillatory activity in the hippocampus . . . 12
- 1.7 Central questions . . . 15

2 Materials & Methods 17
- 2.1 Slice-preparation . . . 17
- 2.2 Electrophysiological recordings . . . 17
  - 2.2.1 Alveus stimulation . . . 18
- 2.3 Fluorescent interneuron staining and confocal imaging . . . 18
- 2.4 Fast CCD voltage imaging . . . 19
- 2.5 Fast glutamate micro-iontophoresis . . . 20
  - 2.5.1 Branch strength potentiation . . . 22
- 2.6 Two photon calcium imaging . . . 22
- 2.7 Data analysis and statistics . . . 22

3 Results 24
- 3.1 Activity dependence of recurrent inhibition . . . 24
  - 3.1.1 Decrease in recurrent inhibition at theta frequency . . . 24
  - 3.1.2 Dichotomy in firing behavior of recurrent inhibitory interneurons . 25
  - 3.1.3 Two populations of interneurons receive distinct input from CA1 pyramidal cells . . . 28
- 3.2 Spatio-temporal dynamics of inhibition in CA1 subfield . . . 28
  - 3.2.1 Morphological differences of the two functionally distinct populations 28
  - 3.2.2 Spatial extent of hyperpolarizing inhibition in CA1 . . . 30
- 3.3 Control of linear input to output conversion by dynamic recurrent inhibition 34
  - 3.3.1 Dynamic and input-site specific control of local dendritic excitation 34
  - 3.3.2 Dynamic and input-location specific control of subthreshold EPSPs 36

3.3.3 Dynamic and input-location specific control of action potential output . . . 39
3.4 Control of nonlinear dendritic spikes by dynamic recurrent inhibition . . 41
3.4.1 Recurrent inhibition of dendritic spikes . . . 41
3.4.2 Recurrent inhibition of action potential output triggered by dendritic spikes . . . 47
3.4.3 Plasticity of dendritic spikes and recurrent inhibition . . . 48

4 Discussion 53
4.1 Design of the stimulation paradigm . . . 54
4.2 Network-state dependent recurrent inhibition . . . 54
4.2.1 Other aspects of inhibition in the CA1 subfield . . . 56
4.3 Network-state dependent inhibition of excitation . . . 58
4.3.1 Inhibition of linear excitatory events . . . 58
4.3.2 Pathway specificity of recurrent inhibition in different network-states 60
4.3.3 Inhibition of supralinear excitatory events . . . 61
4.3.4 Micro-iontophoresis of glutamate: Methodological considerations . 65
4.3.5 Recurrent inhibition and explorative sharp-waves . . . 65
4.3.6 Branch strength potentiation and dendritic spike evoked plasticity 66
4.3.7 Dendritic spikes and assembly coupling . . . 66
4.4 Conclusions & open questions . . . 67

5 Appendix 69
5.1 Additional methods . . . 69
5.1.1 Two-photon uncaging . . . 69
5.1.2 Focal synaptic stimulation . . . 69
5.2 Abbrevations . . . 71

6 Contributions 73

7 Bibliography 74

1 Introduction

1.1 Anatomy of the hippocampus

With its accurately layered architecture and a simpler organization than neocortical regions, the hippocampus is an ideal structure to study the principles of brain physiology. The present study was conducted in the rat (*rattus norvegicus*) hippocampus *in-vitro*. In the acute brain slice preparation the micro-circuitry and physiological function of the hippocampus is preserved. This allows detailed investigation with electrophysiological and imaging techniques. The hippocampus, which forms a crescent-like structure, is part of the medial temporal lobe in all mammals. Apart from a few differences, for example the existence of a commissural system in only the rat and not in the primate dentate gyrus, the hippocampal formation shows a high degree of conservation across the mammalian taxon (Raisman et al., 1965; Gottlieb and Cowan, 1973; Amaral et al., 1984; West, 1990; Manns and Eichenbaum, 2006).

In the hippocampal formation a loop of synaptic connections is formed from the entorhinal cortex to the dentate gyrus, the hippocampus proper, and back to the entorhinal cortex (fig. 1.1). This trisynaptic pathway starts in layer II of the entorhinal cortex. From here information is conveyed to the dentate gyrus granule cells via the perforant path. These fire sparsely *in-vivo* and form huge synaptic boutons on the dendrites of the pyramidal cells in the CA3 subfield of the hippocampus proper (Jung and McNaughton, 1993; Henze et al., 2000). Here, the CA3 pyramidal cell axon collaterals form a recurrent excitatory network, but the main excitatory target of CA3 pyramidal neuron axons is the CA1 region. Finally, the CA1 pyramidal neurons convey information to the subiculum and back to layer V of the entorhinal cortex (Amaral and Witter, 1989; fig. 1.1).

Apart from this trisynaptic loop, a fraction of the perforant path that originates in entorhinal cortex layer III gives rise to the direct pathway (also referred to as the

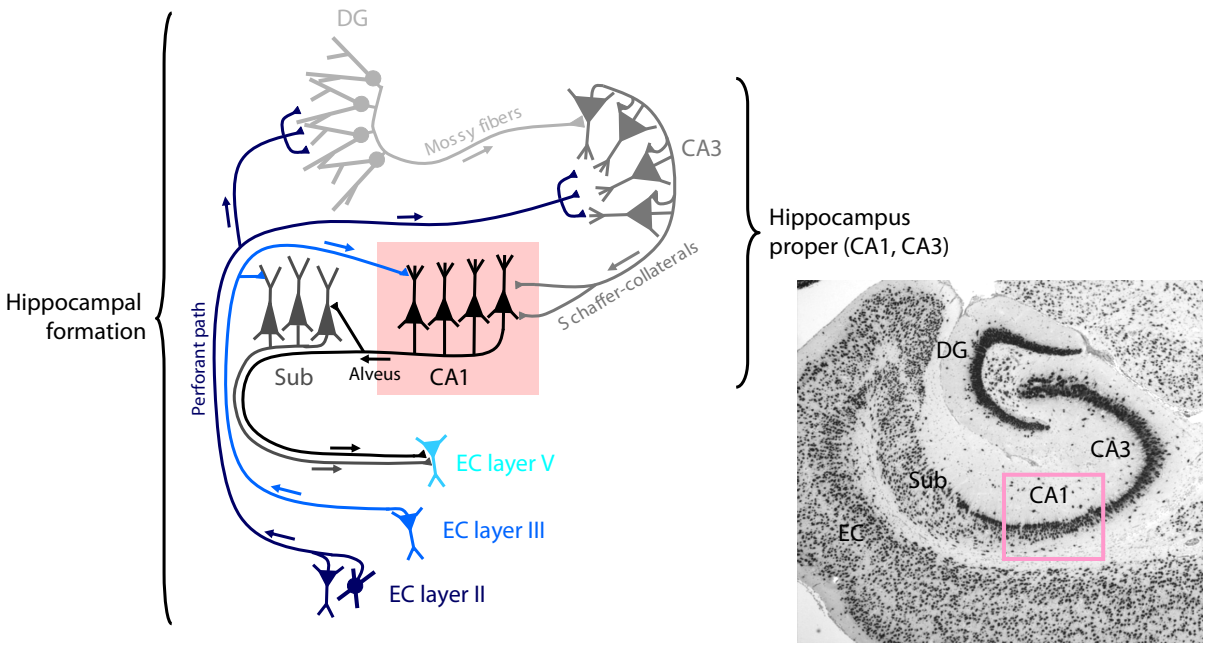

Figure 1.1: Excitatory circuitry in the hippocampal formation. EC: Entorhinal cortex, DG: Dentate gyrus, CA: Cornu ammonis, Sub: Subiculum. Highlighted in red, the CA1 subfield of the hippocampus (Amaral and Witter, 1989; Anderson et al., 2007). Inset: Toluidin-blue staining of a horizontal slice of the rat hippocampus. The red frame again highlights the CA1 subfield (picture: Courtesy of Roland Krüppel and Margit Reitze).

temporo-ammonic pathway; Steward, 1976) that innervates the CA1 pyramidal cells on their apical tuft dendrites. (Amaral and Witter, 1989, fig. 1.1).

In the CA1 subfield the principal glutamatergic cells are the pyramidal cells. Their somata are approximately 15 µm in diameter and lay densely packed in the stratum pyramidale (s.p.; fig. 1.2). From here the thin basal dendrites (diameter: 0.3–0.5 µm) protrude into the stratum oriens (s.o.). A thicker (1.8–2.5 µm) apical trunk gives rise to apical oblique dendrites (diameter: 0.5–0.6 µm) in the stratum radiatum (s.r.) and branches into a dense dendritic tuft (diameter: 0.2–1.2 µm) in the distal stratum lacunosum moleculare (s.l.m.). The total length of the CA1 pyramidal cell dendrites is about 13.5 mm (Pyapali et al., 1998) spanning about one millimeter from the basal dendrites near the alveus to the apical tuft dendrites close to the hippocampal fissure. The myelinated axons of the pyramidal cells are bundled in the alveus and project to the pyramidal cells in the subiculum (Amaral et al., 1991; fig. 1.2).

1.2 Hippocampal function

After the structure and neuronal connectivity in the hippocampus had been elucidated by Ramón y Cajal (Ramón y Cajal, 1911) the investigation of hippocampal function began. Studies in humans revealed evidence for a role of the hippocampus in memory consolidation: In the famous case of the patient H.M., severe deficits in declarative memory consolidation were observed after the patient had both hippocampi removed to cure his epilepsy (Scoville and Milner, 1957). The hippocampus also has been shown to play an important role in spatial navigation: London taxi drivers facing the challenge to find the shortest way to any destination showed significantly enlarged hippocampal volume (Maguire et al., 2000). Apart from these particular examples in humans, *in-vivo* studies in rodents have confirmed the role of the hippocampus in spatial learning tasks (Morris et al., 1982; Wang and Morris, 2010).

A remarkable discovery has been made by O'Keefe and Dostrovsky (1971), who showed that single hippocampal pyramidal cells increased their firing probability, solely depending on the animals location in space. Sensory cues or motor behavior did not change the firing behavior (O'Keefe, 1976). Thus, O'Keefe could confirm an early idea by Tolman (1948) that "...the hippocampus might act as a spatial or cognitive mapping system which would serve as the neural substrate for place learning and exploration". Pyramidal cells in the hippocampus can serve as 'place cells' encoding spatial information on the level of single cells (O'Keefe and Nadel, 1978).

Furthermore, a potential cellular correlate for memory formation has been observed in all excitatory pathways of the hippocampus *in-vitro*: Strong activation of both –a pre- and a postsynaptic neuron– led to a modification of synaptic transmission that lasted for minutes up to several hours (Bliss and Lomo, 1973; Bliss and Gardner-Medwin, 1973; Morris et al., 1990; Frey et al., 1993). It has been hypothesized that plasticity of synapses in the hippocampus is necessary for the formation of transient working memory (McNaughton et al., 1986). Indeed, simple learning paradigms have been shown to induce this long term potentiation (LTP) of synaptic strength *in-vivo* (Whitlock et al., 2006). However, more experimental results are required to prove the direct linkage between LTP and memory function (Neves et al., 2008).

1.2.1 The hippocampus in disease

It has been established that proper function of the hippocampus is crucial to memory consolidation and spatial memory (see previous chapter). Remarkably, the hippocampal formation appears to be specifically vulnerable in neurological diseases. Epilepsy is one of the most common neurological diseases: The chance of experiencing a seizure once during a lifetime is 1.5–5 % (Sander and Shorvon, 1996). Thereof, 60 % of partial epilepsies are manifested by seizures in the temporal lobe (Bruton, 1988; Anderson et al., 2007). As a consequence of epileptiform activity in the hippocampus structural changes like mossy fiber sprouting (Miles et al., 1984; Wuarin and Dudek, 1996; Okazaki et al., 1999; Feng et al., 2003) and selective cell loss have been observed in animal models and epilepsy patients (Sloviter, 1987; Houser and Esclapez, 1996; Morin et al., 1998; Cossart et al., 2001; de Lanerolle et al., 1989; Robbins et al., 1991). Furthermore, functional changes on the cellular level, e.g. the dysregulation of ion-channel function, have been described (Beck and Yaari, 2008).

1.3 Extrinsic inputs to the CA1 subfield

The CA1 region of the hippocampus possesses a unique role in that it receives direct input from the entorhinal cortex directly as well as input that has been processed in the dentate gyrus and the CA3 subfield. The fibers from the CA3 subfield (Schaffer collaterals, Schaffer, 1892) project to the stratum oriens and stratum radiatum and terminate on the basal and apical oblique dendrites of the pyramidal cells. The fibers from the direct entorhinal cortex input on the other hand strictly innervate the dendritic tuft of the principle cells in stratum lacunosum moleculare. Thereby, the CA1 pyramidal neuron receives layer specific excitatory input from distinct input areas (fig. 1.2; Blackstad, 1958; Steward, 1976; Amaral and Witter, 1989).

The synapses of the perforant path on the apical tuft dendrites have been shown to be strongly modulated by dopamine, noradrenalin, and serotonin (Pasquier and Reinoso-Suarez, 1978; Otmakhova and Lisman, 1999, 2000; Otmakhova et al., 2005). In addition, terminals from the thalamus and the amygdala terminate in the apical tuft region of the pyramidal cells (Krettek and Price, 1977; Amaral and Witter, 1989; der Weel and Witter, 1996; der Weel et al., 1997; Kemppainen et al., 2002). This indicates a distinct regulation of the perforant path inputs in the stratum moleculare lacunosum compared

to the Schaffer-collateral inputs in stratum radiatum and oriens.

A CA1 pyramidal cell possesses approximately 30.000 excitatory synapses that are mostly located on dendritic spines (Megías et al., 2001). These synapses exhibit two major types of glutamate receptors: Firstly, AMPA (α-amino-3-hydroxy-5-methyl-4-isoxazolepropionic acid) receptors, that mediate fast synaptic currents by forming a ligand gated pore, permeable predominantly for Na^+. Secondly, the NMDA (N-methyl D-aspartate) receptors that are both voltage and ligand gated and conduct Ca^{2+}, Na^+, and K^+ ions. Their opening leads to excitatory currents slower than those mediated by AMPA receptors (Hestrin et al., 1990; Jonas, 1993). The ratio between these two excitatory receptors on pyramidal neuron dendrites, has been shown to differ in the perforant path integration zone and the Schaffer collateral integration zone. As a consequence the activation of perforant path associated excitatory synapses leads to a relatively greater NMDA receptor activation than activation of Schaffer-collateral associated excitatory synapses (Otmakhova et al., 2002).

The depolarization mediated by the activation of excitatory synapses leads to an opening of NMDA receptors and voltage-gated calcium channels and a subsequent increase in Ca^{2+} concentration in the dendrite (Mainen et al., 1999). This Ca^{2+} increase has been linked to induction of plasticity (Sabatini et al., 2001; Zucker, 1999; Malenka et al., 1988) and can be utilized to indirectly visualize the excitation on the dendrite using Ca^{2+} imaging techniques (Higley and Sabatini, 2008).

In addition to the main extrinsic inputs, the CA1 pyramidal cells also receive extrinsic cholinergic inputs from the medial septum, which plays an important role in rhythmogenesis in the hippocampus (Bland and Bland, 1986; Bland et al., 1988).

1.4 Interneurons and local microcircuits in CA1

The excitatory input on pyramidal cells is delicately counterbalanced by the inhibitory circuitry (Lacaille et al., 1987; Buhl et al., 1994; Miles et al., 1996). Inhibitory interneurons are less abundant than principal neurons (<10% of the total number of neurons). They form about 1700 synapses on the CA1 pyramidal neuron dendrites, predominantly on the soma and proximal aspiny shafts and less densely along the rest of their dendrites (Megías et al., 2001).

When an inhibitory synapse on a pyramidal cell dendrite is activated, gamma-ami-

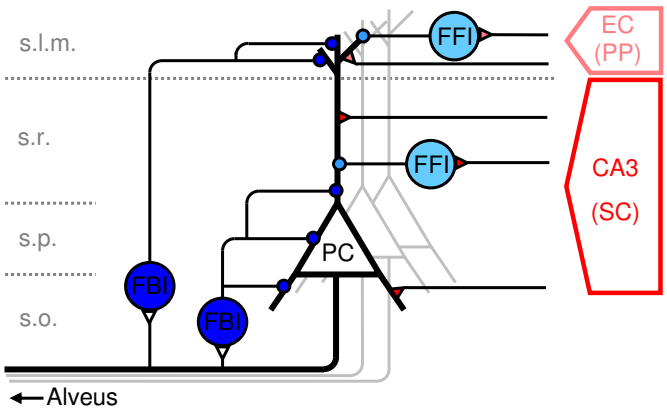

Figure 1.2: Excitatory and inhibitory circuitry in the CA1 subfield of the hippocampus. Feedforward interneurons are directly activated by extrinsic excitation provided by the Schaffer-collateral and the perforant path inputs. Feedback interneurons are activated by the local axon collaterals of CA1 pyramidal cells. Small triangles: Excitatory synapses, small circles: Inhibitory synapses. FBI (dark blue): Feedback inhibitory interneurons, FFI (light blue): Feedforward inhibitory interneurons. PC: Pyramidal neuron, EC: Entorhinal cortex, PP: Perforant path, SC: Schaffer-collaterals. S.o.: Stratum oriens, s.p.: Stratum pyramidale, s.r.: Stratum radiatum, s.l.m.: Stratum lacumosum moleculare.

nobutyric acid (GABA) is released and binds to postsynaptic $GABA_A$ and $GABA_B$ receptors (Bormann, 1988; Dutar and Nicoll, 1988; Pearce, 1993). $GABA_B$ receptors are metabotropic receptors, which mediate a K^+ conductance, that leads to a slow inhibitory postsynaptic potential (IPSP) (Andrade et al., 1986; Dutar and Nicoll, 1988; Misgeld et al., 1995). $GABA_A$ receptors on the other hand are ionotropic receptors that form a ligand gated Cl^- channel. When GABA binds the channel opening results in a fast, phasic, anionic conductance (Kaila, 1994). This $GABA_A$-mediated phasic inhibition, that is generally believed to play a crucial role in network oscillation by synchronizing neuronal output (Cobb et al., 1995; Bartos et al., 2002), is the focus of the present study.

The interneurons in the CA1 subfield of the hippocampus have been shown to be a highly diverse group of at least 16 types. They can be categorized by immunohistochemical markers, their electrophysiological properties, and their axonal target regions (Freund and Buzsáki, 1996; Somogyi and Klausberger, 2005). Among others, the bistratified, trilaminar, and Schaffer-collateral associated interneurons innervate the proximal dendrites of the pyramidal cells in the stratum oriens and radiatum. The oriens lacunosum moleculare interneurons (O-LM cells) in contrast, terminate on the apical dendritic tuft

in the stratum lacunosum moleculare. There are also many other types of interneurons: For example targeting the axon initial segment of the principle cells or targeting other interneurons. Since each interneuron subgroup has preferred axonal target regions on the somato-dendritic axis of pyramidal cells, it can be assumed that their activation inhibits excitation in a compartment specific manner. The classification on the basis of immunohistochemical markers can be helpful, particularly when using genetically expressed fluorescent tags. Immunohistochemical markers can be Ca^{2+}-binding proteins like parvalbumin, which is expressed by fast spiking, proximally innervating interneurons, or peptides like somatostatin, expressed by distally innervating interneurons. However, for exact identification, additional characteristic have to be considered (Somogyi and Klausberger, 2005).

The CA1 inhibitory interneurons can be directly activated by the afferent CA3 Schaffer-collateral pathway and thereby form a feedfoward inhibitory network (fig. 1.2). Feed-forward inhibition is thought to increase the dynamic range of the postsynaptic target cells by preventing the excitatory inputs to become saturated. Furthermore, feedforward inhibition shortens the time-window for summation of excitatory inputs in the pyramidal cells (Pouille and Scanziani, 2001; Pouille et al., 2009).

In addition to their participation in feedforward microcircuits, the local interneurons in the stratum oriens and stratum pyramidale have been shown to be targeted by axon collaterals of the CA1 pyramidal cells (Knowles and Schwartzkroin, 1981), forming a feedback or recurrent inhibitory microcircuit (Buzsáki, 1984). This innervation of the local interneurons by the CA1 pyramidal cells has been shown to reliably activate interneurons *in-vivo* (Csicsvari et al., 1998). The feedback circuitry is only activated when CA1 pyramidal cells fire action potentials and thus constrains excitation of CA1 pyramidal cells. Additionally the time window for Schaffer-collateral and perforant path input integration is shortened with a disynaptic delay (Miles, 1990). Most interneurons are participating in both feedback and feedforward inhibition, but some (O-LM interneurons) are thought to exclusively perform recurrent inhibition (Buzsáki et al., 1983; Frotscher et al., 1984; Blasco-Ibáñez and Freund, 1995; Maccaferri and McBain, 1995).

It has been shown that high frequency stimulation (50–100 Hz) of the recurrent interneuron population leads to a differential recruitment of the proximally and distally innervating interneurons. Over time recurrent inhibition shifts from proximal dendrites to the distal tuft dendrites of the pyramidal neurons (Pouille and Scanziani, 2004). It remains to be determined whether this shift of inhibition along the somatodendritic axis

is also present in response to slower patterns of hippocampal activity occurring *in-vivo*. Moreover, the resulting activity dependent interaction of inhibition and excitation during hippocampal rhythmic activity is still unknown. The present study investigats the effects of recurrent inhibitory dynamics on excitatory signals in response to slower frequencies.

1.5 Dendritic integration in CA1 pyramidal neurons

Dendrites can be regarded as antennas with which neurons receive information from other cells. However, considering the diversity of these thin cell processes in the central nervous system and across different species, they have to be more than passive input receivers: Dendrites have been shown to actively compute synaptic inputs (Stuart et al., 2008).

The structure of the dendrite strongly influences its function: When an excitatory postsynaptic event arrives at the very thin apical tuft dendrites, it has to travel along hundreds of micrometers to the soma and axon (fig. 1.3A). It is predicted by dendritic cable theory that an EPSP from a distal input site will be filtered during passive propagation to the soma. This results in a slowed rise and a decreased EPSP amplitude (fig. 1.3A right panel; Rall, 1967; Rall and Rinzel, 1973; Spruston, 2008). Therefore, a distally evoked EPSP contributes to a lesser extent to neuronal output than an EPSP from a more proximal input site. The passive attenuation of EPSPs on their way to the soma is depending on the cable properties of the dendrites:

i) The membrane resistance is determined by the ion-channels that are open at rest. The more channels are open the smaller the membrane resistance. A reduced membrane resistance leads to a loss in charge across the membrane and subsequent EPSP attenuation (Stuart et al., 2008).

ii) The intracellular resistivity determines how effective the signal can propagate along the dendrite. A low intracellular resistivity for example in thick dendrites facilitates the signal propagation (Koch, 1999).

iii) The capacity of the dendrites is determined by their size and shape and affects how fast a membrane can be charged. In large and ramified neurons, which possess a high membrane capacitance, charging the membrane is slow. This filters fast, transient potential changes (Migliore and Shepherd, 2002; Stuart et al., 2008).

The active dendritic properties are mediated by voltage-gated ion-channels. Two major

currents dampen dendritic excitability: Hyperpolarization activated cation currents (I_h) decrease dendritic excitability by closing at depolarized membrane potentials and thereby shortening EPSPs (Magee, 1998; Williams and Stuart, 2000). Furthermore, voltage-gated potassium conductances (I_A) limit the backpropagation of action potentials and restrain EPSPs size (Hoffman et al., 1997). Additionally, conductances that can increase the excitability can be found: Voltage-gated sodium as well as calcium channels amplify EPSP size and facilitate action potential backpropagation (Lipowsky et al., 1996; Spruston et al., 1995; Gillessen and Alzheimer, 1997).

This passive and active dendritic properties determine the time-course and amplitude of synaptic signals and thereby the time window for summation of inputs. In the CA1 pyramidal neurons the window for integration is comparatively long (Spruston and Johnston, 1992). Thus, CA1 pyramidal neurons are thought to serve as integrators. In contrast, some interneuron subtypes have a shorter membrane time constant. Since this shortens the EPSPs and only highly synchronous inputs can summate, they may serve as coincidence detectors (König et al., 1996).

In CA1 pyramidal neurons EPSPs from the distal input sites are attenuated strongly on their way to the soma leaving them with a minor role for axonal output generation compared to proximal inputs (Golding et al., 2005). This attenuation of excitatory signals along the dendrite has been shown to be partially compensated by a mechanism called synaptic scaling (Magee and Cook, 2000): CA1 oblique dendrites in the Schaffer collateral integration zone compensate for distance dependent attenuation of signals by equipping the more distal synapses with more AMPA receptors (Andrasfalvy and Magee, 2001). This increase in receptor number exactly balances the distance dependent attenuation, so that distance dependence of input is decreased. The equipment with AMPA receptors is lowest in the perforant path integration-zone and the large electrotonical distance is not compensated, leaving inputs from here with little impact on action potential output (Nicholson et al., 2006).

Inhibitory synapses can decrease the overall excitability of the neuron by hyperpolarizing its membrane potential and thus increasing the amount of excitation needed for reaching the action potential threshold. A major contribution to inhibition in CA1 pyramidal neurons is made by phasic GABAergic inhibition mediated by a fast Cl^- conductance (Kaila, 1994). Since the equilibrium potential for Cl^- under physiological conditions is near the resting membrane potential of CA1 pyramidal neurons, the opening of these channels will lead to moderate hyperpolarization of the membrane potential. In addition,

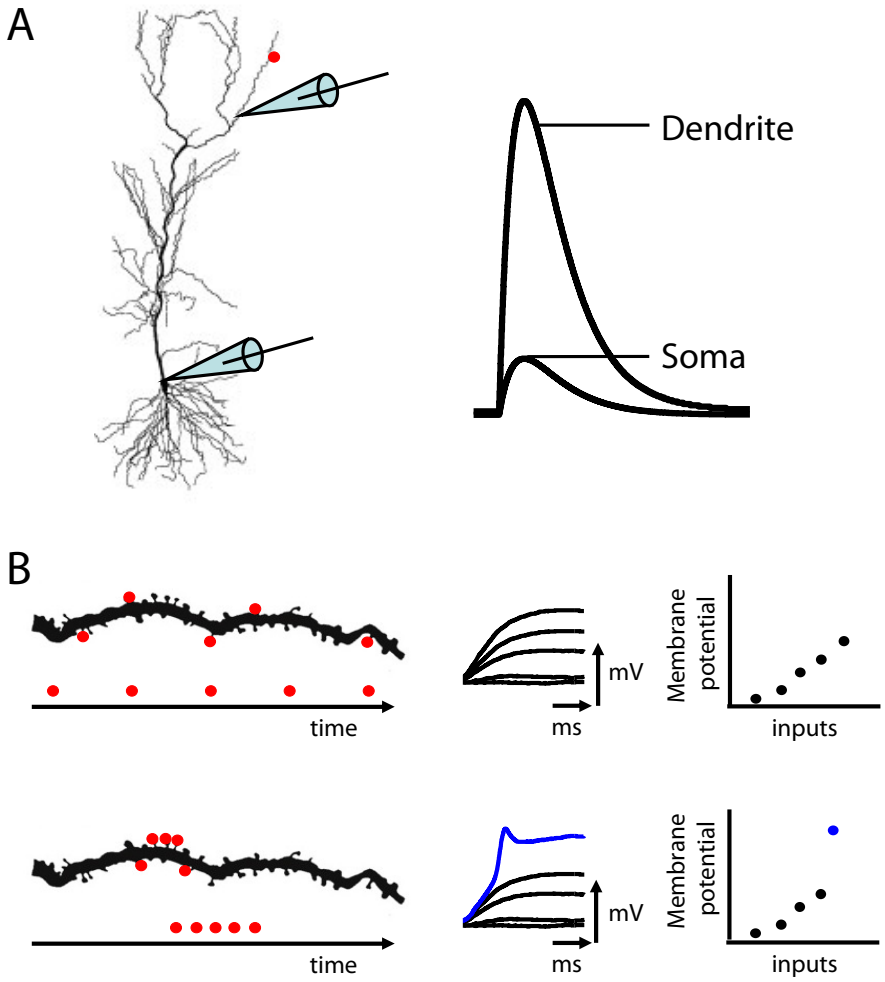

Figure 1.3: **A)** Reconstruction of a CA1 pyramidal cell (full vertical extent 730 µm). Red dot indicates the site of an excitatory input in the distal dendritic tuft. When the excitatory postsynaptic event is recorded at the dendritic site of initiation, it is larger and faster than at the somatic site (adapted from Spruston, 2008 with permission; Magee, 2000). **B)** Dendritic segment of a CA1 pyramidal neuron. Red dots indicate activated excitatory synapses. Upper panels: The excitatory input is spatially distributed and asynchronous. This leads to a linear summation of the postsynaptic excitatory events. Lower panels: The inputs are spatially clustered and synchronous. Above a certain threshold this evokes a nonlinear response: A dendritic spike (blue; dendrites adapted from Spruston, 2008 with permission).

the open Cl^- channels also decrease the resistance of the membrane. When an excitatory potential travels now along the activated inhibitory synapse, it will increase the driving force for Cl^- locally and thus lead to a chloride influx at the inhibitory synapse. This phenomenon called *shunting inhibition* decreases excitatory events only during the time interval the inhibitory conductance is activated. This allows a more precise timing of inhibitory action than with hyperpolarization (which is limited e.g. by the membrane capacitance) alone (Koch et al., 1983; Staley and Mody, 1992; Gulledge and Stuart, 2003). Furthermore, it is spatially more restricted than the effect of hyperpolarizing inhibition and therefore the relative locations of the excitatory and inhibitory synapses determine the amount of inhibition.

1.5.1 Dendritic spikes

Unitary excitatory postsynaptic potentials (EPSPs) can arrive temporally and spatially distributed on the dendritic tree. In that case, they will be integrated in a linear fashion (fig. 1.3B, upper panels): The sum of all EPSPs evoked by the activation of all the single synapses matches the actual voltage deflection evoked by the simultaneous activation of all synapses. However, the first indication for an "additional feature" in excitatory signal integration was given already in the early 1960s by Spencer and Kandel (1961). Many subsequent studies have established that dendrites of CA1 pyramidal neurons can supralinearly integrate excitatory inputs, when they are spatially clustered and highly synchronous. Excitatory inputs to the dendrite will then evoke a stronger excitation than it would be expected by the simple summation of the single events. The postsynaptic response is amplified by the recruitment of dendritic voltage-gated Na^+, Ca^{2+}, and NMDA channels and a dendritic spike is generated locally on the dendrite (fig. 1.3B, lower panels). The fast spikelet (initial component, mainly driven by Na^+) of the dendritic spike facilitates the opening of NMDA receptors responsible for the slower component (Ariav et al., 2003; Losonczy and Magee, 2006; Schiller et al., 2000). This additional, nonlinear dendritic integration mode of pyramidal cells mediated by dendritic spikes may increase information storage capacity of neuronal dendrites. Moreover, dendritic spikes have been shown to trigger neuronal output with high temporal precision (Softky, 1994; Golding and Spruston, 1998; Poirazi and Mel, 2001; Ariav et al., 2003).

Many *in-vitro* experiments provided evidence that basal and apical oblique dendrites of CA1 pyramidal neurons can generate fast sodium spikes (Losonczy et al., 2008; Losonczy

and Magee, 2006; Remy et al., 2009). Also strong excitatory inputs to the apical tuft dendrites of CA1 pyramidal neurons have been shown to evoke dendritic spikes (Jarsky et al., 2005). However, whether these are indeed generated in the tuft dendrites, and not at more proximal sites, remains unclear. In CA1 dendritic spikes have been implicated to contribute to synaptic plasticity in the hippocampus by providing dendritic calcium influx and depolarization, sufficient to induce synaptic plasticity (Golding et al., 2002; Remy and Spruston, 2007). Dendritic spikes on particular branches have been shown to undergo an activity- and experience-dependent form of intrinsic plasticity. This plasticity is mediated by NMDA and muscarinic receptor dependent regulation of K^+ currents that affect dendritic signal propagation (Losonczy et al., 2008). This branch strength plasticity may serve to transform temporally correlated and clustered synaptic inputs on a dendritic branch into long-term changes of branch excitability. It thus provides a putative mechanism of input feature storage. An increase of the propensity for dendritic spikes has been observed *in-vivo* following exposure of the tested animal to an enriched environment (Makara et al., 2009).

The ability to generate dendritic spikes has not only been shown for hippocampal principal neurons (Wong et al., 1979; Golding and Spruston, 1998; Golding et al., 1999), but has also been described for neocortical neurons in layer 5 (Schiller et al., 1997; Stuart et al., 1997), cerebellar Purkinje cells (Rancz and Häusser, 2006), and interneurons (Martina et al., 2000; Traub and Miles, 1995). In addition to fast sodium spikes, slower NMDA (Schiller et al., 2000; Larkum et al., 2009) and Ca^{2+} spikes (Larkum et al., 1999; Helmchen et al., 1999) have been observed in cortical layer V neurons. Since fast dendritic sodium spikes are predominant in CA1 small caliber dendrites, they are the subject of interest in this study.

In-vivo fast sodium spikes have been shown to occur in CA1 during sharp-wave oscillations (Kamondi et al., 1998). During these sharp-waves Schaffer-collateral mediated CA3 input to CA1 is strong and highly synchronous.

1.6 Oscillatory activity in the hippocampus

In the late 1930s Jung and Kornmüller discovered that, when introducing an electrode into the hippocampus of a behaving rabbit, a regular electrical activity at 5 Hz could be recorded (Jung and Kornmueller, 1938; fig. 1.4A). This regular rhythm at 5 Hz is called

theta oscillation and is one of several oscillations in different frequency bands found in the brain (fig. 1.4B). Theta-activity has become one of the most intensely investigated phenomena found in the hippocampal formation.

What causes theta oscillations?

i) The single pyramidal cell in CA1 is found to be well suited to function as an resonator on its own: Voltage-gated ion-channels have been shown to promote membrane potential changes at distinct frequencies. This leads to resonant behavior of the cells in response to specific input frequencies (Leung and Yim, 1991; Leung and Yu, 1998; Peters et al., 2005; Hu et al., 2002).

ii) Interneurons have been suggested to effectively synchronize the pyramidal cells to one another, such that the whole population discharges phase locked to the theta oscillation (Cobb et al., 1995; Fig. 1.4C).

iii) In lesion and pharmacological studies the medial septum and the diagonal band of Broca have been identified to give rise to neuromodulatory and inhibitory inputs to the CA1 population. This functions as the external pacemaker to drive the CA1 cell-population into a state of oscillation (Bland et al., 1996; Buzsáki, 2002; Lawson and Bland, 1993).

Theta oscillations occur during voluntary movement in space (Vanderwolf, 1969) and the speed of the animal is affecting the frequency (Rivas et al., 1996; Slawinska and Kasicki, 1998). It is also present in states of arousal, for example after a noxious stimulus, and during REM sleep (Sainsbury et al., 1987a,b). Furthermore, theta oscillations have not only been found in the CA1 subfield of the hippocampus but also in the entorhinal cortex, the dentate gyrus, and even in regions not belonging to the hippocampal formation like the prefrontal cortex (Hyman et al., 2005; Jones and Wilson, 2005; Siapas et al., 2005) and the amygdala (Paré and Gaudreau, 1996; Seidenbecher et al., 2003). Thus, theta activity could be a means to synchronize different brain regions and thereby bind regions involved in related tasks.

The regular theta oscillation gives rise to a phase code, depending on the firing of neurons relative to the theta cycle. In this regard, it has been shown that some pyramidal neurons fire phase locked, when the animal is located in a specific place field (see chapter 1.2). The phase angle changes depending on whether the animal is approaching or departing the place field (Kamondi et al., 1998; Jensen and Lisman, 2000). However, the average firing frequency of CA1 pyramidal neurons is fairly low ($<$1 Hz, Thompson and Best, 1989). It has been hypothesized that this is due to strong feedback inhibitory control

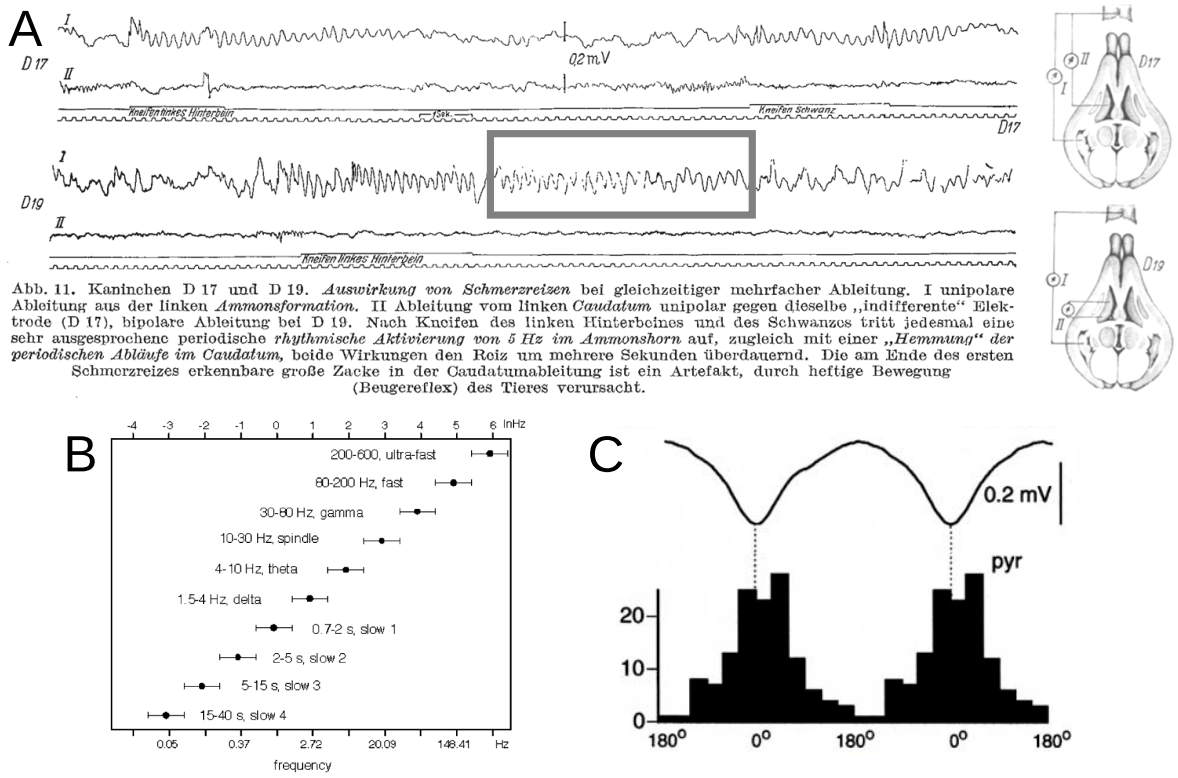

Abb. 11. Kaninchen D 17 und D 19. *Auswirkung von Schmerzreizen* bei gleichzeitiger mehrfacher Ableitung. I unipolare Ableitung aus der linken *Ammonsformation*. II Ableitung vom linken *Caudatum* unipolar gegen dieselbe „indifferente" Elektrode (D 17), bipolare Ableitung bei D 19. Nach Kneifen des linken Hinterbeines und des Schwanzes tritt jedesmal eine sehr ausgesprochene periodische *rhythmische Aktivierung von 5 Hz im Ammonshorn* auf, zugleich mit einer *„Hemmung" der periodischen Abläufe im Caudatum*, beide Wirkungen den Reiz um mehrere Sekunden überdauernd. Die am Ende des ersten Schmerzreizes erkennbare große Zacke in der Caudatumableitung ist ein Artefakt, durch heftige Bewegung (Beugereflex) des Tieres verursacht.

Figure 1.4: A) First recording of theta activity, performed by Jung and Kornmueller (1938) in the rabbit: After a noxious stimulus a very regular rhythmic activity at 5 Hz can be observed (theta frequency; adapted from Jung and Kornmueller, 1938 with permission). **B)** Oscillation frequency bands present in the brain (adapted from Penttonen and Buzsáki, 2003 with permission). **C)** Theta activity in the local field potential (upper trace) and firing histogram of CA1 pyramidal neurons showing a phase preference of the population around the trough (adapted from Buzsáki, 2002 with permission; Csicsvari et al., 1999b)

(Thompson and Best, 1989). In contrast, during exploratory theta oscillations, when the place field of a cell is entered, the firing frequency is strongly increased (Thompson and Best, 1989; O'Neill et al., 2006).

Another prominent oscillation found in the hippocampus is the sharp-wave oscillation. These large amplitude oscillations last only about 50–100 ms and occur when the animal is immobile, e.g. during awake immobility and slow wave sleep. They occur irregularly with a frequency of less than 0.5 Hz in phases of low background activity (Buzsáki, 1986; O'Neill et al., 2006). Sharp-waves mainly appear in the CA1 subfield, where they are thought to be generated by strong synchronous CA3 input onto the CA1 pyramidal cell dendrites (Csicsvari et al., 2000). Characteristically, smaller, very fast oscillations, the

ripple complexes (140–200 Hz), are riding on a sharp-wave. These are hypothesized to be caused by very fast discharge of CA1 perisomatic interneurons (O'Keefe and Nadel, 1978; Buzsáki et al., 1992; Ylinen et al., 1995; Csicsvari et al., 1999a). Sharp-waves can spread to the subiculum and the entorhinal cortex but appear to be more restricted to the hippocampal formation than theta activity (Chrobak and Buzsáki, 1996) .

During exploration assemblies of CA3 and CA1 cells fire together, and are reactivated during sleep (Kudrimoti et al., 1999; Hirase et al., 2001). The sleep sharp-waves have been identified to be crucial for this reactivation (Girardeau et al., 2009; Ego-Stengel and Wilson, 2010). Therefore it has been proposed that sharp-waves provide a mechanism for cell-assembly reactivation that may be crucial for memory consolidation (Buzsáki, 1989; Nádasdy et al., 1999; Kudrimoti et al., 1999).

Hippocampal interneurons also exhibit phase-locked firing during network oscillations. Early studies in behaving animals discovered cells that fired reliably at theta frequency, and therefore were termed theta cells (Ranck, 1973). Their non- bursting behavior, the high frequency discharges and their narrow action potentials, strongly suggest that these cells are interneurons (Csicsvari et al., 1998). Experiments under anesthesia revealed that proximally innervating interneurons fire preferentially at a different phase of the theta cycle than the dendritically innervating cells (Klausberger et al., 2003). The proximally innervating interneurons receive pacing input from the medial septum (Freund and Antal, 1988). These in turn rhythmically inhibit the somatic compartment of the pyramidal cells. Together with the excitation in the stratum lacumosum moleculare, this interaction is thought to generate the extracellular oscillating fields measurable during theta (Buzsáki, 2002).

Phase-locked firing of somatically innervating interneurons is also found during sharp-waves and the resulting inhibition is thought to be responsible for the ripple activity described above (Ylinen et al., 1995). In contrast, the distal dendritically innervating O-LM cells virtually stop firing during sharp-wave ripple events (Klausberger et al., 2003).

1.7 Central questions

The present study investigated, whether rhythmic firing activity of the CA1 neuronal ensemble leads to activity dependent regulation of recurrent inhibition. The core issue

was, how distinct patterns of recurrent inhibition control excitatory inputs arriving on the different dendritic compartments of the CA1 pyramidal cell. Special focus was laid on the role of supralinear dendritic spikes in the interaction of excitatory and inhibitory inputs during hippocampal rhythmic activity. Finally it was examined, whether plasticity of dendritic branch excitation could serve as an intrinsic mechanism by which CA1 pyramidal neurons modify the interaction of excitation and inhibition on their dendrites.

2 Materials & Methods

2.1 Slice-preparation

Male Wistar rats (P21–P28, Charles River) were deeply anesthetized with an injection of ketamine (100 mg/kg, Pfizer, Germany) and xylazine (15 mg/kg, Bayer, Leverkusen, Germany) and then decapitated. The brain was quickly removed and transferred to ice cold standard artificial sucrose-based cerebrospinal fluid ($ACSF_{sucrose}$) containing (in mM): 60 NaCl, 100 sucrose, 2.5 KCl, 1.25 NaH_2PO_4, 26 $NaHCO_3$, 1 $CaCl_2$, 5 $MgCl_2$, 20 glucose. Then 300 µm thick slices were cut with a vibratome (Leica, Wetzlar, Germany) and incubated in $ACSF_{sucrose}$ at 35 °C for 30 min. In the $ACSF_{sucrose}$ solution sodium was reduced and magnesium increased to minimize aberrant activity during slicing. Subsequently slices were transferred to a submerged holding chamber containing normal ACSF solution (in mM: 125 NaCl, 3 KCl, 1.25 NaH_2PO_4, 26 $NaHCO_3$, 2.6 $CaCl_2$, 1.3 $MgCl_2$, 15 glucose) at room temperature. All extracellular solutions were constantly carbogenized (95 % O_2, 5 % CO_2) to saturate the solution with oxygen and to keep the pH stable. During all experiments $GABA_B$ receptors were blocked with 1 µM CGP55845 hydrochloride (Tocris).

All experiments were conducted in wild type rats except the control cell-attached recordings in EGFP labeled interneurons, which where performed in brain slices of GAD2 EGFP mice (fig. 3.5). The EGFP expression facilitated the visual interneuron identification.

2.2 Electrophysiological recordings

Current-clamp whole-cell recordings were performed at 34±1 °C using a BVC-700A (DAGAN, USA) or Multiclamp 700B amplifier (Molecular Devices, Union City, CA, USA) at 100 kHz sampling rate using a Digidata (1322A, Axon Instruments) interface

controlled by the pClamp software (Molecular Devices, Union City, CA, USA). Recording pipettes were pulled with a vertical puller (Narishige PP-830) to 3–5 MΩ resistance resulting in series resistances ranging from 8–25 MΩ. To visualize somata and dendrites we used Dodt-contrast infrared illumination (TILLPhotonics, Gräfelfing, Germany), a Zeiss (Axioskop 2 FS) upright microscope with a water immersion objective (Olympus 60x/NA 0.9, Tokyo, Japan) and a TILL-IMAGO (TILLPhotonics, Gräfelfing, Germany) camera. For fluorescent imaging a monochromator with an integrated light source (TILLPhotonics, Gräfelfing, Germany) was used to excite intracellular Alexa Fluor 488 (Invitrogen). To minimize photo-damage during imaging we repetitively switched the light source on and off (exposure times ranged from usually 10 to 30 ms).

Most whole-cell recordings were performed using an intracellular solution yielding a physiological Cl^- driving force (contents in mM): 140 K-gluconate, 7 KCl, 5 HEPES (4-(2-hydroxyethyl)-1-piperazineethanesulfonic) -acid , 0.5 $MgCl_2$, 5 phosphocreatine, 0.16 EGTA (ethylene glycol tetraacetic acid). In some recordings (fig. 3.1) a lower intracellular Cl^- concentration (1 mM) was used. The cell-attached recordings were conducted with an Axopatch 200B amplifier (Molecular Devices, Union City, CA) in voltage-clamp mode and patch pipettes (5–7 MΩ resistance) were filled with normal ACSF.

2.2.1 Alveus stimulation

To exclusively recruit the recurrent inhibitory interneuron population, the CA1 pyramidal cell axons in the alveus were electrically stimulated. To achieve an isolated stimulation of CA1 axons the subiculum was cut off, sparing the alveus. In addition, the CA3 subfield was separated. A cluster electrode (CE2F75, FHC, Bowdoin, ME) was placed onto the alveus on the subicular side of the cut and a theta burst protocol was applied: Bursts, containing 3 biphasic current pulses (0.15–0.2 ms, 0.01–0.3 mA) at 100 Hz, were repeated 10 times (or 15 times in dendritic spike experiments) at 5 Hz (theta frequency). To generate the current pulses a biphasic stimulus isolator (A-M Systems, Model 2100) was used.

2.3 Fluorescent interneuron staining and confocal imaging

The interneurons were recorded with an intracellular solution (see above) containing 0.3–0.5 % biocytin (Sigma) for at least 15 minutes. After the experiment slices were

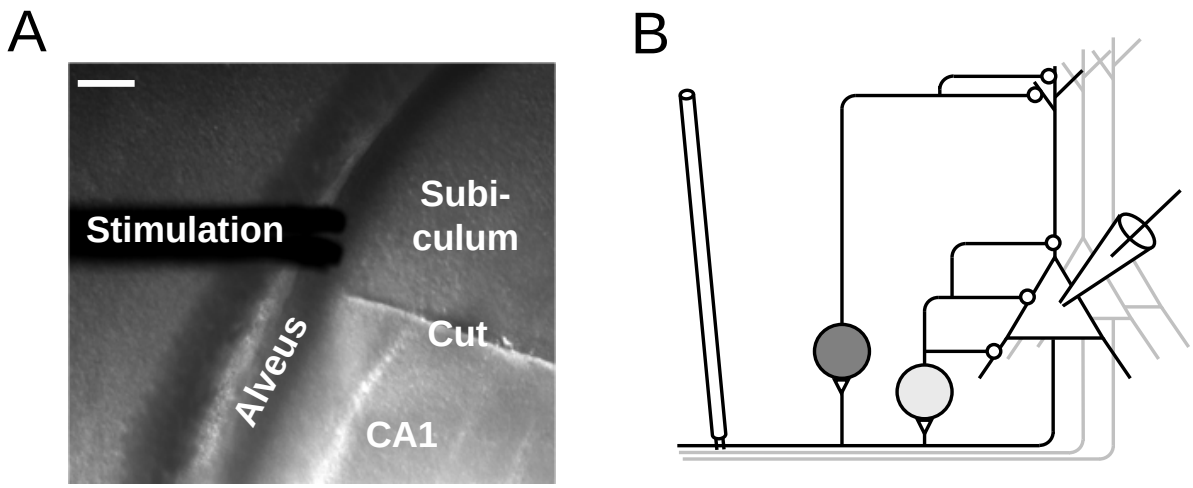

Figure 2.1: A) Infrared image showing electrode position and location of the cut that separated the subiculum but preserved the CA1 axons in the alveus (scale bar: 170 µm). **B)** Recording configuration: Alveus stimulation was performed together with electrophysiological recordings from pyramidal neurons (indicated by the schematic recording pipette) or interneurons in the CA1 subfield of the rat hippocampus.

transferred to 4 % paraformaldehyde (PFA) for 12 hours. For fluorescent staining and post-hoc reconstruction of the axonal arbor, the slices were washed with 0.1 M phosphate-buffer (PB, Sigma Aldrich) and 0.05 M tris-buffer salt solution (TBS, Sigma Aldrich) at room temperature. Subsequently, slices were incubated with (1:500) Streptavidin-Alexa Fluor 488 conjugate (Invitrogen) in TBS for 2 hours in the dark. After washing the slices thoroughly in 0.1 M PB, they were embedded in Vectashield mounting medium (Vector Labs) and kept at 4 °C in the dark. Images were acquired with a confocal microscope (DM RBE, Leica, Wetzlar, Germany) using Leica imaging the software (Leica Confocal Software 2.00) at either 10- or 40- fold magnification. Maximum intensity projections of confocal image stacks were performed with imageJ (NIH). Axonal arborization was reconstructed using Adobe Photoshop CS5.

2.4 Fast CCD voltage imaging

To visualize voltage changes of excitable membranes in the CA1 field, 350 µm thick slices were cut. They were kept in an interface chamber at 35 °C for 30 minutes. Before the experiments the slice was incubated for 15 minutes before the experiment in an interface-chamber with a naphthylstyryl-pyridinium dye, di-3-ANEPPDHQ (Invitrogen) solved

in ACSF (dye-stock: di-3-ANEPPDHQ was solved in 50 µl ethanol. From this stock 1 µl was solved in 300 µl in ACSF shortly before each experiment. Final concentration approximately 100 µM). During incubation the slices were kept in the dark. After incubation it was transferred to the recording interface chamber.

While stimulating the alveus (chapter 2.2.1) epifluorescence images were acquired with a fast CCD camera with 1 kHz frame rate (80×80 pixels, NeuroCCD; RedShirtImaging, Fairfield, CT). The fluorescent dye was excited using a 150 W xenon lamp driven by a stable power supply (Opti Quip, Highland Mills, NY). Theta burst protocol was applied at least 0.3 s after the start of image acquisition to exclude mechanical noise resulting from shutter opening. We acquired images of the whole CA1 subfield by using a low magnification objective (XLFLUOR 4×, 0.28 NA, Olympus, Tokyo, Japan). All technical instruments were switched on at least 30 minutes before recordings to avoid thermal drift. Recordings were performed at 34±1 °C.

Of each slice 12 recordings were obtained with an interval of 20 s in between recordings. These 12 recordings were averaged. Data were analyzed using custom-made routines in IGOR PRO (Wavemetrics, Lake Oswego, OR). Correction for bleaching was warranted by subtracting a double exponential fit of the recording. Peak changes in fluorescence (ΔF/F%) of excitatory signals (fast, negative peaks) were obtained in a 50 ms time window during the first and the last burst of simultaneous alveus stimulation. Peak inhibitory signals (slower, positive peaks) were obtained in a 160 ms time-window after the excitatory signal. The average fluorescence 20 ms before stimulation was used as baseline. To match electrophysiolocical convention in current-clamp mode excitatory events were indicated as positive and inhibitory events as negative values (fig. 2.2; Carlson and Coulter, 2008). The range displayed in the pseudo-color images was set from -12×10^{-3} ΔF/F% to -100×10^{-3} ΔF/F% and a 3x3 pixel smoothing kernel was applied.

2.5 Fast glutamate micro-iontophoresis

Fine, high resistance electrodes (40–90 MΩ) were pulled with a horizontal puller (Sutter Instruments P-97). Pipette glass with a filament 80 mm long and a 1.5 mm diameter was used. The pipettes were filled with a solution of 150 mM glutamatic acid in H_2O_{bidest} and the pH was adjusted to 7.0 with NaOH. 50 µM Alexa Fluor 488 hydrazide (Invitrogen) was added to aid visualization. A micro-iontophoresis amplifier (MVCS-02, NPI, Tamm,

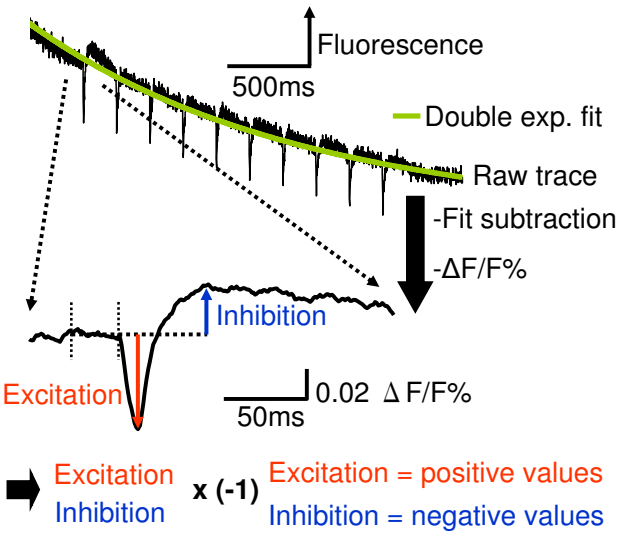

Figure 2.2: Schematic illustration of voltage imaging data analysis. A double exponential fit (green line) of the raw trace was subtracted to correct for bleaching. Relative change in fluorescence ($\Delta F/F$) was calculated. Signals were then inverted to result in positive values for excitation and negative values for inhibition.

Germany) was used, which allowed to compensate the capacitance of high resistance pipettes. Therefore, very brief square current pulses with defined amplitudes could be applied (Murnick et al., 2002).

Before approaching a neuron it was tested under fluorescent illumination, if a leakage of solution was detectable visually. If this was the case, the pipette was rejected. Little bubbles or congested tips could in most cases be cleared with strong current pulses. Appropriate pipettes could then be used for several experiments, however, capacitance compensation had to be frequently controlled and adjusted. The pipette tip was placed close to the dendrite (<1 µm) and short negative current pulses (0.1–0.4 ms, -0.01–(-1) µA) were applied to eject glutamate and evoke EPSPs, dendritic spikes, or action potentials. To achieve a physiological timing of excitation and recurrent inhibition we applied the iontophoretic current and the alveus stimulation synchronously (t0). Therefore, the onset of the EPSP preceded the onset of recurrent inhibition, which is disynaptically delayed. In some experiments, excitation was timed to occur closer to the peak of recurrent inhibition (t0+5 ms).

2.5.1 Branch strength potentiation

A theta pairing protocol was used to potentiate the strength of specific branches that exhibited dendritic spikes (Losonczy et al., 2008). In the theta pairing protocol 3 dendritic spikes were evoked with 200 ms intervals in between. The first two dendritic spikes were elicited together with three short somatic current injections (5 ms, 900 pA) resulting in a 2–3 action potential burst. The third dendritic spike was used as a control to determine, whether the iontophoretic glutamate pulse was successfully and reliably initiating dendritic spikes. This pairing protocol was repeated 15 times with a 10 s intermediate interval. The whole stimulation-paradigm was then repeated 3 times with a 5 minute interval between the repetitions.

2.6 Two photon calcium imaging

Ca^{2+}-signals from small caliber dendrites of the CA1 pyramidal cells were imaged, using two-photon excitation of Oregon Green BAPTA-1 (OGB-1, Invitrogen) and Alexa 594 at a wavelength of 820 nm. A Ti:Sapphire ultrafast, pulsed laser (Chameleon Ultra II, Coherent) and a galvanometer-based scanning system (Prairie Technologies, Middleton, Wisconsin) on an Olympus BX51 upright microscope with a high NA (60×, 0.9 NA, Olympus) objective were used. Cells were patched with the standard intracellular solution, additionally containing 200 µM of the high affinity Ca^{2+} indicator OGB1 and 50 µM Alexa Fluor 594. EGTA was not included in the intracellular solution for Ca^{2+} imaging experiments. Fixed linescans were performed on the dendrites of interest with a frequency of 420 Hz or more. The micro-iontophoretically evoked Ca^{2+}-signals were acquired alone and together with alveus-stimulation. From the raw fluorescence the normalized change in fluorescence $\Delta F/F\%$ was calculated using 100 ms before stimulation onset as baseline.

2.7 Data analysis and statistics

Electrophysiological data were recorded using Clampex 9.0 software (Molecular Devices, Union City, CA) and analyzed with IGOR PRO (Wavemetrics, Lake Oswego, OR), Clampfit 10.0 (Molecular Devices, Union City, CA) and Excel (Microsoft, Redmond, WA). Peak $\Delta V/\Delta t$ values of the dendritic spikes were obtained from the first derivative of the 15 kHz low-pass and boxcar-filtered (23 smoothing points) voltage trace. In all

experiments the peak $\Delta V/\Delta t$ relative to baseline was calculated, except in the branch strength potentiation experiments. Here, it was necessary to exclude EPSP contribution to the $\Delta V/\Delta t$, to isolate the plasticity dependent changes in the fast Na^+ mediated component of the dendritic spikes alone. All results are given as mean ±standard error of mean (SEM), if not indicated otherwise. Statistical significance was tested using appropriate tests in Prism4 (GraphPad Software, San Diego, CA). The statistical tests used are indicated in the figure legends.

3 Results

3.1 Activity dependence of recurrent inhibition

3.1.1 Decrease in recurrent inhibition at theta frequency

In the present study I investigated the temporal dynamics of recurrent inhibition by antidromically firing an ensemble of CA1 pyramidal neurons using alvear stimulation (figs. 2.1, 3.1A). The stimulation paradigm consisted of a burst of three stimuli at 100 Hz. This burst was repeated 10 to 15 times at 5 Hz (theta frequency). In response to a single burst, a compound recurrent inhibitory postsynaptic potential (IPSP) in CA1 pyramidal neurons could be observed (fig. 3.1B). This recurrent IPSP strongly attenuated in response to repetitive burst stimulation at theta frequency (mean attenuation: 40±3 %, n=11; figs. 3.1B_1, 3.2, 3.3). A similar attenuation was also observed when the number of stimuli within each burst was reduced (fig. 3.2). The mean attenuation, when comparing the peak amplitudes of the compound recurrent IPSP in response to a single stimulus was 48±6 % and to a double stimulus 40± 4% (fig. 3.2). The observed attenuation in response to the theta burst protocol decreased with lower burst frequency. The attenuation in response to a 10 and 5 Hz repetition of the burst stimulus was highly significant, whereas at frequencies of 1 and 0.5 Hz no significant attenuation could be observed (fig. 3.3). The activity dependent regulation of recurrent inhibition required at least a two second interval to recover.

Out of the three components evoked by a burst containing 3 stimuli at 100 Hz, the first component predominantly contributed to the overall amplitude (63±3 %), while the other two contributed to a lesser extent (second: 21±3 %, third: 16±1 %; fig. 3.1B_2 and B_3). Interestingly, following theta repetition only the first IPSP component underwent a pronounced reduction (54±4 %, $p<0.001$), which was mainly responsible for the total observed attenuation. The third IPSP component remained unchanged (fig. 3.1B_2, B_3, C) throughout the stimulation. This component-specific regulation of IPSPs could be

due either to different dynamics at the interneuron pyramidal cell synapse or to different interneuron subtypes with functionally distinct action potential output dynamics.

3.1.2 Dichotomy in firing behavior of recurrent inhibitory interneurons

To test the hypothesis that two groups of physiologically different interneurons mediate the differential dynamics of the IPSP components, I performed cell-attached recordings of visually identified interneurons (fig. 3.4A). This recording technique does not rupture the cell-membrane and the composition of intracellular ions is maintained, which is important for preserving the physiological firing behavior. The recorded interneurons were located in the stratum oriens and stratum pyramidale, the target region of CA1 pyramidal neuron axon collaterals. As described above (chapter 2.2.1), electrical stimulation of the alveus was used to determined the action potential firing probability of the interneurons in response to a single burst stimulus. One group of interneurons showed the highest firing probability in response to the first intra-burst stimulus (62±8 %) and a decreased firing probability to the third (15±8 %; n=8; see example: Fig. 3.4B_1). Accordingly, these interneurons were likely to contribute mainly to the first IPSP component that was observed in pyramidal neurons described in chapter 3.1.1.

A second group of interneurons responded with the highest firing probability following the third intra-burst stimulus (50±4 %) and a lower firing probability in response to the first stimulus in a burst (25±5 %; n=16; see example: Fig. 3.4C_1). This indicates a predominant contribution of these late responding interneurons to the third IPSP component measured in the pyramidal neurons the previous chapter.

Consistent with the dynamics of the IPSPs in pyramidal neurons, theta repetition resulted in a reduced firing probability of the early responding interneurons (decrease of 31±6 %, $p<0.01$), whereas the delayed responding interneurons maintained their firing probability (fig. 3.4D).

Occasionally, the identification of interneurons in cell-attached mode is difficult, since the commonly used electrophysiological criterions used in whole cell recordings are lacking. Therefore, a similar dataset from GAD2-EGFP mice (fig. 3.5) was obtained. Interneurons in these mice express EGFP, which enhances the visual interneuron identification. In the GAD2-EGFP mice fast and delayed responding interneurons could also be observed. The early responding interneurons decreased their firing probability in response to the stimulation repeated at theta frequency (28±7 %, $p<0.01$ for fast responding interneurons),

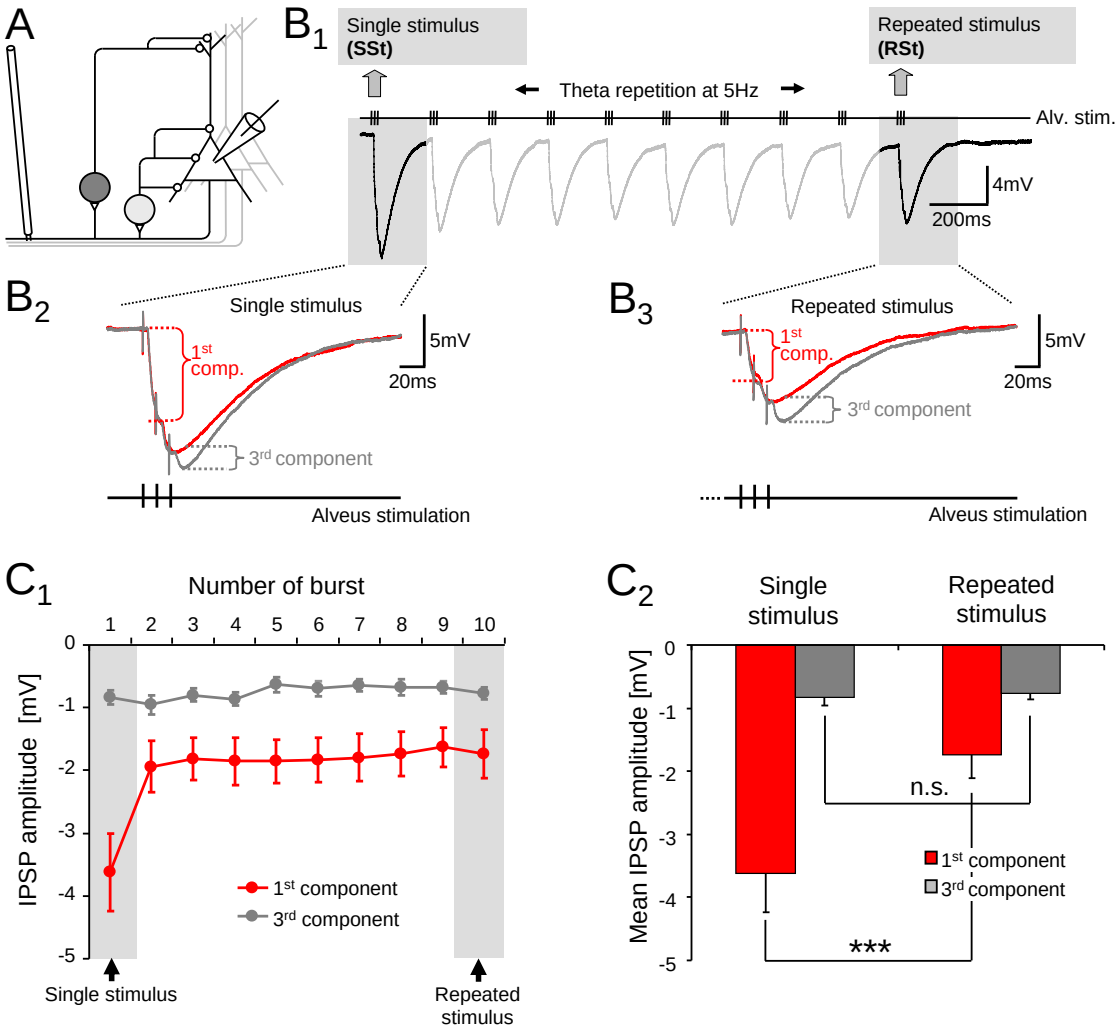

Figure 3.1: **A)** Schematic recording configuration: Alveus stimulation and whole cell recordings from pyramidal cells. **B_1)** IPSPs recorded in current-clamp mode in response to a single 100 Hz burst stimulus (SSt) and following repetition of the burst at 5 Hz (RSt). **B_2)** Magnification of the compound recurrent IPSP in response to a single burst (SSt) compared to **B_3)** the response to a theta repeated stimulus (RSt). **C_1)** Time course of theta attenuation of recurrent IPSP components and **C_2)** comparison of mean IPSP components in response to either a SSt or RSt, red bars: Amplitude of the 1st IPSP component; gray bars: amplitude of the 3rd IPSP component, (n=11 pyramidal neurons; $p<0.001$, paired t-test).

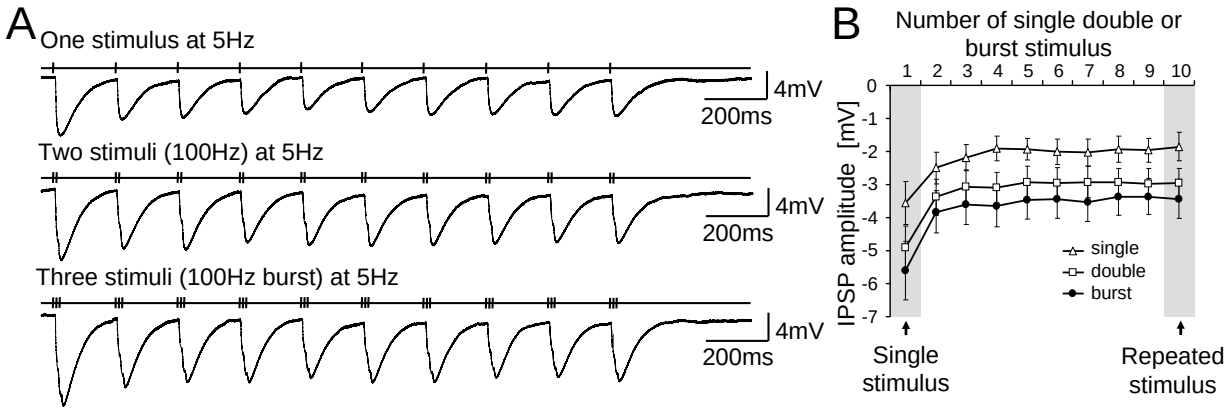

Figure 3.2: Theta dependent dynamics of recurrent inhibition elicited by a single, double, or burst stimulus. **A)** Current clamp recordings of a CA1 pyramidal cell showing IPSP dynamics in response to a single, double, and triple 100 Hz burst alveus-stimulation repeated at theta frequency (5 Hz). **B)** IPSP amplitudes in response to a single (open triangles), double (open squares), and burst (solid circles) stimulus at 5 Hz (n=11 pyramidal neurons).

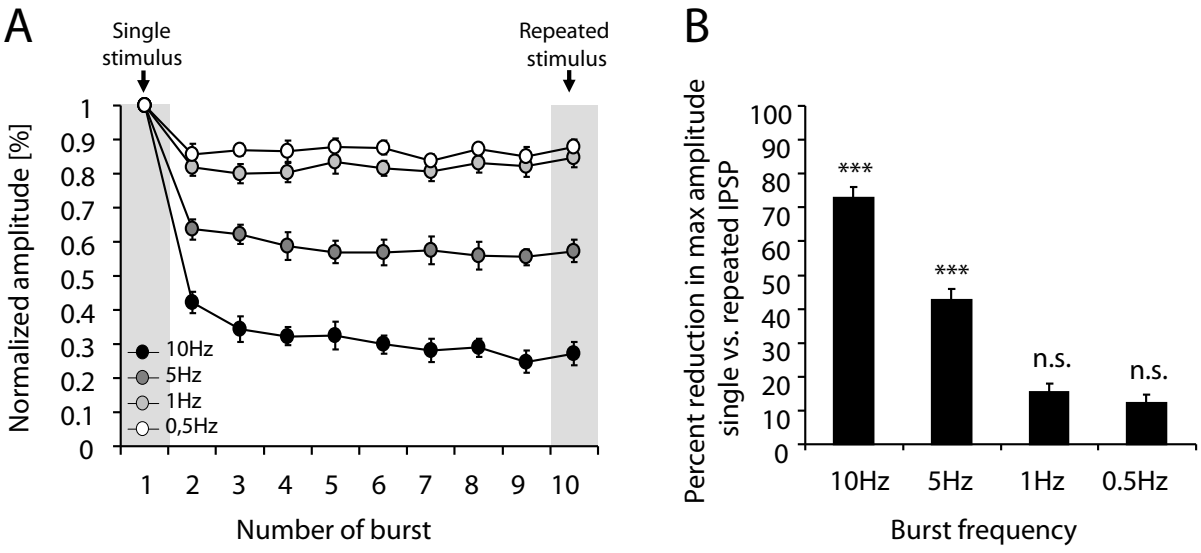

Figure 3.3: **A)** Normalized IPSP amplitude in response to a burst stimulation at 0.5, 1, 5, and 10 Hz. **B)** Percent reduction of IPSP maximal amplitude in response to a single or repeated burst stimulus applied to the alveus normalized to the single stimulus. Percent reduction for burst stimulation at 0.5, 1, 5, and 10 Hz

whereas the late responding interneurons showed an persistent with an tendency to an increasing firing probability (42 ±19, p>0.05 for late responding interneurons; fig. 3.5). These data confirmed the results measured in wild type rats, where interneurons were only identified by location and appearance.

3.1.3 Two populations of interneurons receive distinct input from CA1 pyramidal cells

The difference of interneuron firing patterns in response to a repeated stimulation at 5 Hz could be attributed to a different integration of excitatory inputs from the CA1 pyramidal cell population. Thus, whole cell current-clamp recordings in 122 visually and electrophysiologically identified hippocampal interneurons were performed. In response to a repetitive 5 Hz burst stimulation two opposing interneuron response-patterns could be observed:

i) Interneurons receiving depressing input from CA1 axon collateral synapses. Here, the EPSP amplitude decreased about 36±3 % (n=74; fig. 3.6A, C).

ii) Interneurons receiving facilitating input from the CA1 pyramidal cell population showed an EPSP amplitude increase of 103±20 % (n=48; fig. 3.6B, C). The total interneuron population could then be divided into two groups according to the direction of amplitude change from the response to a single stimulus to the response to the repeated stimulus (fig. 3.6D). The overall theta-dependent attenuation of recurrent inhibition on CA1 pyramidal neurons indicated a more pronounced contribution of the theta-depressing population to the somatically recorded IPSPs (fig. 3.1B_1).

When stimulated at a higher frequency (10 stimuli at 50 Hz) the difference between the two interneuron groups receiving facilitating and depressing inputs was even more pronounced (fig. 3.7).

3.2 Spatio-temporal dynamics of inhibition in CA1 subfield

3.2.1 Morphological differences of the two functionally distinct populations

The stronger contribution of theta depressing interneurons to the inhibitory dynamics observed in pyramidal cell suggests a systematic difference between theta facilitating and theta-depressing interneurons in their dendritic target domains on the CA1 pyramidal cells.

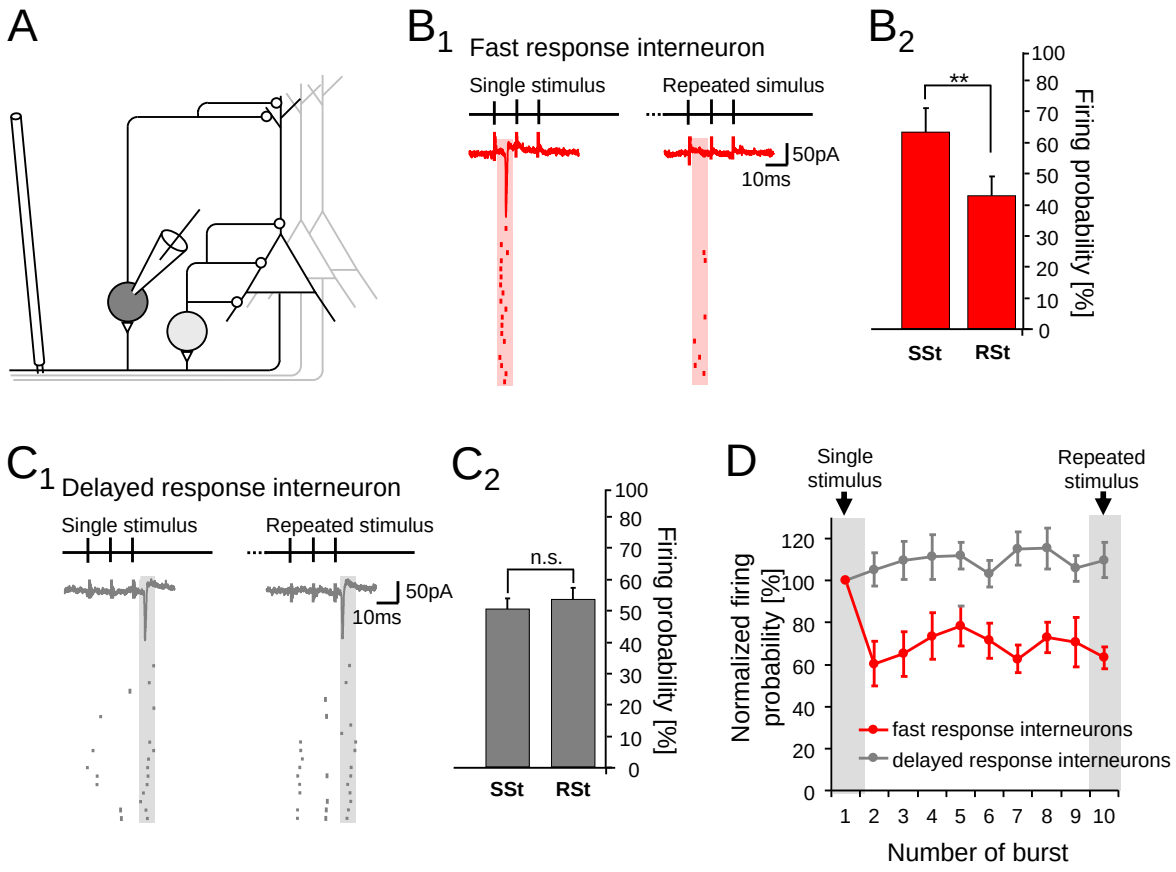

Figure 3.4: **A)** Recording configuration: Cell-attached patch-clamp recordings of CA1 interneurons together with alveus-stimulation. **B_1)** Representative cell-attached recording of a CA1 interneuron responding with action currents preferentially to the 1st stimulus within a burst (fast responding interneurons). **B_2)** Firing probability of the fast responding cells in response to a single burst (SSt) and to a repeated stimulus (RSt; $p<0.01$, Wilcoxon-test). **C_1)** Interneuron responding preferentially to the 3rd stimulus in a burst (delayed responding interneurons). **C_2)** Comparison of action current probability in response to a SSt or a RSt. **D)** Temporal dynamics of normalized firing probabilities of fast (n=8) and delayed responding interneurons (n=16 cells) in response to a repeated stimulus at theta frequency.

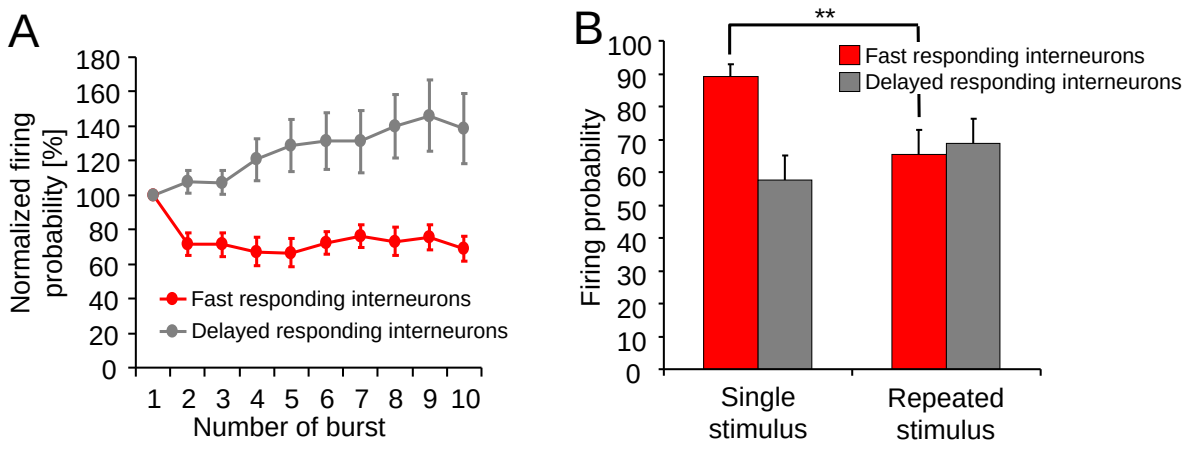

Figure 3.5: A) Cell-attached voltage-clamp recording in visually identified EGFP expressing interneurons in GAD2-EGFP mice, responding predominantely to the 1^{1st} stimulus in a burst (fast responding interneurons: Red; n=9 cells) in comparison to delayed responding interneurons (grey; n=14). Normalized firing probabilities in response to repeated (5 Hz) burst stimulation. **B)** Comparison of firing probabilities in response to a sharp-wave stimulus and to a theta stimulus ($p<0.01$; Wilcoxon test).

To test this hypothesis, I combined the electrophysiological analysis with morphological reconstructions using biocytin in the recording pipette. The subsequent fluorescent streptavidin staining allowed me to reconstruct the axonal morphology using confocal imaging. Interestingly, the functional dichotomy observed in the CA1 interneurons correlated with their axonal target domains (fig. 3.8). Out of 15 interneurons receiving theta-depressing input 14 exhibited an axonal termination in stratum radiatum and oriens (fig. 3.8A, B). In these regions CA1 pyramidal neurons integrate excitatory Schaffer-collateral input from area CA3 (SC integration-zone). In contrast, the majority of interneurons (12 out of 16 interneurons) receiving theta-facilitating CA1 input targeted the distal apical dendrites of pyramidal neurons (fig. 3.8C, D). There, pyramidal neurons almost exclusively integrate excitatory input from the entorhinal cortex layer III via the perforant-path (PP integration-zone).

3.2.2 Spatial extent of hyperpolarizing inhibition in CA1

Next, the interaction of interneuron physiology and axonal connectivity on the hippocampal circuit level was addressed. Therefore, I combined alvear stimulation with voltage

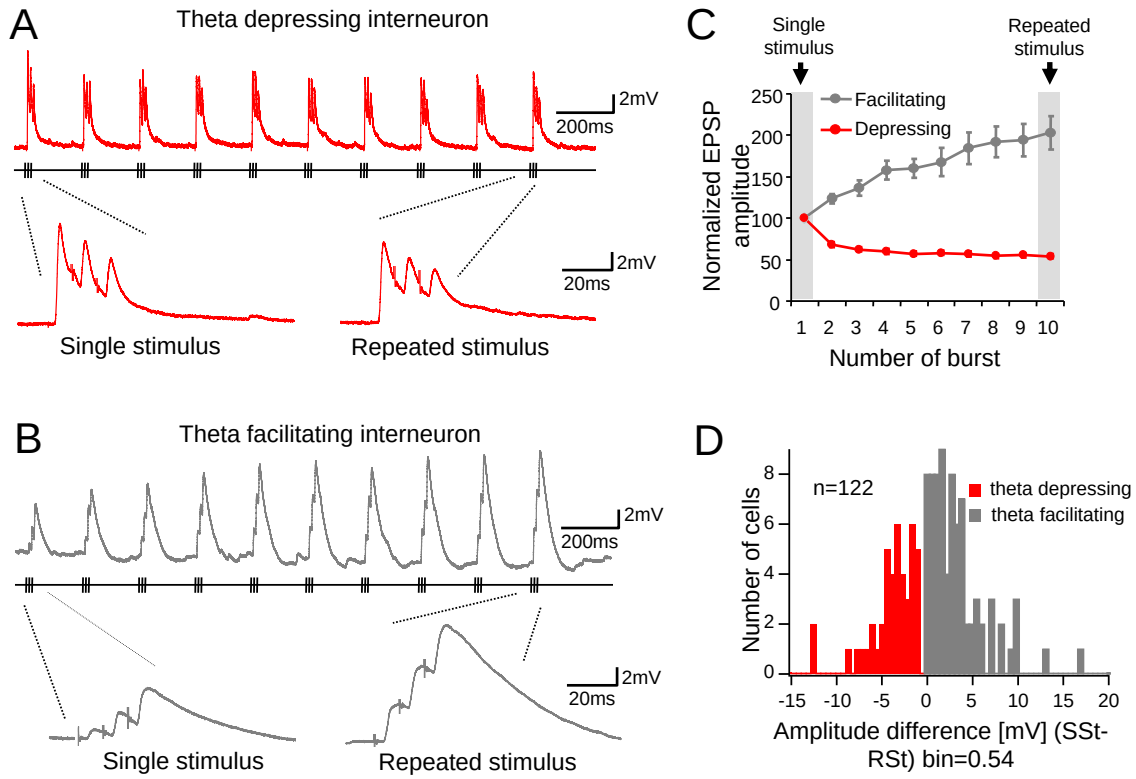

Figure 3.6: **A)** Whole-cell current-clamp recordings of CA1 interneurons in response to theta repeated stimulation: Representative interneuron receiving depressing (red) and **B)** interneuron receiving facilitating (gray) input from CA1 pyramidal neurons to theta repeated stimulation. **C)** Time course of theta-dependent changes in normalized EPSP amplitudes (red, n=74; gray, n=48). **D)** Distribution of interneurons according to the EPSPs amplitude difference in response to a single stimulus (SSt) compared to a repeated stimulus (RSt).

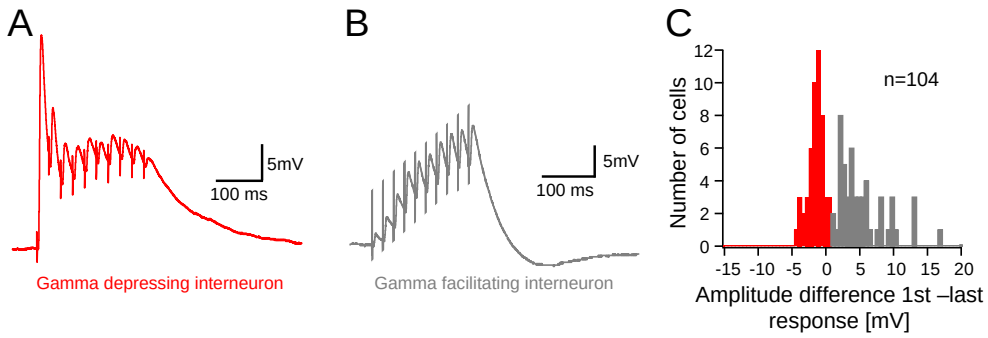

Figure 3.7: Interneurons divided by their response-patterns to alveus stimulation at gamma frequency (50 Hz). **A)** Example of an interneuron receiving depressing excitatory input (red) and **B)** of an interneuron receiving facilitating input (gray) in response to 10 stimuli at 50 Hz. **C)** Distribution of interneurons according to the EPSPs amplitude difference in response to the 1st and last stimulus in a 50 Hz-train; n=104 cells.

sensitive dye imaging using di-3-ANEPPDHQ and fast full frame CCD image acquisition (chapter 2.4; fig. 2.2). According to the results shown before, the theta-dependent dynamics of distinct interneuron groups and the differences in axonal targeting of these interneurons, it can be hypothesized that there is a transition from proximal dendritic inhibition towards distal dendritic inhibition during repetitive theta rhythmic pyramidal neuron firing. The slower inhibitory signal could be isolated from the excitation in time (fig. 2.2). The inhibitory signal reflected the amount of hyperpolarization and gave no evidence about the amount of shunting inhibition.

A single alvear stimulus evoked a hyperpolarizing inhibitory signal, which extended spatially throughout all layers in the CA1 field (fig. 3.9A). This inhibition was most pronounced throughout stratum oriens and stratum radiatum (-0.034±0.003 $\Delta F/F\%$), in the Schaffer-collateral integration-zone. The stratum lacunosum moleculare, the perforant path integration zone, exhibited a weaker but clearly detectable hyperpolarizing inhibitory signal (-0.013±0.001 $\Delta F/F\%$).

Theta rhythmic repetition resulted in a significant reduction (75±4 %; $p<0.01$; fig. 3.9B, C, D) of the inhibitory signal in the Schaffer-collateral integration-zone (s.r. and s.o.). This disinhibition clearly resembled the decrease in discharge probability observed in proximally projecting interneurons (fig. 3.8A, B). In contrast, a significant reduction of recurrent hyperpolarizing inhibition in stratum lacunosum-moleculare could not be observed (25±12 %, $p>0.05$; fig. 3.9C, D). The persistent signal is in accordance with response pattern observed electrophysiologically in distally projecting interneurons, when

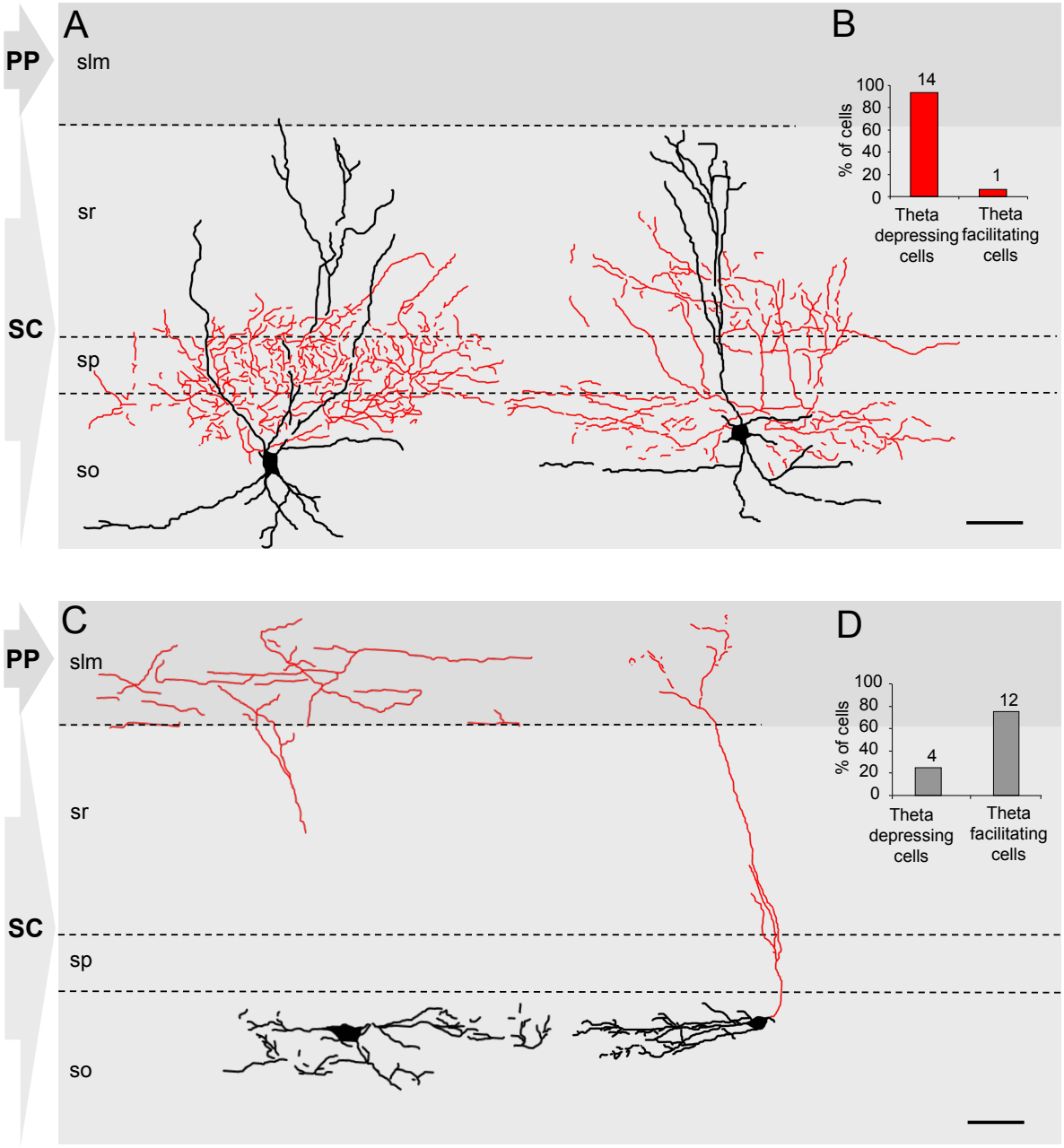

Figure 3.8: **A)** Biocytin reconstructions of two theta depressing interneurons; red: Axonal arbor, black: Dendritic arbor. **B)** Theta response-pattern based distribution of CA1 interneurons targeting Schaffer-collateral integration-zone (stratum radiatum and oriens). **C)** Biocytin reconstructions of two theta facilitating interneurons **D)** Theta response-pattern based distribution of CA1 interneurons targeting the perforant-path integration zone (stratum lacunosum moleculare); scale-bars: 50 µm.

stimulated with a single or a repeated burst-stimulus (fig. 3.8C, D).

As a control the excitation, reflecting the discharge of a subset of CA1 pyramidal preceding the activation of feedback inhibitory neurons, was evaluated. In response to a single alvear burst stimulation, the CA1 pyramidal neurons fired a burst of action potentials. Induced by the antidromic action potentials, excitation in stratum pyramidale and stratum oriens/alveus could be observed. This excitatory signal did not change in amplitude, when the burst stimulus was repeated at theta frequency (fig. 3.10). This result confirmed that the firing of a subset of the pyramidal cell remained constant during theta burst stimulation and that the observed dynamics are not due to intrinsic changes of pyramidal neuron excitability.

3.3 Control of linear input to output conversion by dynamic recurrent inhibition

3.3.1 Dynamic and input-site specific control of local dendritic excitation

In CA1 pyramidal neurons integration of Schaffer-collateral (SC) and perforant path (PP) excitatory inputs depends on the passive cable properties and the recruitment of dendritic ionic conductances, which exhibit layer specific differences (Hoffman et al., 1997; Magee, 1998, 2000; Otmakhova et al., 2002). So far the presented data suggest that there is an additional, activity dependent regulation of excitatory synaptic integration by recurrent inhibition. This mechanism may serve to balance dendritic excitatory input from entorhinal cortex layer III (PP integration-zone) and CA3 (SC integration-zone). To test this hypothesis, local EPSPs were evoked on single dendritic branches using fast micro-iontophoresis of glutamate (chapter 2.5). The depolarization resulted in associated Ca^{2+}-transients that could be visualized by two-photon Ca^{2+} imaging (fig. 3.11). The measured depolarization dependent Ca^{2+}-transients are most likely mediated by NMDA receptors and voltage-gated Ca^{2+} channels (Higley and Sabatini, 2008).

The visualisation of Ca^{2+}-transients allowed to monitor the excitation locally on the dendrites in the different integration zones (fig. 3.11). Glutamate micro-iontophoresis on radial oblique and basal dendrites evoked clear EPSP-associated Ca^{2+}-transients (fig. 3.12A_1, black trace). Next, a single recurrent inhibitory stimulus was evoked simultaneously. This resulted in a significant reduction of the proximally evoked peak

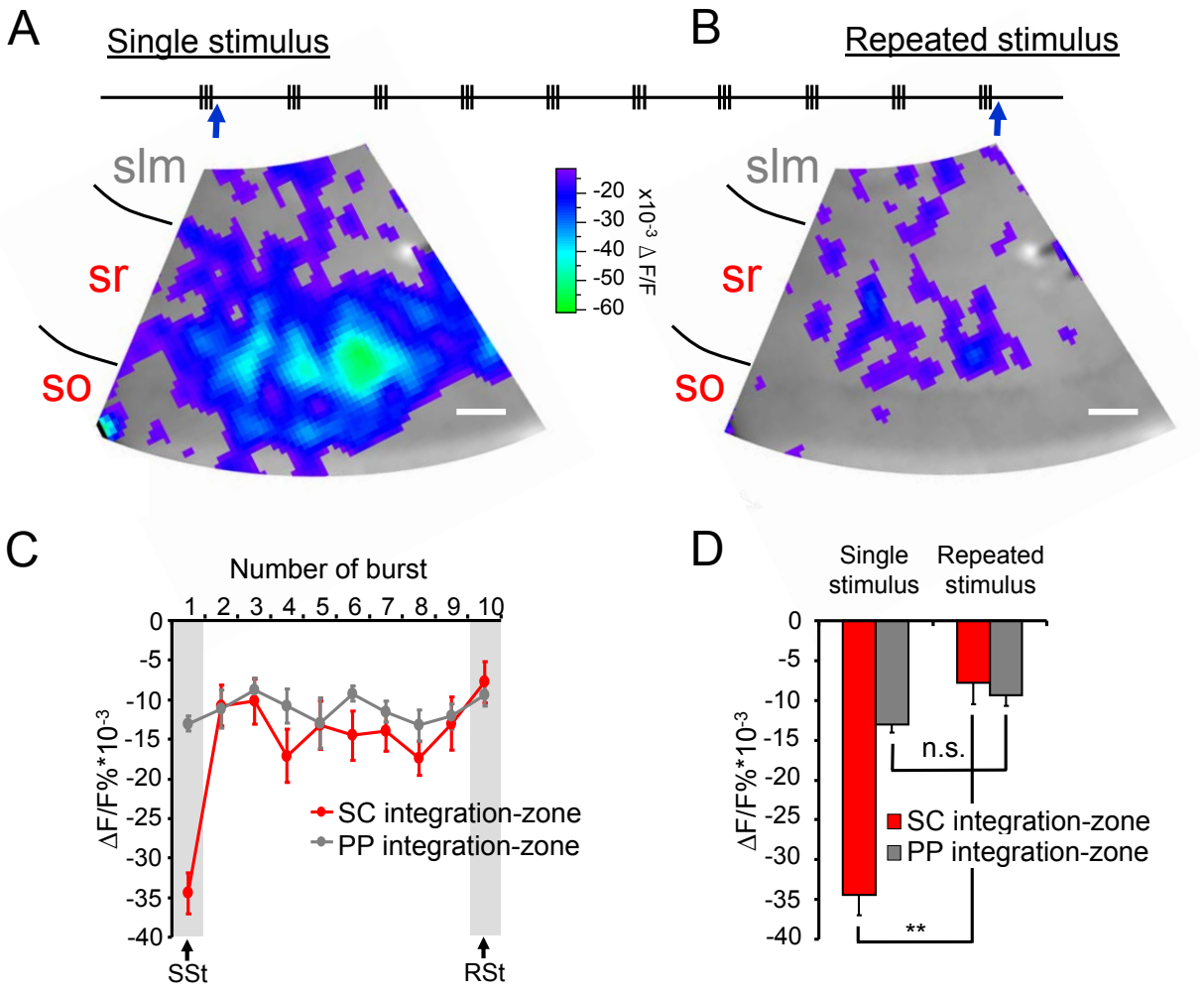

Figure 3.9: **A)** Voltage imaging using di-3-ANEPPDHQ and fast 1 kHz CCD image acquisition: Inhibitory voltage signals across the CA1 subfield in response to a single alveus stimulation. **B)** Inhibitory signal in response to a repeated stimulus (scale bars: 200 µm). **C)** Time-course of inhibition in response to theta repetition of the burst stimulus. Average inhibitory signal in the Schaffer-collateral integration-zone (red) compared to the perforant path integration-zone (gray; n=10 slices). **D)** Comparison of the integration zone specific inhibitory signal in response to a SSt and a RSt ($p<0.01$, Wilcoxon matched pairs test).

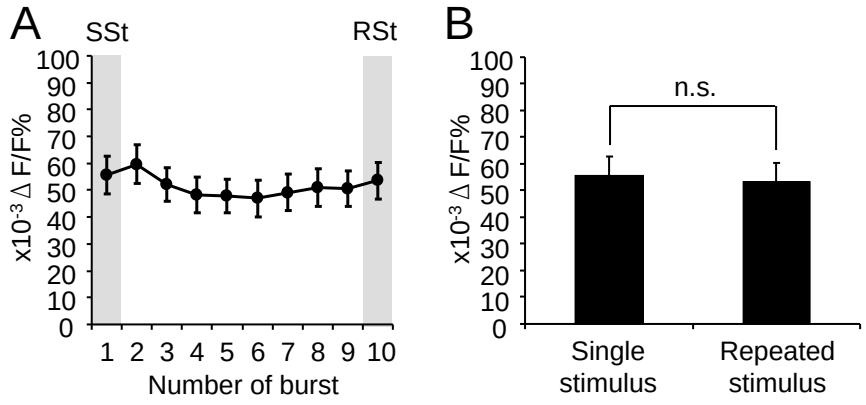

Figure 3.10: A) Excitatory voltage-signal (preceding inhibitory signals, fig. 2.2) in response to a theta burst stimulation measured in stratum oriens, alveus, and the proximal dendritic region of the CA1 pyramidal cells together (n=10 slices). **B)** Comparison of the excitatory voltage signal in response to a single and repeated stimulus reveals no difference ($p>0.05$; Wilcoxon matched pairs test)

.

calcium response by 22±4 % ($p<0.01$; fig. 3.12A_1, red trace; fig. 3.12B).

Theta rhythmic repetition of this stimulus almost completely decreased the proximal inhibition as shown before. When combined with this theta repeated stimulus the local Ca^{2+}-transient on the branch could not be significantly inhibited anymore (reduction: 11±4 %; $p>0.05$; fig. 3.12A_2, B). This reveals a disinhibited proximal dendritic branch after theta repetition of alvear stimulation.

Remarkably, we found that recurrent inhibition inversely regulated excitation on the apical tuft (fig. 3.12C_1, D). There, recurrent inhibition evoked by a single stimulus could not reduce the EPSP-associated Ca^{2+}-transient evoked locally on tuft branches (reduction: 4±4 %; fig. 3.12C_1). However, when the stimulus was repeated at theta frequency, the tuft inhibition became stronger and significantly reduced the EPSP-associated Ca^{2+}-signals (11±2 %; $p<0.01$; fig. 3.12C_2, D).

3.3.2 Dynamic and input-location specific control of subthreshold EPSPs

The dendritic Ca^{2+}-transient is a result of the local depolarization. On the dendrite the observed Ca^{2+}-signal is locally restricted. The underlying depolarisation, however, propagates throughout the dendritic tree and contributes to the somatic and axonal membrane potential. The axo-somatic membrane potential determines, whether the

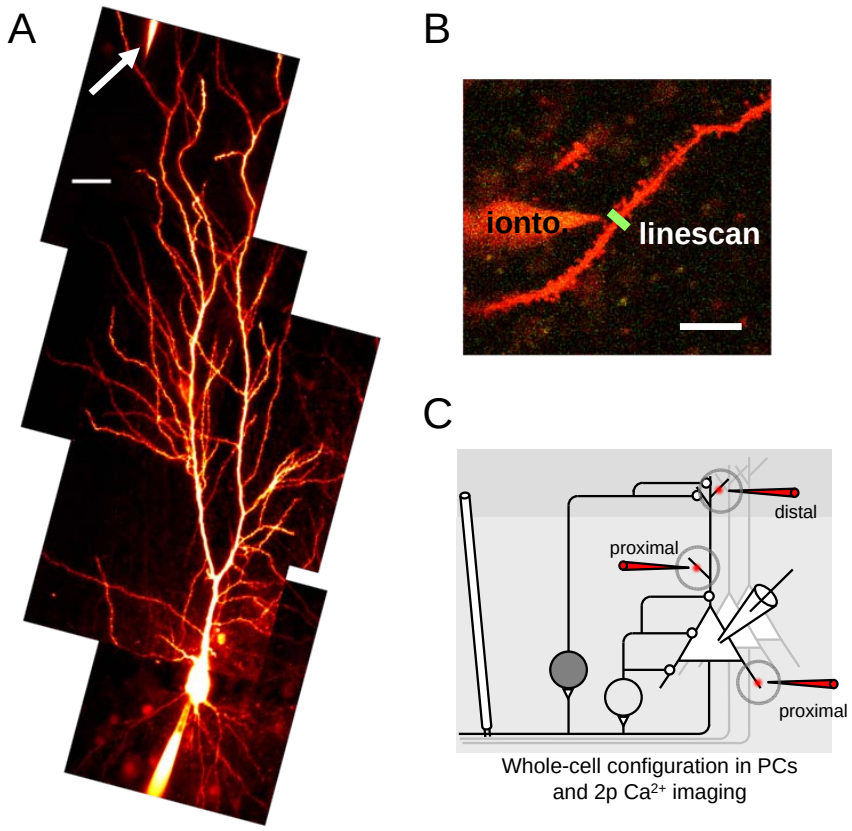

Figure 3.11: A) Two photon maximal intensity projection of an image stack showing a CA1 pyramidal neuron filled with Alexa 594 (50 µM) and Oregon-Green-BAPTA 1 (200 µM). The arrow indicates the position of the micro-iontophoretic pipette in the apical tuft; (scale-bar: 23 µm). **B)** Representative linescan during micro-iontophoresis and simultaneous two-photon Ca^{2+} imaging of a CA1 pyramidal cell dendrite; (filled with Alexa 594/OGB-1; scale bar: 8.3 µm). **C)** Recording configuration: Two photon linescans of iontophoretically evoked Ca^{2+}-signals either on radial oblique and basal dendrites (proximal) or on apical tuft dendrites (distal) and co-activation of recurrent inhibition.

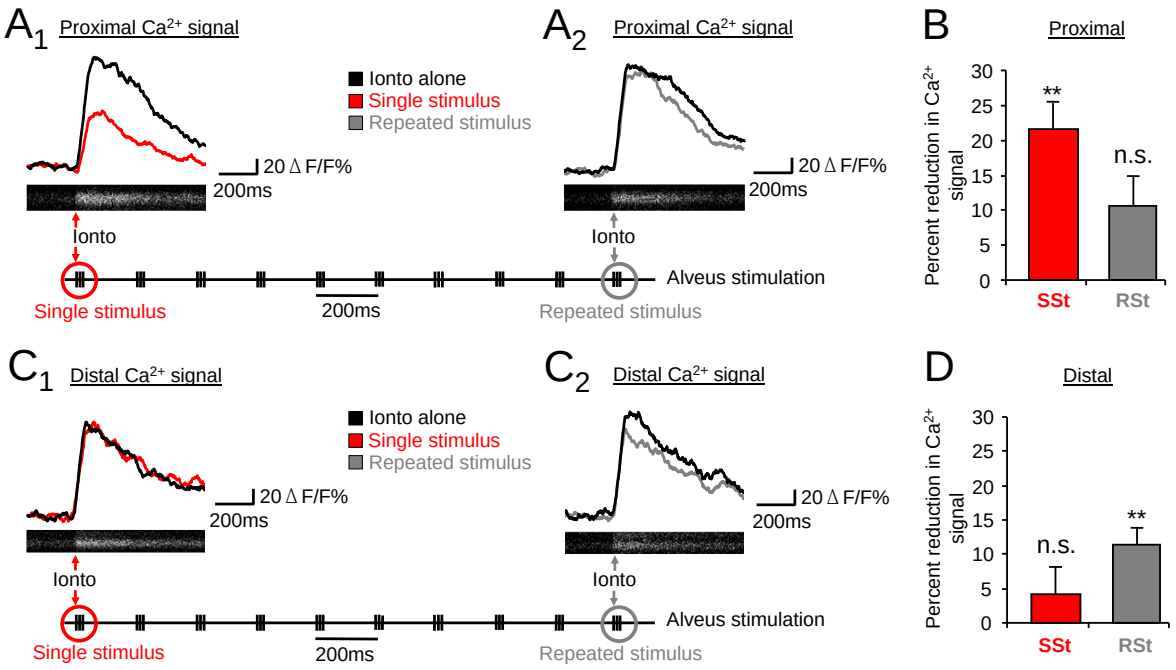

Figure 3.12: **A_1)** Iontophoretically evoked Ca^{2+}-signal on a proximal dendrite alone (black trace) and together with coactivated recurrent inhibition (single stimulus: Red trace). **A_2)** Iontophoretically evoked Ca^{2+}-signal on a proximal dendrite alone (black trace) and together with coactivated recurrent inhibition (repeated stimulus: Gray trace). **B)** Percent reduction of proximal Ca^{2+}-signals by recurrent inhibition activated by the two stimuli (single stimulus: n=9 dendritic branches; $p<0.01$, Wilcoxon matched pairs test. RSt: n=6 dendritic branches; n.s.). **C_1)** Iontophoretically evoked Ca^{2+}-signal on a distal dendrite alone (black trace) and together with coactivated recurrent inhibition (single stimulus: Red trace). **C_2)** Iontophoretically evoked Ca^{2+}-signal on a distal dendrite alone (black trace) and together with coactivated recurrent inhibition (repeated stimulus: Gray trace). **D)** Percent reduction of proximal Ca^{2+}-signals by recurrent inhibition activated by the two stimuli (SSt: n=15, n.s.; RSt: n=15; $p<0.01$, Wilcoxon matched pairs test).

threshold for action potential generation is crossed. Therefore, the effect of recurrent inhibition on the somatically recorded EPSP amplitude was tested. EPSPs were evoked either proximally on basal and radial oblique dendrites or distally on the apical tuft (fig. 3.13A). In both cases, we observed that EPSPs increased linearly in amplitude with increasing micro-iontophoretic current. Proximally evoked 3–6 mV EPSPs (mean amplitude= 4.53±0.13 mV) were significantly reduced by a single inhibitory stimulus by about 41±5 % ($p<0.001$ reduction by SSt compared to control, ANOVA and Bonferroni post hoc; fig. 3.13B, D). Distally evoked 3–6 mV EPSPs (mean amplitude= 4.53±0.11 mV) were reduced by a single recurrent inhibitory stimulus even stronger (56±4 %; $p<0.05$ when compared to proximal with Man-Whitney test; $p<0.001$ reduction by SSt, ANOVA and Bonferroni post hoc; fig. 3.13C, D).

When activated repetitively at theta frequency however, this suppression was clearly reduced for proximally evoked EPSPs (23±6 %, $p<0.001$) and distally evoked EPSPs (37±4 %, $p<0.001$, reduction by RSt compared to control, ANOVA and Bonferroni post hoc; fig. 3.13B, C, D). The impact of recurrent inhibition on the excitatory events originating form different input sites was significantly stronger for distally evoked EPSPs than for proximally evoked EPSPs under both stimulus conditions (fig. 3.13D). Since inhibitory synapses are distributed along the whole somatodendritic axis of the apical dendrite, the considerably longer path length for distal EPSPs suggests that they pass a higher number of shunting synapses.

3.3.3 Dynamic and input-location specific control of action potential output

By controlling the axo-somatic membrane potential, recurrent inhibition may provide a powerful regulation of action potential firing. To investigate the inhibitory control of neuronal output, the micro-iontophoretic current was increased step-wise until the action potential threshold was crossed. Then the stimulus intensity was adjusted to obtain sub-maximal action potential firing probabilities in the absence of inhibition. Both, inputs from proximal and distal input sites were able to evoke axonal action potentials.

As expected, delivering the suprathreshold iontophoretic stimulus together with a recurrent inhibitory single stimulus, strongly suppressed the firing probability of a proximally evoked EPSP (86±5 % reduction; fig. 3.14A, B). However, recurrent inhibition could not significantly suppress action potential output following alveus stimulation repeated at theta frequency (29±8 % reduction; fig. 3.14A, B).

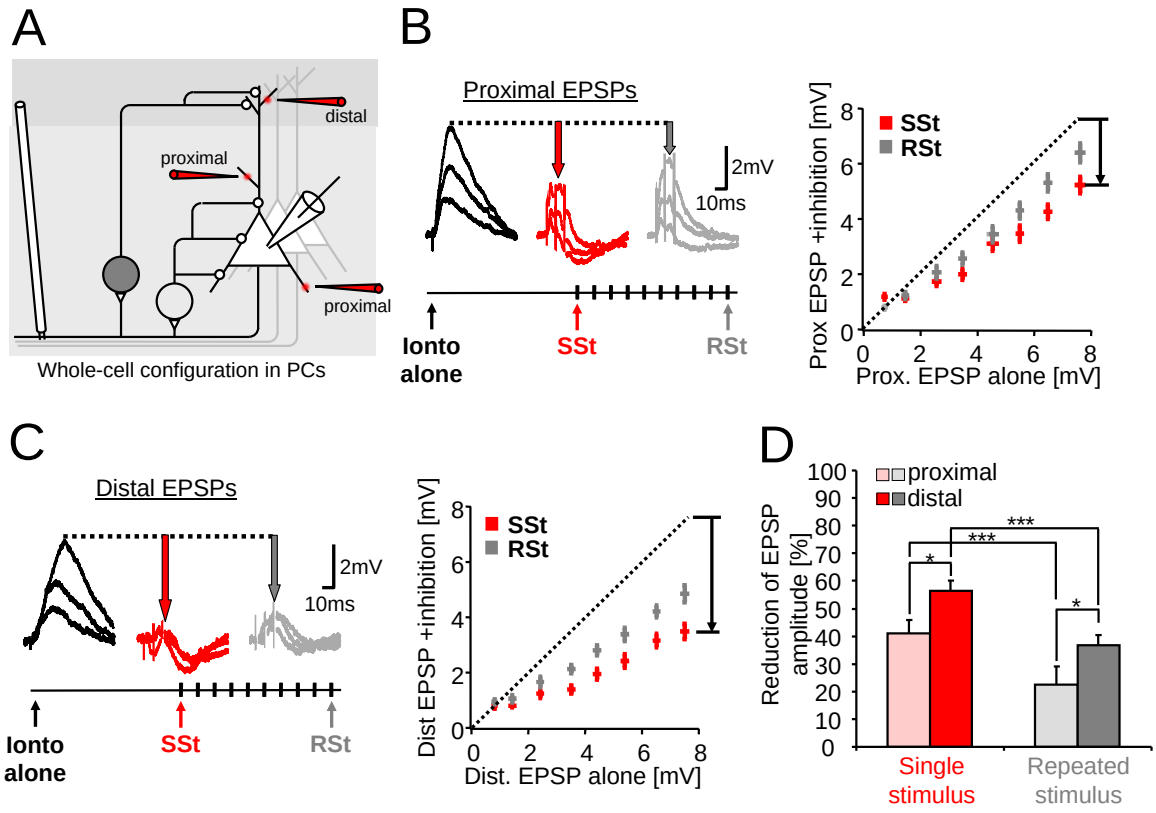

Figure 3.13: **A)** Recording configuration: Somatic whole-cell current-clamp recordings of iontophoretically evoked distal and proximal excitatory events (EPSPs) with and without coactivation of recurrent inhibition. **B)** Input-output relation of proximally evoked EPSPs with increasing iontophoretic stimulation strength, alone and together with recurrent inhibition. Example (left panel) and summarized data (SSt or RSt, n=18 branches; dotted line: angle bisector). **C)** Input-output relation of distally evoked EPSPs with increasing iontophoretic stimulation strength, alone and together with recurrent inhibition, example (left panel) and summarized data (SSt or RSt, n=12). **D)** Amplitude reduction compared to control of proximally and distally evoked EPSPs together with coactivated recurrent inhibition (SSt or RSt; difference SSt/RSt: $P<0.001$, Wilcoxon test. Difference proximal/distal: $P<0.05$ Man-Whitney test).

Similarly, recurrent inhibition evoked by a single stimulus markedly reduced firing probability in response to distal inputs (99±1 %; fig. 3.14C, D). In marked contrast to action potentials evoked by proximal input, theta-repeated recurrent inhibition still significantly suppressed action potentials evoked by distal input (83±7 %; fig. 3.14C, D). These results indicate that recurrent inhibition controls distal dendritic tuft input in two ways: i) Locally on the tuft dendrite excitatory input is only suppressed by recurrent inhibition when it is occurs repeatedly at theta frequency. ii) At the site of action potential initiation the influence of distal dendritic excitation is controlled by recurrent inhibition in a persistent, network-state independent manner, potently segregating distal inputs from output generation.

3.4 Control of nonlinear dendritic spikes by dynamic recurrent inhibition

3.4.1 Recurrent inhibition of dendritic spikes

CA1 principal cell dendrites promote synchronous and spatially clustered input by generating fast, supralinear dendritic spikes (Gasparini et al., 2004; Losonczy and Magee, 2006; Remy et al., 2009). It was shown above that recurrent inhibition provides a powerful mechanism to suppress subthreshold, linear excitatory input (fig. 3.13). However, different regulatory rules may apply for all-or-nothing events such as dendritic spikes. To experimentally address this, dendritic spikes were elicited using fast glutamate micro-iontophoresis (chapter 2.5). The iontophoretic current, used to locally release glutamate onto the dendrite, was systematically increased. In all branches studied, the iontophoretically evoked EPSPs exhibited linear increase with increasing iontophoretic current (fig. 3.13). However, exclusively in the Schaffer-collateral integration-zone (radial oblique and basal dendritic branches) a subset of branches exhibited supralinear dendritic spikes (fig. 3.15). In the somatic recording, the dendritic spike manifested as a fast spikelet riding on the EPSP followed by a slower spike component. The spikelet could be easily detected as rapid increase in the temporal derivative of the voltage signal ($\Delta V/\Delta t$; fig. 3.15B, lower panels).

Using glutamate micro-iontophoresis, dendritic spikes could be repeatedly evoked for up to 260 times without detectable dendritic damage and glutamate toxicity. When plotting

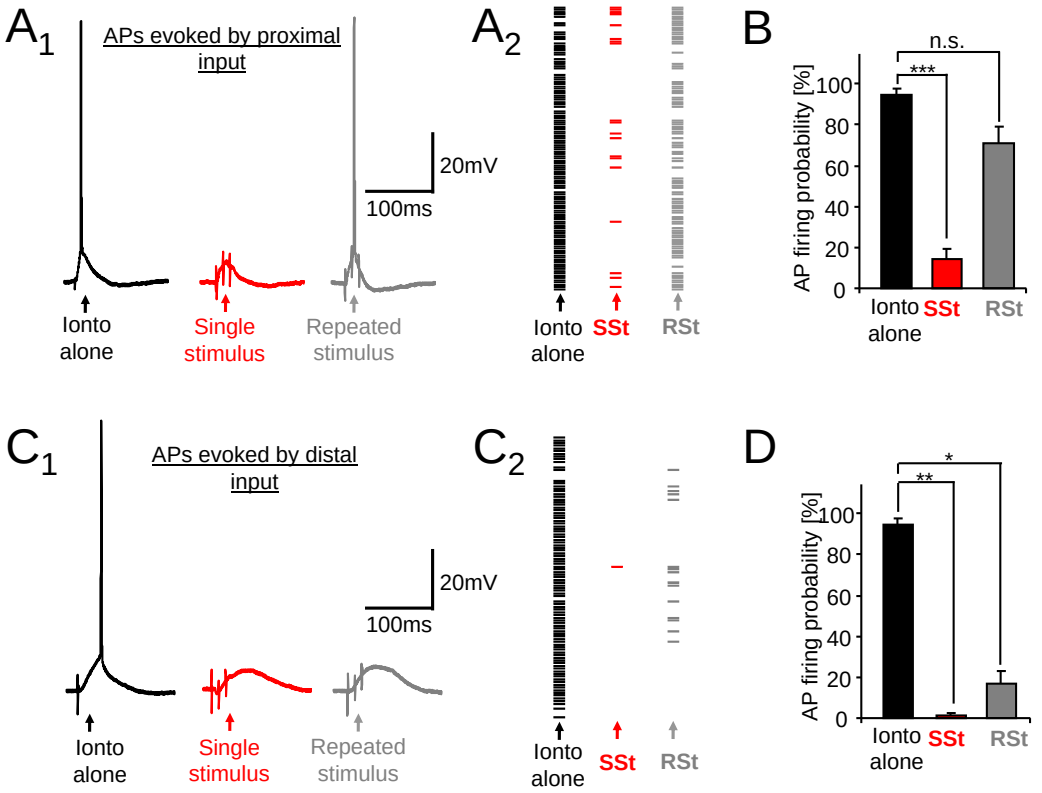

Figure 3.14: **A_1)** Action potentials (APs) evoked by proximal inputs alone and together with recurrent inhibition (SSt: red; RSt: gray). **A_2)** Dot-plot showing probability of proximally evoked APs alone (black) and together with recurrent inhibition (SSt: red; RSt: gray). **B)** Mean firing probabilities of proximally evoked APs alone (black) and together with recurrent inhibition (SSt: red, $p<0.001$, Friedman test; RSt: gray, $n=10$ cells). **C_1)** APs evoked by distal iontophoresis alone (black) and together with recurrent inhibition (SSt: red; RSt: gray). **C_2)** Dot-plot showing probability of distally evoked AP alone (black) and together with recurrent inhibition (SSt: Red; RSt: Gray). **D)** Mean firing probabilities of distally evoked APs alone (black) and together with recurrent inhibition (SSt: red, $p<0.01$; RSt: gray, $p<0.05$, Friedman test; $n=7$ cells).

the number of spikes over the maximum of the temporal derivative of the voltage signal a two-peaked distribution could be observed (fig. 3.15C). This revealed two populations of dendritic spikes according to the branch excitability of the branch they were initiated on. According to this distribution, weak spikes were defined as dendritic spike with a $\Delta V/\Delta t$ below 6.5 V/s (n=48) and strong spikes as dendritic spike with a $\Delta V/\Delta t$ above 6.5 V/s (n=13; fig. 3.15C). This distribution of dendritic Na^+ spikes in CA1 pyramidal neurons has also been previously described using two-photon uncaging of MNI-glutamate (Losonczy and Magee, 2006; Remy et al., 2009). Somatic fast spikelets could only be detected after iontophoretic glutamate release on proximal dendrite (SC integration-zone) and not following micro-iontophoretic stimulation in apical tuft dendrites (PP integration-zone).

When I assessed the effect of recurrent inhibition on dendritic spikes using a physiological timing of recurrent inhibition and dendritic excitation (chapter 2.5), remarkable differences in the processing of weak and strong dendritic spikes could be observed. Weak dendritic spikes (n= 15 dendritic branches of 15 cells) were reliably suppressed by recurrent inhibition evoked by a single stimulus (51±8 % reduction, $p<0.001$; fig. 3.16A, C). The failure of initiation was accompanied by a loss of supralinearity of the voltage response at the given iontophoretic current. When further increasing the iontophoretic current, while keeping inhibition constant, the dendritic spikes reinitiated at approximately 30 % higher stimulus intensities (fig. 3.17A, C).

Next, we tested whether the theta dependent decrease of recurrent inhibition, observed in the Schaffer-collateral integration-zone, influenced the probability of dendritic spike initiation. Remarkably, we found –in the case of weak spikes– that due to theta attenuation, remaining recurrent inhibition failed to decrease weak dendritic spike probability (fig. 3.16A, C).

In contrast, strong dendritic spikes consistently resisted recurrent inhibition (control: 84±3 % strong dendritic spike probability, combined with a single alvear stimulus: 77±4 % probability, repeated stimulation: 82±4 % probability (n=11 dendritic branches of 11 cells; fig. 3.16B, C). Even when proximal recurrent inhibition was maximal, in response to a single stimulus, strong dendritic spikes were able to persist.

In addition, the data revealed a significant difference in the temporal jitter of peak excitation between weak and strong dendritic spikes, reflected in the broader distribution of the time-point weak dendritic spikes (peak in $\Delta V/\Delta t$). The median of the latencies however, did not differ significantly (fig. 3.17D).

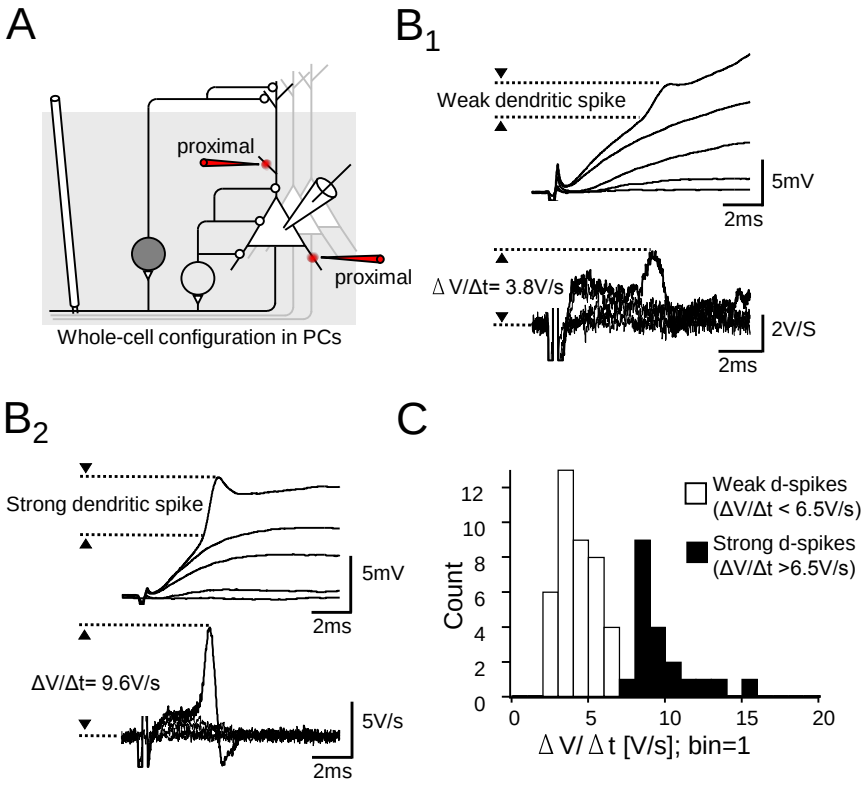

Figure 3.15: **A)** Recording configuration: Proximally (basal and radial oblique dendrites) evoked excitatory events together with recurrent inhibition evoked by alveus stimulation. **B_1)** Representative subthreshold EPSPs and weak dendritic spike (upper panel) and corresponding $\Delta V/\Delta t$ traces (lower panel). **B_2)** Subthreshold EPSP and strong dendritic spike (upper panel) and corresponding $\Delta V/\Delta t$ traces (lower panel). **C)** Histogram of dendritic spike $\Delta V/\Delta t$ (n= 61 branches) iontophoretically evoked on basal and radial oblique dendrites.

In-vivo, the timing of excitation and recurrent inhibition may be more variable. Therefore, it was tested, whether a delay of the onset of excitation by 5 ms would have an effect on the inhibition of strong dendritic spikes. Under these conditions, where the dendritic spikes are shifted nearer to the peak of inhibition, and therefore being inhibited more, strong dendritic spikes were minorly but significantly affected (fig. 3.17E). However, when compared to the strong inhibition of weak dendritic spikes at the control time-point, the effect of recurrent inhibition was much weaker (fig. 3.17E, fig. 3.16C). This indicates that the resistance of strong dendritic spikes to recurrent inhibition is minorly depended on the relative timing of excitation and inhibition.

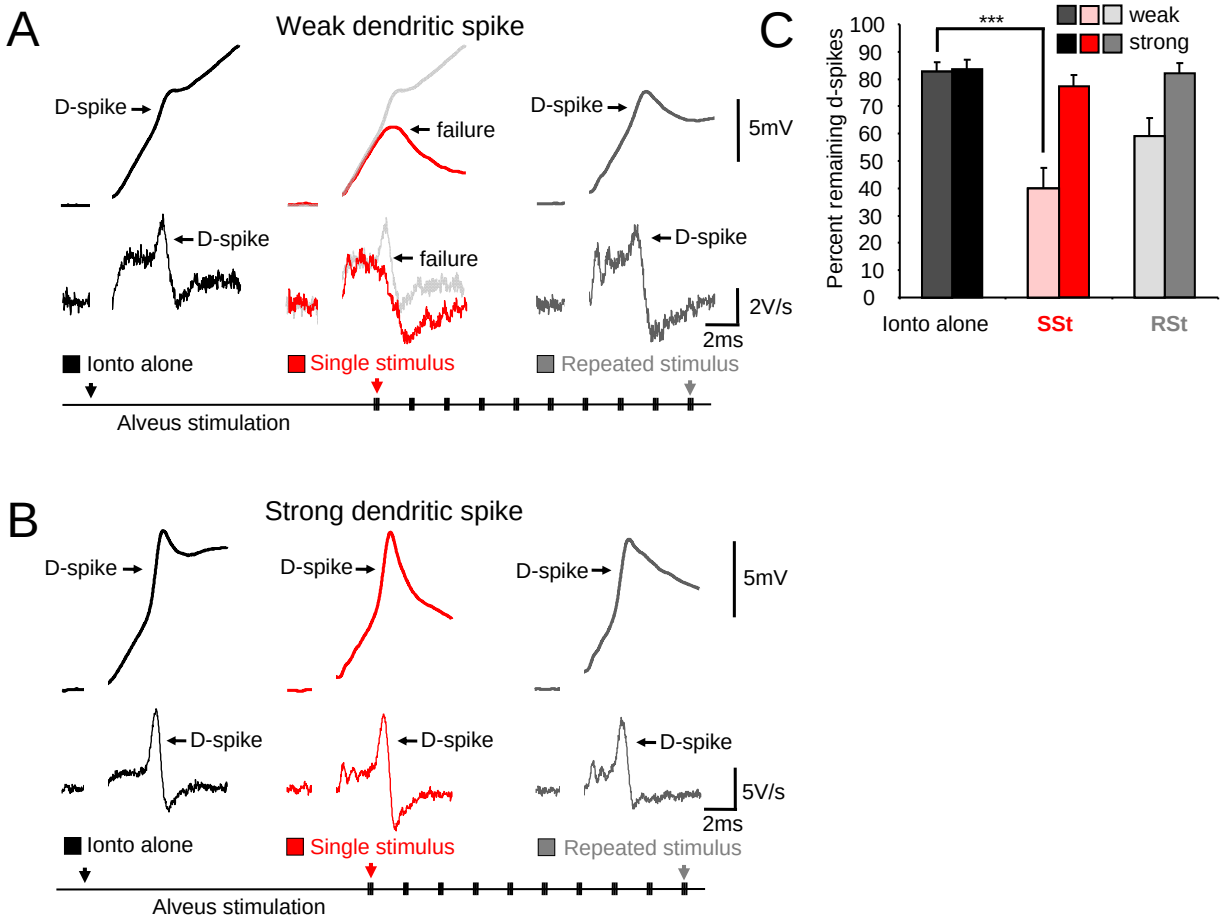

Figure 3.16: **A)** Example of a weak dendritic spike alone (black trace) and with coactivated recurrent inhibition (SSt: Red; RSt: Dark-Gray). **B)** Example of a strong dendritic spike alone (black trace) and with coactivated recurrent inhibition (SSt: red; RSt: gray). **C)** Dendritic spike probabilities (weak dendritic spikes: Light bars, n= 14; strong dendritic spikes: Dark bars, n= 11) alone (black) and together with recurrent inhibition (SSt: Red; RSt: Gray; $p<0.001$, Friedman test).

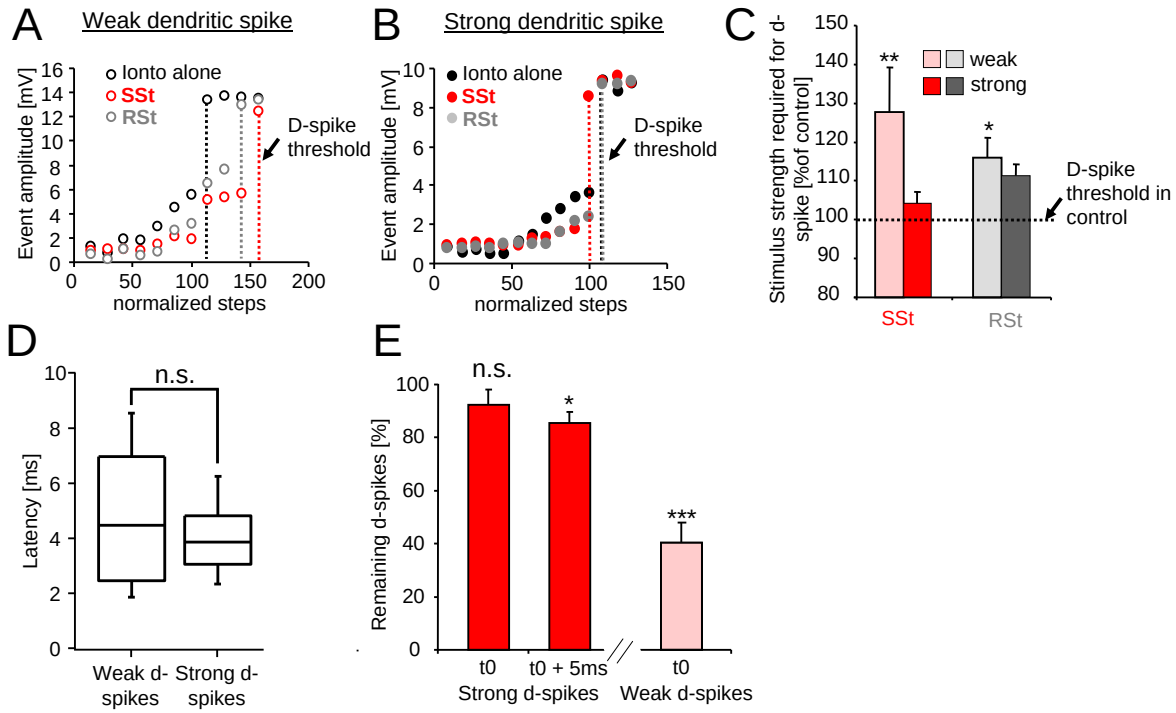

Figure 3.17: **A)** Input-output relation of a weak dendritic spike alone (black open circles) and together with recurrent inhibition (SSt: Red, RSt: Gray). **B)** Input-output relation of a strong dendritic spike (black solid circles) and together with recurrent inhibition (SSt: red, RSt: gray). **C)** Increase in stimulus strength required to elicit a dendritic spike in the presence of inhibition compared to control conditions (SSt: $p<0.01$; RSt: $p<0.05$, Friedman test). **D)** Box and whisker plot (median, quartiles and SD) of dendritic spike latencies shows no difference of medians ($p>0.05$; Mann-Whitney test) but a difference in variance (f-test). **E)** Probability of dendritic spike generation compared to control conditions determined at two different timings of recurrent inhibition (t0; t0+5 ms= dendritic spikes are elicited 5 ms later). Strong dendritic spikes at t0-timing of a SSt (red, n=4 branches $p>0.05$) and same strong dendritic spikes at t0+5ms ($p<0.05$ Wilcoxon test). Weak dendritic spikes at t0 (light bar; compare: Fig. 3.16C).

3.4.2 Recurrent inhibition of action potential output triggered by dendritic spikes

Both, strong and weak dendritic spikes have been shown to serve as efficient triggers of neuronal action potential output (Losonczy and Magee, 2006; Remy et al., 2009; Ariav et al., 2003; Antic et al., 1999; Schiller et al., 2000). As described above, the dendritic spikes consisted of a fast spikelet and a slower component. In the experiments shown here, dendritic spikes could efficiently trigger action potential output with the Na^+ spikelets, resulting in fast, temporally precise neuronal discharges (median latency: 5.4±2.9 ms SD; n=60; fig. 3.18A). In contrast, when action potentials were triggered by the slower NMDA receptor and Ca^{2+} channel dependent dendritic spike components they were initiated delayed (median latency: 12.8±3.1 ms SD; n=191; fig. 3.18B). Furthermore, the data revealed that strong dendritic spikes were the major contributor to fast spikelet triggered output (82 % of all spikelet-triggered APs) whereas weak dendritic spikes were more likely to trigger action potentials with their slow component (18 % of spikelet triggered APs; fig. 3.18).

How recurrent inhibition affects the generation of dendritic spike triggered action potential output has never been investigated before. Weak and strong dendritic spike triggered action potentials were evoked alone, simultaneously with a single and with a theta repeated alvear stimulation. Action potentials triggered by strong dendritic spikes were more resistant to recurrent inhibition than those triggered by weak dendritic spikes (fig. 3.19). Single-burst stimulation led to a selective recurrent inhibition of temporally delayed, weak dendritic spike triggered output (fig. 3.19A–C, middle panels). As a result of this temporal selectivity, the sum of all dendritic spike (weak and strong) triggered action potential output had a significantly shorter latency (5.0±4.0 ms; n=45; fig. 3.19E) than under control conditions or following repetitive theta-activity (median of control latency: 11.1±4.1 ms SD, n=251; TSt latency: 8.1±8.5 ms, n=116 APs; fig. 3.19A–C and E).

Following theta dependent regulation of recurrent inhibition, both weak and strong dendritic spikes participated in triggering output. Therefore, under theta network-state conditions, this led to action potential output that was temporally more distributed (fig. 3.19A–C, right panels). In comparison to a single burst recruitment of recurrent inhibition, the theta dependent reduction of recurrent inhibition resulted in a significantly stronger dendritic spike dependent input to output coupling (fig. 3.19A–D).

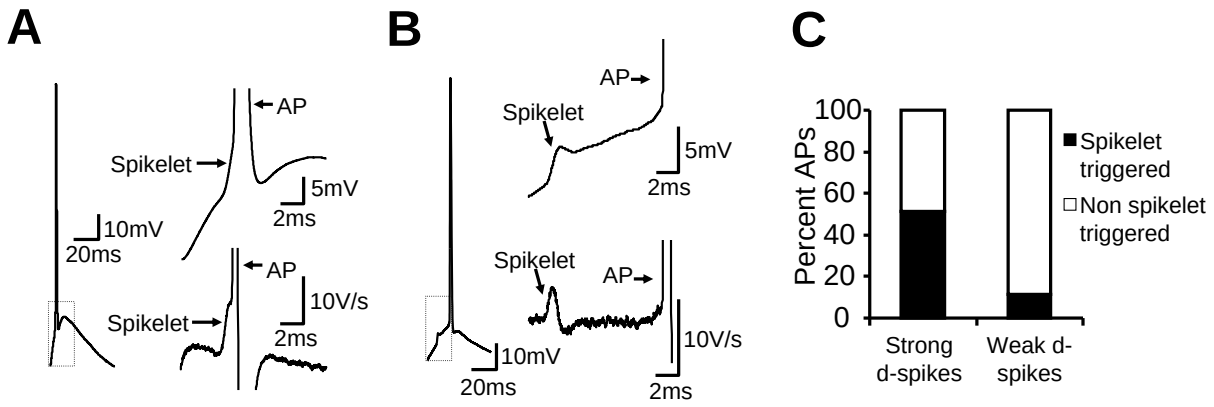

Figure 3.18: **A)** Example of a spikelet triggered action potential (left inset). Magnification and corresponding $\Delta V/\Delta t$ (right panels). **B**) Example of a non-spikelet triggered AP (left inset). Magnification and corresponding $\Delta V/\Delta t$ (right panels). **C)** Probability of strong (n=11) and (n=15) weak dendritic spikes to elicit spikelet triggered APs.

3.4.3 Plasticity of dendritic spikes and recurrent inhibition

It is known, that dendritic spike strength can undergo plasticity, following either physiological theta rhythmic pairing of action potential output and dendritic spikes, or cholinergic modulation (Losonczy et al., 2008). Regarding the interaction of dendritic excitation and inhibition, a strengthening of weak dendritic spikes could serve as a powerful intrinsic plasticity mechanism to counteract recurrent inhibition. To test this hypothesis a theta-pairing paradigm was applied: Glutamate micro-iontophoresis to branches that gave rise to weak dendritic spikes were simultaneously evoked with an action potential burst, elicited by a strong somatic current injection (chapter 2.5.1). Indeed, a pronounced branch spike potentiation, lasting for at least 20 minutes could be observed: Initially weak dendritic spikes (n=7) were thereby converted into stronger dendritic spikes. Following induction; the spikelet $\Delta V/\Delta t$ increased by 73±25 % ($p<0.05$; fig. 3.20).

To address, whether a conversion of weak dendritic spikes into stronger spikes could provide an intrinsic mechanism to counteract recurrent inhibition, dendritic spike probability before and following branch strength potentiation in the presence of recurrent inhibition was observed. Remarkably, within 8 minutes after the induction of branch strength potentiation, weak dendritic spikes, which were initially inhibited by a single alvear stimulus resulting in strong proximal inhibition (53 ±10 % reduction, $p<0.01$; fig. 3.21A, B), were strengthened to withstand the potent recurrent inhibitory control

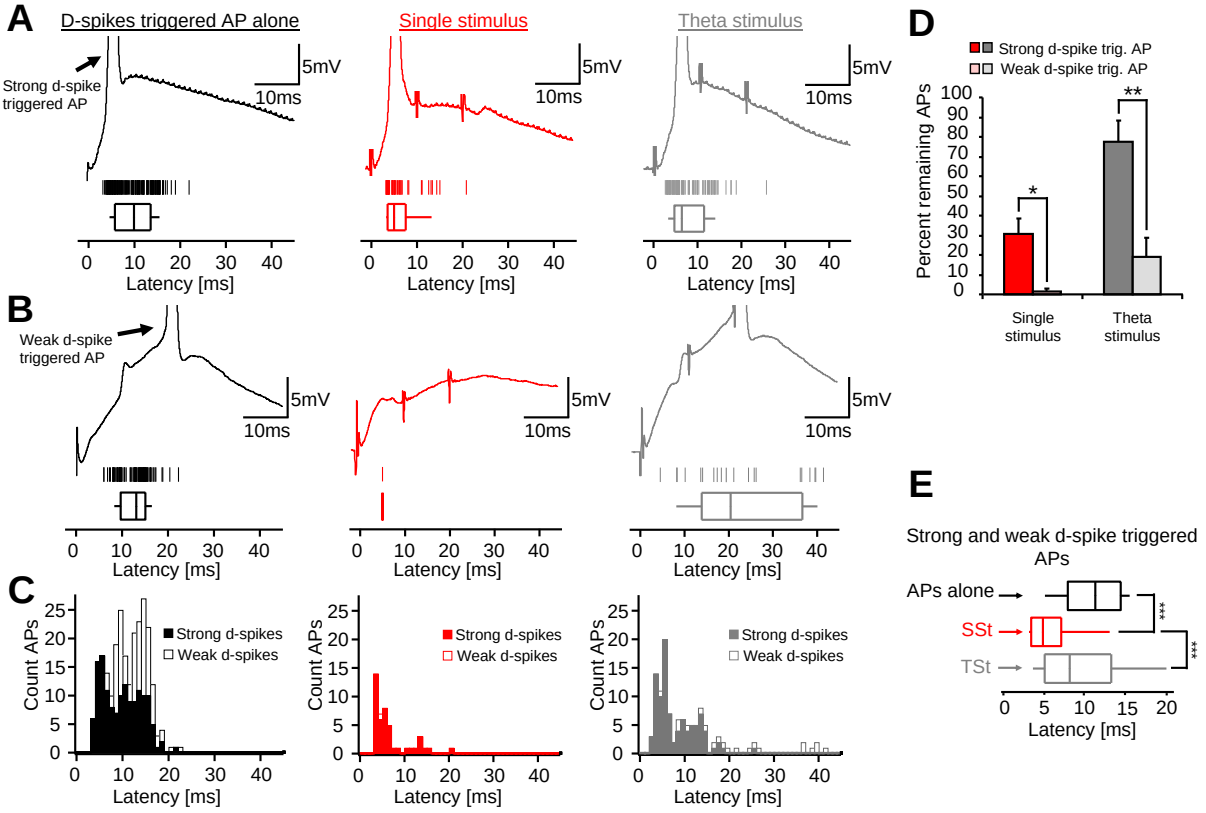

Figure 3.19: **A)** Strong dendritic spike triggered AP alone (black; lower panels: Box- and dotplot of AP latencies) and together with recurrent inhibition (SSt: Red, and RSt: Gray; lower panels: Box and dotplot of AP latencies). **B)** Weak dendritic spike triggered AP alone (black; lower panels: Box- and dot-plot of AP latencies) and together with recurrent inhibition (SSt: Red, and RSt: Gray; lower panels: Box- and dotplot of AP latencies). **C)** Histogram of all dendritic spike triggered (light bars: Weak dendritic spike and dark bars: Strong dendritic spike triggered) APs alone (black) and in the presence of recurrent inhibition (SSt: Red; RSt: Gray). **D)** Percent remaining dendritic-spike triggered APs in the presence of recurrent inhibition (SSt: Red; RSt: Gray) comparing weak dendritic spike (n=15 branches) and strong dendritic spike triggered APs (n=9; $p<0.05$; Mann-Whitney test). **E)** Box and whisker plot of all dendritic spike triggered (weak and strong) APs alone (black) and in the presence of recurrent inhibition (SSt: Red; RSt: Gray; $p<0.001$, ANOVA).

(10±5 % reduction, p>0.05; fig. 3.21D, E).

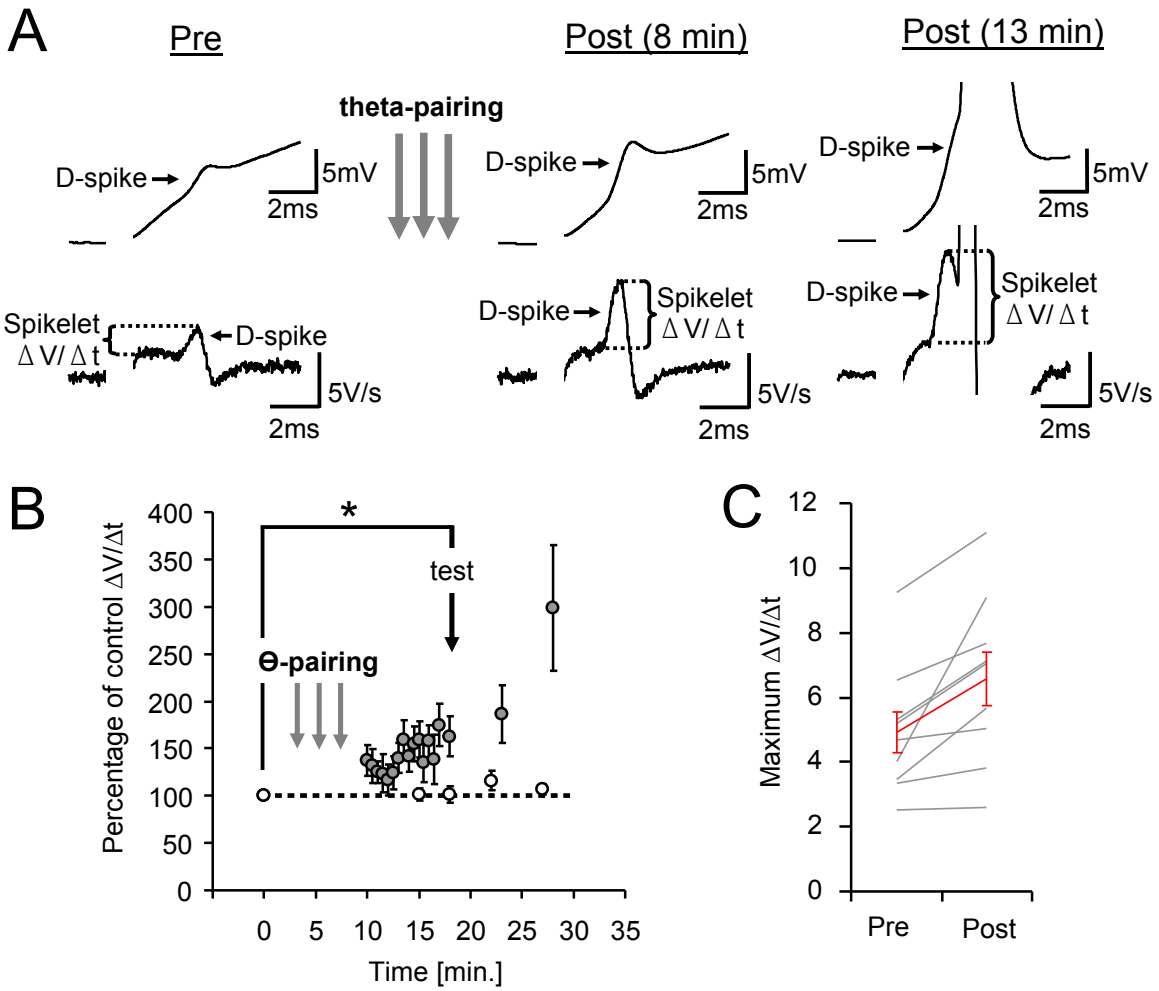

Figure 3.20: **A)** Dendritic spike and corresponding $\Delta V/\Delta t$ before theta pairing and 8 or 13 minutes after the paring. **B)** Percentage of spikelet $\Delta V/\Delta t$ at sequential time-points after the pairing compared to control (before pairing). Significant increase in spikelet $\Delta V/\Delta t$ at testing time-point (n=7, $p<0.05$; Wilcoxon test). Open circles: $\Delta V/\Delta t$ of non potentiated dendritic spikes (n=7–2). **B)** Maximum $\Delta V/\Delta t$ before and after the potentiation. Red: Mean $\Delta V/\Delta t$.

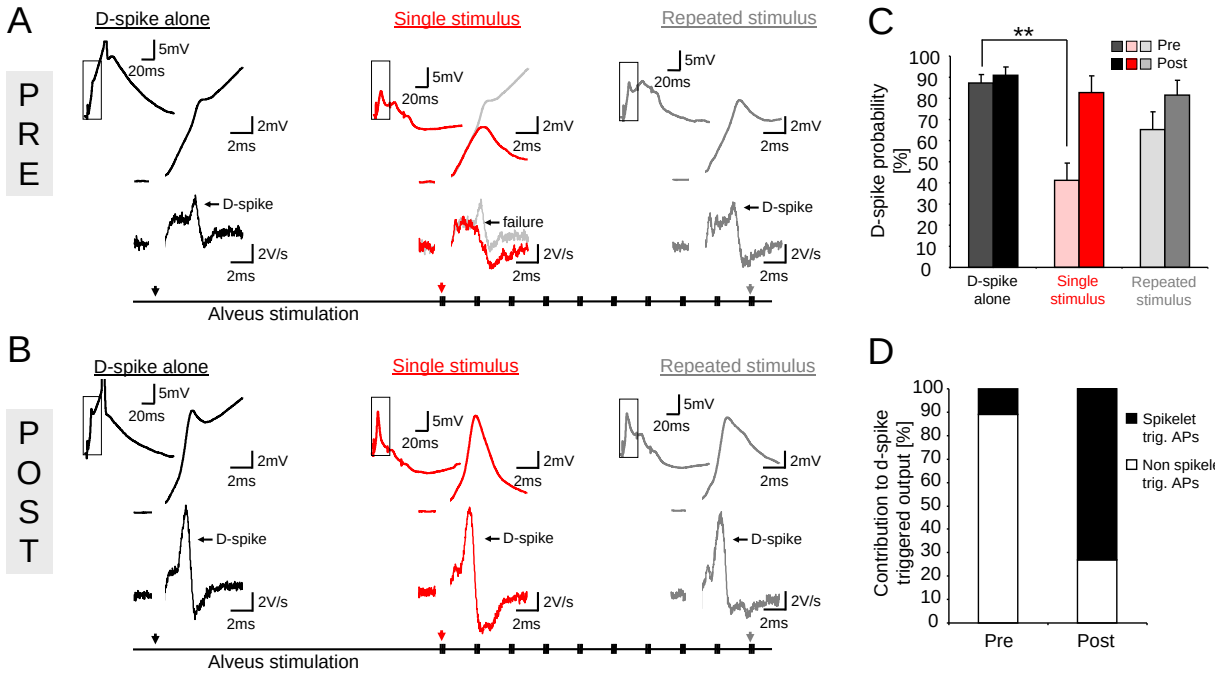

Figure 3.21: **A)** Example of a weak dendritic-spike and corresponding $\Delta V/\Delta t$ alone (black) and in the presence of recurrent inhibition (SSt: Red; RSt: Gray). Insets: Voltage trace at lower magnification. **B)** Same dendritic spike after the pairing paradigm alone (black) and in the presence recurrent inhibition (SSt: Red; RSt: Gray). **C)** Comparison of dendritic spike probability alone (black) and together with inhibition (red, gray), before (light bars) and after (dark bars) pairing paradigm (n=7 cells, $p<0.01$; Friedman test). **D)** Dendritic spike triggered AP probability regarding relative contribution of spikelet (black) and non spikelet (white) triggered APs before and after pairing paradigm.

4 Discussion

The presented data reveal novel insights into how excitatory signal integration in the hippocampus is dynamically controlled by recurrent inhibition during different network-states. The major findings are:

- The impact of recurrent inhibitory circuitry in the hippocampal CA1 field is downregulated by activation of CA1 pyramidal neurons at theta frequency.
- On a low activity background initial inhibition is strong in the proximal integration zone, which potently inhibits the excitatory input on proximal dendritic branches.
- During theta rhythmic activity the inhibition is dynamically regulating the CA3 and PP inputs in an oppositional manner.
- Strong dendritic spikes are specialized excitatory signals that can resist strong inhibitory control.
- Weak dendritic spikes are inhibited like EPSPs but can undergo plasticity, strengthening them to withstand inhibition.
- In a network that is sparsely active, recurrent inhibition reduces neuronal output generated by EPSPs and weak dendritic spikes.
- Under these conditions strong dendritic spikes are most likely to generate more resistant neuronal output, which increases the overall output precision.
- Theta dependent down-regulation of recurrent inhibition leads to a higher contribution of EPSPs and weak dendritic spikes to output generation, which results in more numerous and more imprecise output.

4.1 Design of the stimulation paradigm

To investigate the regulation of recurrent inhibition a physiological theta burst protocol consisting of 10–15 bursts at 5 Hz was applied to the alveus. Thereby, a CA1 pyramidal cell sub-population was discharged that recurrently recruited inhibitory interneurons. Each stimulus train was preceded by 15 seconds without stimulation. Therefore, the first stimulus in each train occurred in a non-regulated network. During slow-wave sleep and awake immobility (Buzsáki, 1986) sharp-waves occur irregularly (below 0.5 Hz; O'Neill et al., 2006) with underlying low background activation (mean firing rate: 1.0–1.5 Hz including intra-sharp-wave firing; Thompson and Best, 1989). Thus, the first stimulus in each train resembled the activation found in sharp-wave states *in-vivo*.

During place related theta activity, however, the average place-related firing of the pyramidal cells is clearly higher (8.8 Hz; Thompson and Best, 1989; O'Neill et al., 2006). Therefore, the last stimulus in each train of theta rhythmic repetition was intended to resemble the network conditions found during theta activity.

The observed regulation of the recurrent inhibition is depended on the preceding discharge frequency of the pyramidal cell population (fig. 3.3). Since, the recurrent inhibition was significantly reduced only in the theta frequency range (5 and 10 Hz) and a decrease could not be observed with lower stimulation frequencies, it is most likely to occur selectively during theta oscillations and not during isolated sharp-waves *in-vivo*.

In the following I will discuss the results in the context of two distinct network states found *in-vivo*: The sharp-wave state and the theta state.

4.2 Network-state dependent recurrent inhibition

The results show that discharging a group of pyramidal cells reliably evoked recurrent inhibition (figs. 3.1, 3.2, 3.3). In CA1 *in-vivo* it was observed that less than 3 ms (monosynaptic delay) after the pyramidal cells, a population of interneurons is discharging (Csicsvari et al., 1998, 1999b). This implies that the recurrent interneurons are reliably activated by the firing of the CA1 pyramidal neurons *in-vivo*.

During a sharp-wave CA1 pyramidal neurons discharge a single brief burst of several action potentials at approximately 100 Hz (Ylinen et al., 1995). The experiments revealed that this pattern of low background activity in CA1 neuronal induced strong, widespread proximal recurrent inhibition. Thus, the population discharge found during sharp-wave

will most likely evoke strong recurrent proximal inhibition that is not downregulated by previous activity.

During hippocampal theta oscillations on the other hand, which occur during explorative behavior and rapid-eye-movement sleep (O'Keefe and Nadel, 1978), CA1 pyramidal neurons repetitively discharge single or bursts of action potentials at frequencies of 4–12 Hz (Ranck, 1973; Csicsvari et al., 1998). The presented data show that this CA1 neuronal activity pattern can induce a state of reduced proximal recurrent inhibition.

In the distal dendritic tuft compartment in contrast, the inhibition, was increased.

A similar activity dependent spatial regulation of inhibition has been observed for gamma activity patterns in the hippocampus by Pouille and Scanziani (2004) and also in the piriform cortex (Stokes and Isaacson, 2010). In the study of Pouille and Scanziani (2004) it was shown that a CA1 neuronal spike series at 50–100 Hz induced a shift of recurrent inhibition along the somatodendritic axis of the pyramidal neurons: At the beginning of a spike series, the recurrent inhibition in the proximal compartment of the recorded pyramidal cell was strong, whereas at the end of a spike series distal compartments of the CA1 pyramidal neurons were inhibited. Consistent with our data, this shift of inhibition is provided by two functional groups of recurrent interneurons, characterized by opposing physiological response patterns. However, the study by Pouille and Scanziani (2004) did not answer the question, how this regulatory mechanism interacts with excitatory inputs.

The interneurons participating in feedback inhibition are a highly diverse group (Freund and Buzsáki, 1996; McBain and Fisahn, 2001). The interneurons shown here were characterized with respect to their axonal arborization. According to previous studies on the morphology of interneurons, my data suggest that interneurons showing a theta depressing response pattern are a heterogeneous group of basket-, bistratified-, trilaminar- and axo-axonic cells, whereas the facilitating interneurons correspond to oriens-lacunosum moleculare (O-LM) cells (Freund and Buzsáki, 1996; Ali et al., 1998; Ali and Thomson, 1998).

Direct antidromic firing of the pyramidal cell axons to excite recurrent interneurons will generate the same amount of pyramidal cell firing throughout the stimulation (fig. 3.10). Therefore, the interneuron type specific regulation is most likely occurring at the synapse between the CA1 pyramidal neuron and the interneuron. This implicates that synapses formed onto distinct interneuron subtypes by the same presynaptic partner can exhibit different short-term plasticity: Some synapses show facilitation and some depression. A

group with theta depressing and a group with theta facilitating properties in response to theta burst stimulation could be discerned in my experiments (fig. 3.6). This phenomenon has been reported previously for proximally innervating basket and bistratified cells, both targeted by CA1 pyramidal cell axon collaterals. In double intracellular recordings from presynaptic CA1 pyramidal cells and postsynaptic interneurons, basket and bistratified interneurons showed a decrease in EPSP-amplitude with repetitive presynaptic firing (Ali et al., 1998). In contrast, in double recordings of presynaptic CA1 pyramidal neurons and postsynaptic O-LM cells the EPSPs displayed facilitation (Ali and Thomson, 1998). These data are in high accordance with the results presented here, confirming that distally innervating cells receive facilitating and proximally innervating interneurons receive depressing input from the CA1 pyramidal cell population (fig. 3.6).

A use-dependent form of plasticity that can last for minutes is most likely underlying this regulation at the CA1 pyramidal neuron to interneuron synapse. Short-term facilitation and short-term depression can be mediated presynaptically amongst others by: Changes in the Ca^{2+} concentration and its detection in the terminal. Changes in the pool of available vesicles, or by presynaptic receptors activated by the release from the terminal (Thomson, 2000; Zucker and Regehr, 2002). Postsynaptically the active and passive properties of the dendrites, which determine the time-window for summation of simultaneous synaptic signaling, may also play role (Johnston et al., 1996; Larkum et al., 1999; Häusser et al., 2001; Stuart and Häusser, 2001; Anderson et al., 2007).

Furthermore, *in-vivo* studies investigated the discharge rates of interneurons situated in the innervation zone of CA1 axon collaterals. They showed an overall decrease in firing rate during theta activity while the animal explored a novel environment (Wilson and McNaughton, 1993; Nitz and McNaughton, 2004). This is consistent with the idea that many proximally innervating interneurons in the stratum pyramidale exhibit theta dependent depression (fig. 3.8).

4.2.1 Other aspects of inhibition in the CA1 subfield

During sharp-waves and theta rhythmic activation, excitatory input via the Schaffer-collaterals and the perforant path arrives on the CA1 pyramidal cell dendrites. The two pathways are additionally recruiting feedforward inhibitory interneurons. This means that a stronger activation will also lead to a stronger feedforward inhibition, thereby controlling directly the excitatory inputs to the pyramidal neurons. Feedforward

inhibition is thought to adjust the dynamic range of pyramidal neurons. This guaranties that pyramidal neurons are sensitive to weak inputs, but still remain responsive to stronger inputs (Pouille et al., 2009). Furthermore, feedforward inhibition is thought to shorten the time window for summation of excitatory inputs (Pouille and Scanziani, 2001). Thus, feedforward inhibition has the potential to control summation of excitatory events that ultimatively leads to CA1 neuronal output. Feedforward inhibition controls the postsynaptic input strength and determines, if a cell fires, whereas recurrent inhibition controls the persistance of the neuronal output. By restricting prolonged firing, recurrent inhibition could help to terminate short lasting sharp-wave activity. During sharp-waves the excitation from CA3 outweighs the feedforward inhibition and discharges the CA1 population within a time window of less than 20 ms (Csicsvari et al., 2000). The strong proximal inhibition during sharp-wave stimulation demonstrated here could then prevent the population from prolonged firing after the synchronous discharge.

O-LM cells are thought to be the only interneuron sub-type that exclusively participates in the recurrent inhibitory network, whereas the proximally innervating interneurons like bistratified and basket cells may participate in both feedforward and feedback inhibition (Blasco-Ibáñez and Freund, 1995; Maccaferri and McBain, 1995). Dendritically targeting interneurons like the Schaffer collateral associated and neurogliaform cells, however, may exclusively provide feedforward inhibition (Klausberger et al., 2004; Price et al., 2005). The main contributor to feedforward inhibition in the perforant path integration zone is the neurogliaform cell (Price et al., 2005). Upon excitatory synaptic input this cell type shows pronounced short-term depression. This indicates that the activity dependent regulation in the feedforward circuitry leads to a depression of inhibition in both the Schaffer-collateral and perforant path integration-zone. Therefore, the integration-zone specific regulation of inhibition, as described here for recurrent inhibition, is not likely to be observed in the feedforward inhibitory circuitry.

In this study $GABA_B$ dependent slow inhibitory signaling was blocked to focus on phasic $GABA_A$ mediated inhibition. There is direct evidence that $GABA_B$ receptors play only a minor role in the inhibition mediated by the recurrent inhibitory network in CA1 (Newberry and Nicoll, 1984; Alger and Nicoll, 1982a,b). In contrast, the feedforward inhibitory network induces both, $GABA_A$ and $GABA_B$ mediated inhibition. The $GABA_B$ mediated inhibition is primarily found on the dendrites and to a lower extent on the perisomatic region. Additionally, there is evidence for a stronger contribution of $GABA_B$ mediated inhibition especially in the perforant path integration zone (Williams and

Lacaille, 1992; Nurse and Lacaille, 1997). Since both receptors exhibit different properties this could indicate a layer specific regulation of feedforward inhibition, however, this idea has yet to be further investigated.

In addition to the difference in inhibition mediated by $GABA_A$ or $GABA_B$ receptors, the $GABA_A$ mediated inhibition can have different timecourses. Tonic inhibition is a slow GABAergic conductance mediated by extrasynaptic $GABA_A$ receptors that are suggested to be activated by synaptic GABA spillover. This form of inhibition is less regulated and less specific than phasic $GABA_A$ mediated inhibition (Farrant and Nusser, 2005). There is recent evidence that neurogliaform cells in the cortex, which possess a dense axonal arborization, release GABA in the extracellular space and hyperpolarize the neurons in their surrounding unspecifically. This "volume transmission" of GABA can suppress the local circuitry persistently (Oláh et al., 2009). Neurogliaform cells can also be found in the stratum lacunosum moleculare of the hippocampus and similar neurons, the ivy cells, in the innervation zone of CA1 pyramidal neuron axon collaterals (Fuentealba et al., 2008; Tricoire et al., 2010). Therefore, this type of long lasting non-synaptic $GABA_A$ mediated inhibition could also play a role in the feedback inhibitory circuitry.

4.3 Network-state dependent inhibition of excitation

4.3.1 Inhibition of linear excitatory events

Here, we show that linearly integrated excitatory events received from proximal input sites are potent triggers of action potential output. Excitatory postsynaptic events (EPSPs) are integrated linearly when distributed synapses are activated asynchronously (Gasparini et al., 2004). In that case, synaptically distinct input patterns are not favored over others. How the EPSP contributes to the axosomatic membrane potential deflection, is not only determined by the passive and active cable properties of the dendrites, but critically depends on inhibition. When recurrent inhibition was activated by a single sharp-wave stimulus, it strongly decreased EPSP amplitude and the resulting action potential firing probability (fig. 3.13, 3.14).

Following theta rhythmic activation and the observed downregulation of proximal inhibition, EPSPs and action potential output were inhibited less (fig. 3.13, 3.14). Consequently, the upregulation of the recurrent inhibition in the apical tuft dendrites only weakly affected proximally evoked EPSPs: The hyperpolarization in the tuft may

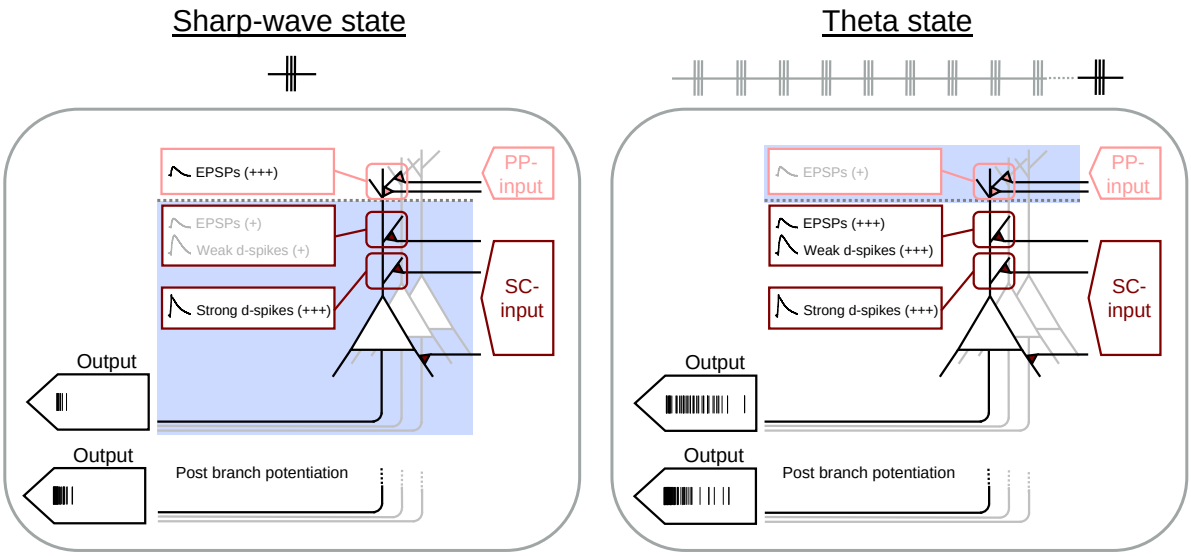

Figure 4.1: Network-state dependent control of action potential output. Left panel: In response to a sharp-wave like pattern of CA1 ensemble activity (single burst stimulation paradigm, trace above) proximal inhibition is strongest (left panel). In this state, action potential output probability in response to Schaffer collateral (SC) input is reduced. EPSPs and weak dendritic spikes are effectively inhibited. Strong dendritic spikes can resist recurrent inhibition and trigger temporally precise output. Weak dendritic spikes can be transformed into strong dendritic spikes by activity-dependent branch strength potentiation and gain the ability to withstand recurrent inhibition. In the perforant path integration-zone inhibition is lower than during theta activity. After dendritic branch strength potentiation, the output increases while remaining precise.
In contrast, in a state of repetitive theta patterned activity (theta burst stimulation paradigm, trace above) proximal inhibition is strongly attenuated (right panel). EPSPs, weak and strong dendritic spikes jointly contribute to action potential output, resulting in a higher action potential probability but lower output precision. Inhibition of perforant path input onto the apical tuft dendrites is stronger than during sharp-wave activity. After dendritic branch strength potentiation, the output gains additional precise discharges.

attenuate by propagation and may be reduced at the site of proximal excitatory input. Furthermore, the off-path inhibitory synapses would not contribute to shunting inhibition of proximal EPSPs.

Due to the distance of propagation along the dendrite, distally evoked EPSPs are generally attenuated more strongly than proximal EPSPs (Magee, 1998; Golding et al., 2005). When coactivated together with a single sharp-wave stimulus that elicits potent proximal inhibition, they are even more effectively inhibited than proximal evoked EPSPs. This is most likely due to the shunting inhibition mediated by the activated proximal inhibitory synapses that the distal EPSPs pass on their path to the soma (fig. 1.3A, 3.13). In the sharp-wave state the contribution of distally evoked EPSPs to action potential output is weak. In contrast, locally in the distal dendritic tuft, inhibition is low and EPSPs and their corresponding Ca^{2+}-signals remain unaffected by a sharp-wave stimulus.

Following theta repeated activation and decreasing proximal inhibition, distal inhibition becomes more effective. Therefore, contribution of distal input to output becomes less likely. Locally in the tuft dendrites, the impact of perforant path associated excitatory inputs is stronger under sharp-wave state conditions (fig. 3.12). Calcium influx evoked by strong inputs from the perforant path to the CA1 pyramidal neurons –also when not combined with action potential output– has been proposed to contribute to LTP induction (Golding et al., 2002). The induction of synaptic plasticity could be facilitated in a state of reduced distal inhibition during sharp-waves.

Taken together, this work reveals a pathway specific, network-state dependent regulation of excitatory inputs, which will be discussed in the following section.

4.3.2 Pathway specificity of recurrent inhibition in different network-states

In the hippocampus, place-related information is conveyed via the perforant path input from entorhinal cortex layer III (O'Keefe and Nadel, 1978; Brun et al., 2002). In addition, the perforant path input to CA1 pyramidal neurons is thought to be critically involved in spatial memory consolidation (Remondes and Schuman, 2004) and appears to play a role in novelty detection (Hasselmo, 2005; Lee et al., 2005; Leutgeb et al., 2004). It has been proposed that feedback inhibition in the CA1 area can segregate the contribution of the perforant path and the Schaffer-collateral to the CA1 subfield differentially in distinct functional network-states (Ang et al., 2005).

Here we propose, that in addition to the known distinct neuromodulatory regulation

of Schaffer-collateral inputs and perforant path inputs (Pasquier and Reinoso-Suarez, 1978; Otmakhova and Lisman, 1999, 2000; Otmakhova et al., 2005) and the differences of their post-synaptic receptor composition (Otmakhova et al., 2002), also a network-state dependent oppositional regulation of both pathways exists, which is mediated by the recurrent inhibitory micro-circuitry.

The hippocampus is thought to act as a comparator (Knight, 1996; Vinogradova, 2001; Kumaran and Maguire, 2007). It compares predictions, which are believed to be provided by CA3 inputs via the Schaffer-collaterals, with the actual current sensory input from the perforant path (Kumaran and Maguire, 2007). During sharp-waves, the perforant path input is only weakly inhibited; on the other hand, proximal inhibition is strong. By truncating Schaffer-collateral mediated excitation, this strong proximal inhibition shortens time window for integration of these inputs with the perforant path inputs. In this way, in CA1 pyramidal cell only synchronous inputs from both pathways can summate. In this way pyramidal cells could serve as coincidence detectors during sharp-waves.

The hippocampus appears to be specifically vulnerable in neurological disease. In a study using an animal model of epilepsy it has been shown that dendritically innervating interneurons –the O-LM cells– are selectively lost in the CA1 field (Cossart et al., 2001). In this model, interneurons in general were hyperactive and thus somatic inhibition was increased; however, due to the loss of dendritically innervating interneurons the dendritic compartment of the pyramidal cells was less inhibited. This may lead to a loss of the network-state dependent regulation of the different excitatory integration-zones in this model of epilepsy.

4.3.3 Inhibition of supralinear excitatory events

Hippocampal principal neurons, apart from dentate granule cells (Krueppel et al., 2011), are optimized to integrate excitatory events supralinearly and generate dendritic spikes (Gasparini et al., 2004; Losonczy and Magee, 2006; Larkum et al., 2009; Remy et al., 2009). The data show that a stepwise increase of the stimulation strength, by application of increasing currents to the micro-iontophoretic pipette, could reliably initiate dendritic spikes in the proximal integration-zone of CA1 pyramidal neurons. Dendritic spikes in the Schaffer collateral integration zone have been described in previous experimental studies (Gasparini et al., 2004; Losonczy and Magee, 2006; Remy et al., 2009). According

to a modeling study (Jarsky et al., 2005) the electrotonically more distant apical tuft dendrites could also possess the ability to generate dendritic spikes. Also experimentally dendritic spikes could be elicited by strong stimulation of excitatory inputs applied to the tuft (Golding et al., 2002; Jarsky et al., 2005). However, it is not yet clear, whether these dendritic spikes were indeed generated in the apical tuft or at more proximal locations (Jarsky et al., 2005). Thus, direct experimental evidence for the generation of fast dendritic spikes in the apical tuft dendrites of the CA1 pyramidal neurons is still lacking. Also, it has to be noted that, $GABA_A$ and $GABA_B$ mediated inhibition was blocked in these earlier studies, potentially facilitating dendritic spike induction. In my experiments dendritic spikes could not be evoked in the perforant path integration-zone. Bearing in mind that in the tuft region tonic inhibition mediated by neurogliaform cells is strong (Fuentealba et al., 2008; Tricoire et al., 2010; Oláh et al., 2009) and tonic inhibition was intact in my experiments (only $GABA_B$ mediated inhibition was blocked), this could explain the failure to elicit dendritic spikes in the perforant path integration-zone.

Dendritic spikes can be observed when excitatory inputs appear spatially clustered and synchronous (Gasparini et al., 2004; Losonczy and Magee, 2006; Remy et al., 2009). The fast component of dendritic spikes has been shown to be mediated by voltage-gated Na^+ channels that strongly depolarize the dendrite and thereby open slower NMDA channels (Lorincz and Nusser, 2010; Losonczy and Magee, 2006). The strength of the dendritic spikes is expressed by the maximum of their temporal derivative ($\Delta V/\Delta t$) reflecting the speed of the depolarization dominated by the fast component. The maxima ($\Delta V/\Delta t$) of iontophoretically evoked dendritic spikes were bimodally distributed, revealing a group of strong and weak dendritic spikes and corresponding dendritic branches. This has been shown previously for dendritic spikes evoked by two-photon uncaging (Losonczy et al., 2008; Remy et al., 2009).

The strength of a dendritic spike, triggered by a specific input cluster is dependent on the properties of the dendritic branch on which these inputs impinge. Voltage-gated potassium channels ($K_V4.2$ A-type channels) play a crucial role in determining the excitability of an individual branch (Hoffman et al., 1997; Frick et al., 2004; Losonczy et al., 2008). These channels open at depolarized membrane potentials and mediate the fast repolarization of the dendrites. This affects dendritic spikes propagating along the dendrite: When the branch possesses a high number of these potassium channels, the dendritic spikes, especially the fast component, is strongly attenuated. Dendritic spikes evoked on these branches can be recognized as weak dendritic spikes, when recording

them in the soma. In branches with low $K_V4.2$ mediated potassium conductance, the dendritic spikes are less affected and can be identified as strong dendritic spikes with a prominent somatic spikelet and a higher maximal $\Delta V/\Delta t$ (fig. 3.15, Losonczy et al., 2008).

Little is known about how dendrites and dendritic spikes are regulated by inhibition (Stuart et al., 2008). The data in this thesis show that pronounced proximal inhibition evoked by sharp-wave stimulation failed to suppress the generation of strong dendritic spikes. This allocates a novel, specialized function to strong dendritic spikes, when comparing them to linearly integrating EPSPs and weak dendritic spikes: During sharp-wave state conditions, only branches generating strong dendritic spikes were able to convert correlated branch input to action potential output. This exclusive processing allowed temporally precise dendritic-spike-to-output coupling via the fast spikelet component. Branches which generated weak dendritic spikes were almost excluded from direct output generation. Also, their supralinear input-output relation in the presence of inhibition was suppressed, indicating a failure of dendritic spike initiation (fig. 3.17A–C).

The experiments revealed that weak dendritic spikes show no significant difference in their latency after stimulus onset compared to strong dendritic spikes (fig. 3.17D). However, the temporal jitter of weak dendritic spikes was significantly higher than that of strong dendritic spikes. This could provide an explanation for weak dendritic spikes being more prominently affected by recurrent inhibition: The later portion of the evoked weak dendritic spikes would face a stronger amount of recurrent inhibition, since it occurs closer to the peak of inhibition. Also strong dendritic spikes could be significantly inhibited when shifted closer to the peak of inhibition. Yet, even in the presence of much stronger inhibition at a latter timepoint, the strong dendritic spikes clearly remained more resistant to recurrent inhibition than weak dendritic spikes (fig. 3.17E).

In neurological diseases the balance of inhibition and excitation can be disturbed: In chronic epilepsy a downregulation of of $K_V4.2$ subunits in CA1 pyramidal neurons has been described (Bernard et al., 2004). This could lead to an increase in strong dendritic spike mediated signaling that has been observed in $K_V4.2$ knock out mice (Andrásfalvy et al., 2008). This disease related difference could result in a reduced control by recurrent inhibition and a less pronounced network-state dependent regulation.

The synchronous and spatially clustered excitatory inputs required for dendritic spike initiation (Gasparini et al., 2004; Losonczy and Magee, 2006; Remy et al., 2009) are thought to be provided by a synchronous and correlated firing of a CA3 neuronal assembly.

In-vivo, these input requirements are likely present during sharp-waves (Buzsáki, 1986; Csicsvari et al., 1999a). In a sharp-wave up to 10 % of presynaptic CA3 neurons are coactivated and excite CA1 pyramidal neurons by simultaneously activating at least several tens of excitatory synapses within a narrow time window of less than 20 ms (Csicsvari et al., 2000). In accordance with this, dendritic spikes have been observed in intra-dendritic recordings, predominantly during sharp-waves (Kamondi et al., 1998). The presented data show that in the presence of recurrent inhibition the strong dendritic spikes, which resisted inhibition, triggered action potentials with a high precision and low temporal jitter.

During hippocampal theta oscillations, which occur during explorative behavior and rapid-eye-movement sleep (O'Keefe and Nadel, 1978), CA1 pyramidal neurons repetitively discharge single or bursts of action potentials at frequencies of 4–12 Hz (Ranck, 1973; Csicsvari et al., 1998). In this thesis it could be shown that this CA1 neuronal activity pattern induced a state of reduced proximal inhibition. In this state, the conversion of Schaffer-collateral input to output is facilitated and strong dendritic spikes, EPSPs, and weak dendritic spikes in concert contribute to action potential output. This heterogeneous contribution of linear and nonlinear events to action potential output also implies that during theta input clustering and synchrony are less stringently required for output generation. Congruently, the data reveal a lower amount of precise and fast spikelet-triggered output. A more asynchronous activation of the Schaffer-collateral input as observed in the sharp-wave state may, in addition, contribute to the lower output precision observed during theta states (Gasparini and Magee, 2006).

It has been hypothesized that the sparse CA1 pyramidal firing during different network-states is a result of a strong inhibitory control of CA1 activity (Thompson and Best, 1989). The results in this study suggest that during theta states the inhibitory control of pyramidal neuron firing is reduced, by which the probability of action potential output is increased. The reduction of proximal inhibition is expected when CA1 pyramidal neurons have a high probability of burst discharge at frequencies from 4–12 Hz. These conditions are met when subsets of CA1 pyramidal neurons exhibit place-field related firing (Ranck, 1973; Thompson and Best, 1989; Csicsvari et al., 1998).

Direct antidromic firing of the CA1 pyramidal cell, from which whole recording were obtained, was unlikely (approximately one in 30–40 recordings). This suggests that only a small group of the whole CA1 pyramidal cell population is fired by the stimulation. Consequently, the assumption can be made that one activated CA1 principle cell assembly

does not inhibit itself but controls another assembly of CA1 pyramidal neurons.

4.3.4 Micro-iontophoresis of glutamate: Methodological considerations

In the present study fast micro-iontophoresis of glutamate was used to elicit excitatory events as described previously for cell culture experiments (Murnick et al., 2002). Due to the fast compensation of the pipette capacitance the glutamate could be applied very precisely. Several synapses could be activated reliably at defined spots without causing photo-damage, as it is regularly observed in long-term experiments with photo-releasable glutamate. In addition, caged glutamate compounds have been shown to block $GABA_A$ receptors (Fino et al., 2009). Therefore, glutamate micro-iontophoresis is especially useful for the experimental investigation of dendritic spike generation. Furthermore, triggering dendritic spikes with glutamate iontophoresis does not require a pharmacological block of inhibition, as it is often required when using focal synaptic stimulation. Thus, this technique is ideally suited to study the interaction of dendritic spikes and inhibition. The evoked dendritic spikes are similar to those elicited by other techniques (fig. 5.1). However, the slow component of iontophoretically and two photon uncaging evoked dendritic spikes may be bigger, compared to synaptically evoked dendritic spikes.

4.3.5 Recurrent inhibition and explorative sharp-waves

The data shown here suggest that in theta states, highly synchronous and clustered glutamatergic branch input excites proximal CA1 dendrites in a state of reduced recurrent inhibition. In this situation the initiation of dendritic spikes would be facilitated *in-vivo*. Does highly synchronous, clustered Schaffer-collateral input actually occur during theta? Exploratory sharp-waves may represent an activity-pattern fulfilling the initiation requirements of dendritic spikes by providing a high input synchrony from CA3 during ongoing theta activity (O'Neill et al., 2006). These exploratory sharp-waves occur at approximately 0.1 Hz either "nested" within or in brief interruptions of theta activity during exploratory and consummatory behavior. Interestingly, exploratory sharp-waves increased background firing while maintaining place-related firing of CA1 neurons (O'Neill et al., 2006). This resulted in a supralinear increase of peak firing rate, exceeding the sum of both firing rates (O'Neill et al., 2006). Due to their supralinear nature and effective output-triggering, dendritic spikes might be well suited to be mechanistically involved in

this supralinear summation of exploratory sharp-waves and place-selective inputs.

4.3.6 Branch strength potentiation and dendritic spike evoked plasticity

The differences between branches that generate weak or strong dendritic spikes is mediated by the properties and density of A-type potassium channels (Hoffman et al., 1997; Losonczy et al., 2008). The composition of these channels has been shown to be regulated in a NMDA receptor dependent manner by the dendritic spikes, when combined with simultaneous action potential generation. This intrinsic dendritic spike dependent potentiation was first described by Losonczy et al. (2008) and is attributed to a down-regulation of the Kv4.2 A-type K^+ conductance. In the present study it is shown that branch strength plasticity endows specific branches and their correlated branch inputs with the potential to generate strong dendritic spikes and to withstand recurrent inhibition. In my experiments a potentiation protocol was used, that allowed to evoke more dendritic spikes than the theta potentiation protocol described by Losonczy et al. (2008). This could partially be responsible for the stronger and faster branch strength potentiation observed in the present study compared to the results observed by Losonczy et al. (2008).

4.3.7 Dendritic spikes and assembly coupling

The high reliability of dendritic spike dependent signaling in both the sharp-wave and the theta-state may play a specific role in hippocampal mnemonic function: Sequential activity of specific CA3-CA1 cell assemblies during the exploratory theta-state is reactivated by sharp-waves during sleep (sleep SWRs, Skaggs and McNaughton, 1996; O'Neill et al., 2008). This reactivation of assembly activity by sharp-waves has been proposed to be critically involved in spatial memory consolidation (Skaggs and McNaughton, 1996; Wilson and McNaughton, 1993; Nakashiba et al., 2009; Girardeau et al., 2009). It has been hypothesized further that strengthening of assembly interconnections is a necessary requirement (O'Neill et al., 2008, 2010) for assembly reactivation. Increasing the reliability of input-output coupling by plasticity of branch strength could provide a cellular mechanism of CA3-CA1 assembly coupling, which is, as shown in this study, independent of the network-state. In this context, the high temporal precision of strong dendritic spike-triggered action potentials may facilitate the sequence preservation of

temporally condensed firing patterns replayed during sharp-waves (Nádasdy et al., 1999; Lee and Wilson, 2002).

Another mechanism by which CA3-CA1 neuronal assemblies could be coupled is synaptic plasticity. Synaptic plasticity can be reliably evoked by brief bursts of synaptic activity in the presence of inhibition (Wigström et al., 1986; Golding et al., 2002; Remy and Spruston, 2007). In dendritic spike-dependent forms of synaptic plasticity, dendritic spikes can serve as associative signals. They provide a more localized postsynaptic depolarization and/or dendritic Ca^{2+} influx than back-propagating action potentials and the repetition in a specific sequence with the EPSP does not appear to be a necessary requirement for plasticity induction (Golding et al., 2002; Remy and Spruston, 2007; Lisman and Spruston, 2010; Wittenberg and Wang, 2006). These properties suggest participation of dendritic-spike dependent synaptic plasticity during brief, solitary events, such as sharp-waves. However, whether dendritic spikes are indeed involved in synaptic plasticity and contribute to assembly connectivity during different network-states *in-vivo*, still remains to be shown.

4.4 Conclusions & open questions

Taken together, the data presented in this thesis reveal that hippocampal network-state dependent regulation by recurrent inhibition controls the input to output coupling of CA1 pyramidal neurons. Brief, solitary bursts of CA1 pyramidal neuron firing, which occurs during the sharp-wave state, and repetitive, theta rhythmic activation differentially utilized the recurrent inhibitory circuitry to modify excitatory input efficacy. This activity-dependent activation of recurrent inhibition is sufficient to control the precision and probability of CA1 action potential firing.

This thesis identified dendritic spikes as specialized signals that are able to withstand recurrent inhibition, and that produce highly precise action potential output. This could promote correlated excitatory input features, representing input from specific cell assemblies. Moreover, the plasticity of dendritic spikes could be identified as a dendritic branch specific mechanism that promotes specific input patterns to be resistive against inhibitory control in different network-states of the hippocampus.

This raises the question, if the input features required for dendritic spikes are actually represented by the activity of distinct presynaptic assemblies *in-vivo*. It has been

proposed that reactivation of assembly firing during sharp-wave sleep that could serve to strengthen connections between coactivated assemblies, requires a plasticity mechanism. It is likely that here dendritic spikes play a crucial role, providing a branch intrinsic plasticity mechanism and by potently inducing synaptic plasticity. Thus, by strengthening coactivated neuronal assemblies during sharp-waves, dendritic spikes could provide an important function for learning and memory. However, this has to be verified in future work using *in-vivo* techniques.

5 Appendix

5.1 Additional methods

5.1.1 Two-photon uncaging

Two-photon glutamate uncaging was performed at basal dendrites of CA1 pyramidal neurons a two-photon microscope equipped with two galvanometer-based scanning systems (Prairie Technologies, Middleton, WI) was used to photorelease MNI-caged-L-glutamate (Biozol, Eching, Germany; 10 or 15 mM applied via a patch pipette above slice) at multiple dendritic spines. Multiphoton photorelease was obtained with an ultrafast, pulsed Titan:sapphire laser (Chameleon Ultra, Coherent) tuned to 725 nm with an uncaging dwell time of 1 ms per spine. For uncaging of multiple spines, the laser focus was rapidly moved from spine to spine with a moving time of ≈ 0.1 ms. The laser power was kept below 8 mW at the slice surface to avoid photodamage (text adapted from Remy et al., 2009 with permission).

5.1.2 Focal synaptic stimulation

To evoke dendritic spikes by local extracellular stimulation, a theta glass pipette was placed near a basal dendrite (40–150 µm from the soma) and a bipolar pulse (biphasic 100–150 ms, 6–65 V, Model 2100, A-M Systems, Sequim, WA) was applied. If no dendritic spike could be detected at 65 V stimulation intensity, the stimulating electrode was moved to a different branch. In some experiments the basal dendrite was visualized briefly before recording using epifluorescence (Zeiss HBO 50, 100 µM Alexa 488 in internal solution). In most experiments the basal dendrite was visualized using DIC optics and a fluorescence image was obtained after the experiment to avoid photodamage (text adapted from Remy et al., 2009 with permission).

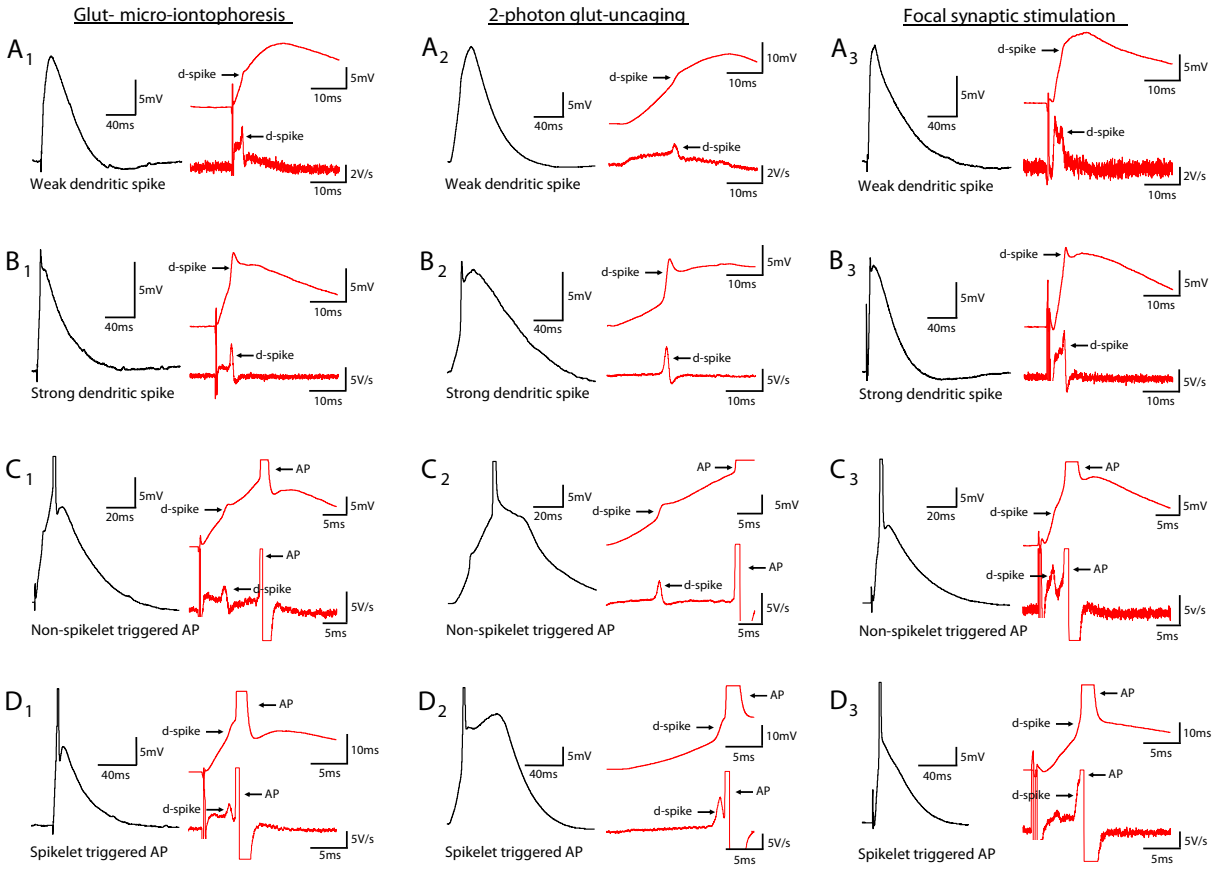

Figure 5.1: Comparison of dendritic spikes evoked by micro-iontophoresis of glutamate, 2-photon-glutamate uncaging, and focal synaptic stimulation. $\mathbf{A_1}$) Weak dendritic-spikes in CA1 pyramidal cells evoked by glutamate iontophoresis, $\mathbf{A_2}$) by 2-photon glutamate uncaging $\mathbf{A_3}$), and by focal synaptic stimulation. Insets (red): Magnification of the voltage-trace and the corresponding $\Delta V/\Delta t$. $\mathbf{B_1}$). Strong dendritic spikes evoked by glutamate iontophoresis, $\mathbf{B_2}$) by 2-photon glutamate uncaging; $\mathbf{B_3}$) and by focal synaptic stimulation. $\mathbf{C_1}$) Non-spikelet triggered AP evoked by glutamate iontophoresis, $\mathbf{C_2}$) by 2-photon glutamate uncaging; $\mathbf{C_3}$) and by focal synaptic stimulation. $\mathbf{D_1}$) Spikelet triggered AP evoked by glutamate iontophoresis, $\mathbf{D_2}$) by 2-photon glutamate uncaging; $\mathbf{D_3}$) and by focal synaptic stimulation. Two-photon and focal synaptic stimulation data was provided by Dr. Stefan Remy.

5.2 Abbrevations

ACSF	artificial cerebrospinal fluid
AMPA	alpha-amino-3-hydroxy-5-methyl-4-isoxazolepropionic acid
AP	action potential
BAPTA	1,2-bis(o-aminophenoxy)ethane-N,N,N',N'-tetraacetic acid
Ca	calcium
CA1	cornu ammonis (Ammon's horn), subregion 1
CA3	cornu ammonis (Ammon's horn), subregion 3
CCD	charged coupled device
CGP	(2S)-3-[[(1S)-1-(3,4-Dichlorophenyl)ethyl] amino-2-hydroxypropyl] (phenylmethyl)phosphinic acid
Cl	chloride
CNS	central nervous system
Δ	delta
DG	dentate gyrus
di-3-ANEPPDHQ	amino-naphthyl-ethenyl-pyridinium dye
d-spike	dendritic spike
EC	entorhinal cortex
EGFP	enhanced green fluorescent protein
EGTA	ethylene glycol tetraacetic acid
EPSP	excitatory postsynaptic potential
eSWR	exploratory sharp-wave ripples
F	fluorescence
GABA	gamma-aminobutyric-acid
$GABA_A$	ionotropic GABA receptor, type A
$GABA_B$	metabotropic GABA receptor, type B
GAD	glutamic decarboxylase
HEPES	4-(2-hydroxyethyl)-1-piperazineethanesulfonic acid
Hz	hertz
IPSP	inhibitory postsynaptic potential
K	potassium
K_V	voltage dependent potassium channel
l	liter
LTP	long term potentiation
M	mol
min	minute
MNI-glutamate	4-methoxy-7-nitroindolinyl-caged L-glutamate
N	sodium
NA	numerical aperture
ns	not significant
s	second
SC	Schaffer-collateral
SD	standard deviation
SEM	standard error of mean

slm	stratum lacunosum moleculare
so	stratum oriens
sp	stratum pyramidale
sr	stratum radiatum
SSt	single stimulus
SWR	sharp-wave ripples
t	time
TBS	tris-buffer salt solution
TSt	theta stimulus
OGB-1	oregon green BAPTA-1
O-LM	oriens lacunosum moleculare
Ω	ohm
p	probability
PB	phosphate buffer
PFA	paraform aldehyde
PP	perforant path
V	voltage
*****	$p<0.05$
******	$p<0.01$
*******	$p<0.001$

6 Contributions

The experiments, in which dendritic spikes were evoked by two-photon uncaging (fig. 5.1A_2, B_2, C_2, D_2) and synaptic stimulation (fig. 5.1A_3, B_3, C_3, D_3) were performed by Dr. Stefan Remy. Special thanks for that.

7 Bibliography

Alger, B. E. and Nicoll, R. A. (1982a). Feed-forward dendritic inhibition in rat hippocampal pyramidal cells studied in vitro. *J Physiol*, 328:105–123.

Alger, B. E. and Nicoll, R. A. (1982b). Pharmacological evidence for two kinds of GABA receptor on rat hippocampal pyramidal cells studied in vitro. *J Physiol*, 328:125–141.

Ali, A. B., Deuchars, J., Pawelzik, H., and Thomson, A. M. (1998). CA1 pyramidal to basket and bistratified cell EPSPs: dual intracellular recordings in rat hippocampal slices. *J Physiol*, 507 (Pt 1):201–217.

Ali, A. B. and Thomson, A. M. (1998). Facilitating pyramid to horizontal oriens-alveus interneurone inputs: Dual intracellular recordings in slices of rat hippocampus. *J Physiol*, 507 (Pt 1):185–199.

Amaral, D. G., Dolorfo, C., and Alvarez-Royo, P. (1991). Organization of ca1 projections to the subiculum: A PHA-L analysis in the rat. *Hippocampus*, 1(4):415–435.

Amaral, D. G., Insausti, R., and Cowan, W. M. (1984). The commissural connections of the monkey hippocampal formation. *J Comp Neurol*, 224(3):307–336.

Amaral, D. G. and Witter, M. P. (1989). The three-dimensional organization of the hippocampal formation: A review of anatomical data. *Neuroscience*, 31(3):571–591.

Anderson, P., Morris, R., Amaral, D., Bliss, T., and O'Keefe, J., editors (2007). *The Hippocampus Book*. Oxford University Press.

Andrade, R., Malenka, R. C., and Nicoll, R. A. (1986). A G protein couples serotonin and $GABA_B$ receptors to the same channels in hippocampus. *Science*, 234(4781):1261–1265.

Andrasfalvy, B. K. and Magee, J. C. (2001). Distance-dependent increase in AMPA receptor number in the dendrites of adult hippocampal CA1 pyramidal neurons. *J Neurosci*, 21(23):9151–9159.

Andrásfalvy, B. K., Makara, J. K., Johnston, D., and Magee, J. C. (2008). Altered synaptic and non-synaptic properties of CA1 pyramidal neurons in Kv4.2 knockout mice. *J Physiol*, 586(16):3881–3892.

Ang, C. W., Carlson, G. C., and Coulter, D. A. (2005). Hippocampal CA1 circuitry dynamically gates direct cortical inputs preferentially at theta frequencies. *J Neurosci*, 25(42):9567–9580.

Antic, S., Major, G., and Zecevic, D. (1999). Fast optical recordings of membrane potential changes from dendrites of pyramidal neurons. *J Neurophysiol*, 82(3):1615–1621.

Ariav, G., Polsky, A., and Schiller, J. (2003). Submillisecond precision of the input-output transformation function mediated by fast sodium dendritic spikes in basal dendrites of CA1 pyramidal neurons. *J Neurosci*, 23(21):7750–7758.

Bartos, M., Vida, I., Frotscher, M., Meyer, A., Monyer, H., Geiger, J. R. P., and Jonas, P. (2002). Fast synaptic inhibition promotes synchronized gamma oscillations in hippocampal interneuron networks. *Proc Natl Acad Sci U S A*, 99(20):13222–13227.

Beck, H. and Yaari, Y. (2008). Plasticity of intrinsic neuronal properties in CNS disorders. *Nat Rev Neurosci*, 9(5):357–369.

Bernard, C., Anderson, A., Becker, A., Poolos, N. P., Beck, H., and Johnston, D. (2004). Acquired dendritic channelopathy in temporal lobe epilepsy. *Science*, 305(5683):532–535.

Blackstad, T. W. (1958). On the termination of some afferents to the hippocampus and fascia dentata; an experimental study in the rat. *Acta Anat (Basel)*, 35(3):202–214.

Bland, B. H., Colom, L. V., Konopacki, J., and Roth, S. H. (1988). Intracellular records of carbachol-induced theta rhythm in hippocampal slices. *Brain Res*, 447(2):364–368.

Bland, B. H., Trepel, C., Oddie, S. D., and Kirk, I. J. (1996). Intraseptal microinfusion of muscimol: Effects on hippocampal formation theta field activity and phasic theta-on cell discharges. *Exp Neurol*, 138(2):286–297.

Bland, S. K. and Bland, B. H. (1986). Medial septal modulation of hippocampal theta cell discharges. *Brain Res*, 375(1):102–116.

Blasco-Ibáñez, J. M. and Freund, T. F. (1995). Synaptic input of horizontal interneurons in stratum oriens of the hippocampal CA1 subfield: Structural basis of feed-back activation. *Eur J Neurosci*, 7(10):2170–2180.

Bliss, T. V. and Gardner-Medwin, A. R. (1973). Long-lasting potentiation of synaptic transmission in the dentate area of the unanaestetized rabbit following stimulation of the perforant path. *J Physiol*, 232(2):357–374.

Bliss, T. V. and Lomo, T. (1973). Long-lasting potentiation of synaptic transmission in the dentate area of the anaesthetized rabbit following stimulation of the perforant path. *J Physiol*, 232(2):331–356.

Bormann, J. (1988). Electrophysiology of gabaa and gabab receptor subtypes. *Trends Neurosci*, 11(3):112–116.

Brun, V. H., Otnass, M. K., Molden, S., Steffenach, H.-A., Witter, M. P., Moser, M.-B., and Moser, E. I. (2002). Place cells and place recognition maintained by direct entorhinal-hippocampal circuitry. *Science*, 296(5576):2243–2246.

Bruton, C. J. (1988). *The neuropathology of temporal lobe epilepsy*. Oxford University Press.

Buhl, E. H., Halasy, K., and Somogyi, P. (1994). Diverse sources of hippocampal unitary inhibitory postsynaptic potentials and the number of synaptic release sites. *Nature*, 368(6474):823–828.

Buzsáki, G. (1984). Feed-forward inhibition in the hippocampal formation. *Prog Neurobiol*, 22(2):131–153.

Buzsáki, G. (1986). Hippocampal sharp waves: their origin and significance. *Brain Res*, 398(2):242–252.

Buzsáki, G. (1989). Two-stage model of memory trace formation: A role for "noisy" brain states. *Neuroscience*, 31(3):551–570.

Buzsáki, G. (2002). Theta oscillations in the hippocampus. *Neuron*, 33(3):325–340.

Buzsáki, G., Horváth, Z., Urioste, R., Hetke, J., and Wise, K. (1992). High-frequency network oscillation in the hippocampus. *Science*, 256(5059):1025–1027.

Buzsáki, G., Leung, L. W., and Vanderwolf, C. H. (1983). Cellular bases of hippocampal EEG in the behaving rat. *Brain Res*, 287(2):139–171.

Carlson, G. C. and Coulter, D. A. (2008). In vitro functional imaging in brain slices using fast voltage-sensitive dye imaging combined with whole-cell patch recording. *Nat Protoc*, 3(2):249–255.

Chrobak, J. J. and Buzsáki, G. (1996). High-frequency oscillations in the output networks of the hippocampal-entorhinal axis of the freely behaving rat. *J Neurosci*, 16(9):3056–3066.

Cobb, S. R., Buhl, E. H., Halasy, K., Paulsen, O., and Somogyi, P. (1995). Synchronization of neuronal activity in hippocampus by individual GABAergic interneurons. *Nature*, 378(6552):75–78.

Cossart, R., Dinocourt, C., Hirsch, J. C., Merchan-Perez, A., Felipe, J. D., Ben-Ari, Y., Esclapez, M., and Bernard, C. (2001). Dendritic but not somatic GABAergic inhibition is decreased in experimental epilepsy. *Nat Neurosci*, 4(1):52–62.

Csicsvari, J., Hirase, H., Czurkó, A., Mamiya, A., and Buzsáki, G. (1999a). Fast network oscillations in the hippocampal CA1 region of the behaving rat. *J Neurosci*, 19(16):RC20.

Csicsvari, J., Hirase, H., Czurkó, A., Mamiya, A., and Buzsáki, G. (1999b). Oscillatory coupling of hippocampal pyramidal cells and interneurons in the behaving rat. *J Neurosci*, 19(1):274–287.

Csicsvari, J., Hirase, H., Czurko, A., and Buzsáki, G. (1998). Reliability and state dependence of pyramidal cell-interneuron synapses in the hippocampus: An ensemble approach in the behaving rat. *Neuron*, 21(1):179–189.

Csicsvari, J., Hirase, H., Mamiya, A., and Buzsáki, G. (2000). Ensemble patterns of hippocampal CA3-CA1 neurons during sharp wave-associated population events. *Neuron*, 28(2):585–594.

de Lanerolle, N. C., Kim, J. H., Robbins, R. J., and Spencer, D. D. (1989). Hippocampal interneuron loss and plasticity in human temporal lobe epilepsy. *Brain Res*, 495(2):387–395.

der Weel, M. J. D.-V., da Silva, F. H. L., and Witter, M. P. (1997). Nucleus reuniens thalami modulates activity in hippocampal field CA1 through excitatory and inhibitory mechanisms. *J Neurosci*, 17(14):5640–5650.

der Weel, M. J. D.-V. and Witter, M. P. (1996). Projections from the nucleus reuniens thalami to the entorhinal cortex, hippocampal field CA1, and the subiculum in the rat arise from different populations of neurons. *J Comp Neurol*, 364(4):637–650.

Dutar, P. and Nicoll, R. A. (1988). A physiological role for $GABA_B$ receptors in the central nervous system. *Nature*, 332(6160):156–158.

Ego-Stengel, V. and Wilson, M. A. (2010). Disruption of ripple-associated hippocampal activity during rest impairs spatial learning in the rat. *Hippocampus*, 20(1):1–10.

Farrant, M. and Nusser, Z. (2005). Variations on an inhibitory theme: Phasic and tonic activation of $GABA_A$ receptors. *Nat Rev Neurosci*, 6(3):215–229.

Feng, L., Molnár, P., and Nadler, J. V. (2003). Short-term frequency-dependent plasticity at recurrent mossy fiber synapses of the epileptic brain. *J Neurosci*, 23(12):5381–5390.

Fino, E., Araya, R., Peterka, D. S., Salierno, M., Etchenique, R., and Yuste, R. (2009). RuBi-glutamate: Two-photon and visible-light photoactivation of neurons and dendritic spines. *Front Neural Circuits*, 3:2.

Freund, T. F. and Antal, M. (1988). GABA-containing neurons in the septum control inhibitory interneurons in the hippocampus. *Nature*, 336(6195):170–173.

Freund, T. F. and Buzsáki, G. (1996). Interneurons of the hippocampus. *Hippocampus*, 6(4):347–470.

Frey, U., Huang, Y. Y., and Kandel, E. R. (1993). Effects of camp simulate a late stage of ltp in hippocampal ca1 neurons. *Science*, 260(5114):1661–1664.

Frick, A., Magee, J., and Johnston, D. (2004). LTP is accompanied by an enhanced local excitability of pyramidal neuron dendrites. *Nat Neurosci*, 7(2):126–135.

Frotscher, M., Léránth, C., Lübbers, K., and Oertel, W. H. (1984). Commissural afferents innervate glutamate decarboxylase immunoreactive non-pyramidal neurons in the guinea pig hippocampus. *Neurosci Lett*, 46(2):137–143.

Fuentealba, P., Begum, R., Capogna, M., Jinno, S., Márton, L. F., Csicsvari, J., Thomson, A., Somogyi, P., and Klausberger, T. (2008). Ivy cells: A population of nitric-oxide-producing, slow-spiking GABAergic neurons and their involvement in hippocampal network activity. *Neuron*, 57(6):917–929.

Gasparini, S. and Magee, J. C. (2006). State-dependent dendritic computation in hippocampal CA1 pyramidal neurons. *J Neurosci*, 26(7):2088–2100.

Gasparini, S., Migliore, M., and Magee, J. C. (2004). On the initiation and propagation of dendritic spikes in CA1 pyramidal neurons. *J Neurosci*, 24(49):11046–11056.

Gillessen, T. and Alzheimer, C. (1997). Amplification of EPSPs by low Ni^{2+}- and amiloride-sensitive Ca^{2+} channels in apical dendrites of rat CA1 pyramidal neurons. *J Neurophysiol*, 77(3):1639–1643.

Girardeau, G., Benchenane, K., Wiener, S. I., Buzsáki, G., and Zugaro, M. B. (2009). Selective suppression of hippocampal ripples impairs spatial memory. *Nat Neurosci*, 12(10):1222–1223.

Golding, N. L., Jung, H. Y., Mickus, T., and Spruston, N. (1999). Dendritic calcium spike initiation and repolarization are controlled by distinct potassium channel subtypes in CA1 pyramidal neurons. *J Neurosci*, 19(20):8789–8798.

Golding, N. L., Mickus, T. J., Katz, Y., Kath, W. L., and Spruston, N. (2005). Factors mediating powerful voltage attenuation along CA1 pyramidal neuron dendrites. *J Physiol*, 568(Pt 1):69–82.

Golding, N. L. and Spruston, N. (1998). Dendritic sodium spikes are variable triggers of axonal action potentials in hippocampal CA1 pyramidal neurons. *Neuron*, 21(5):1189–1200.

Golding, N. L., Staff, N. P., and Spruston, N. (2002). Dendritic spikes as a mechanism for cooperative long-term potentiation. *Nature*, 418(6895):326–331.

Gottlieb, D. I. and Cowan, W. M. (1973). Autoradiographic studies of the commissural and ipsilateral association connection of the hippocampus and detentate gyrus of the rat. I. the commissural connections. *J Comp Neurol*, 149(4):393–422.

Gulledge, A. T. and Stuart, G. J. (2003). Excitatory actions of gaba in the cortex. *Neuron*, 37(2):299–309.

Hasselmo, M. E. (2005). The role of hippocampal regions CA3 and CA1 in matching entorhinal input with retrieval of associations between objects and context: Theoretical comment on lee et al. *Behav Neurosci*, 119(1):342–345.

Helmchen, F., Svoboda, K., Denk, W., and Tank, D. W. (1999). In vivo dendritic calcium dynamics in deep-layer cortical pyramidal neurons. *Nat Neurosci*, 2(11):989–996.

Henze, D. A., Urban, N. N., and Barrionuevo, G. (2000). The multifarious hippocampal mossy fiber pathway: A review. *Neuroscience*, 98(3):407–427.

Hestrin, S., Perkel, D. J., Sah, P., Manabe, T., Renner, P., and Nicoll, R. A. (1990). Physiological properties of excitatory synaptic transmission in the central nervous system. *Cold Spring Harb Symp Quant Biol*, 55:87–93.

Higley, M. J. and Sabatini, B. L. (2008). Calcium signaling in dendrites and spines: Practical and functional considerations. *Neuron*, 59(6):902–913.

Hirase, H., Leinekugel, X., Czurkó, A., Csicsvari, J., and Buzsáki, G. (2001). Firing rates of hippocampal neurons are preserved during subsequent sleep episodes and modified by novel awake experience. *Proc Natl Acad Sci U S A*, 98(16):9386–9390.

Hoffman, D. A., Magee, J. C., Colbert, C. M., and Johnston, D. (1997). K^+ channel regulation of signal propagation in dendrites of hippocampal pyramidal neurons. *Nature*, 387(6636):869–875.

Houser, C. R. and Esclapez, M. (1996). Vulnerability and plasticity of the GABA system in the pilocarpine model of spontaneous recurrent seizures. *Epilepsy Res*, 26(1):207–218.

Hu, H., Vervaeke, K., and Storm, J. F. (2002). Two forms of electrical resonance at theta frequencies, generated by M-current, h-current and persistent Na^+ current in rat hippocampal pyramidal cells. *J Physiol*, 545(Pt 3):783–805.

Häusser, M., Major, G., and Stuart, G. J. (2001). Differential shunting of EPSPs by action potentials. *Science*, 291(5501):138–141.

Hyman, J. M., Zilli, E. A., Paley, A. M., and Hasselmo, M. E. (2005). Medial prefrontal cortex cells show dynamic modulation with the hippocampal theta rhythm dependent on behavior. *Hippocampus*, 15(6):739–749.

Jarsky, T., Roxin, A., Kath, W. L., and Spruston, N. (2005). Conditional dendritic spike propagation following distal synaptic activation of hippocampal CA1 pyramidal neurons. *Nat Neurosci*, 8(12):1667–1676.

Jensen, O. and Lisman, J. E. (2000). Position reconstruction from an ensemble of hippocampal place cells: Contribution of theta phase coding. *J Neurophysiol*, 83(5):2602–2609.

Johnston, D., Magee, J. C., Colbert, C. M., and Cristie, B. R. (1996). Active properties of neuronal dendrites. *Annu Rev Neurosci*, 19:165–186.

Jonas, P. (1993). AMPA-type glutamate receptors–nonselective cation channels mediating fast excitatory transmission in the CNS. *EXS*, 66:61–76.

Jones, M. W. and Wilson, M. A. (2005). Theta rhythms coordinate hippocampal-prefrontal interactions in a spatial memory task. *PLoS Biol*, 3(12):e402.

Jung, M. W. and McNaughton, B. L. (1993). Spatial selectivity of unit activity in the hippocampal granular layer. *Hippocampus*, 3(2):165–182.

Jung, R. and Kornmueller, A. (1938). Eine Methodik der Ableitung lokalisierter Potentialschwankungen aus subcorticalen Hirngebieten. *Arch Psychiatry*, 109:1–30.

Kaila, K. (1994). Ionic basis of $GABA_A$ receptor channel function in the nervous system. *Prog Neurobiol*, 42(4):489–537.

Kamondi, A., Acsády, L., and Buzsáki, G. (1998). Dendritic spikes are enhanced by cooperative network activity in the intact hippocampus. *J Neurosci*, 18(10):3919–3928.

Kemppainen, S., Jolkkonen, E., and Pitkänen, A. (2002). Projections from the posterior cortical nucleus of the amygdala to the hippocampal formation and parahippocampal region in rat. *Hippocampus*, 12(6):735–755.

Klausberger, T., Magill, P. J., Márton, L. F., Roberts, J. D. B., Cobden, P. M., Buzsáki, G., and Somogyi, P. (2003). Brain-state- and cell-type-specific firing of hippocampal interneurons in vivo. *Nature*, 421(6925):844–848.

Klausberger, T., Márton, L. F., Baude, A., Roberts, J. D. B., Magill, P. J., and Somogyi, P. (2004). Spike timing of dendrite-targeting bistratified cells during hippocampal network oscillations in vivo. *Nat Neurosci*, 7(1):41–47.

König, P., Engel, A. K., and Singer, W. (1996). Integrator or coincidence detector? The role of the cortical neuron revisited. *Trends Neurosci*, 19(4):130–137.

Knight, R. (1996). Contribution of human hippocampal region to novelty detection. *Nature*, 383(6597):256–259.

Knowles, W. D. and Schwartzkroin, P. A. (1981). Axonal ramifications of hippocampal CA1 pyramidal cells. *J Neurosci*, 1(11):1236–1241.

Koch, C. (1999). *Biophysics of computation: Information processing in single neurons*. Oxford University Press.

Koch, C., Poggio, T., and Torre, V. (1983). Nonlinear interactions in a dendritic tree: Localization, timing, and role in information processing. *Proc Natl Acad Sci U S A*, 80(9):2799–2802.

Krettek, J. E. and Price, J. L. (1977). Projections from the amygdaloid complex and adjacent olfactory structures to the entorhinal cortex and to the subiculum in the rat and cat. *J Comp Neurol*, 172(4):723–752.

Krueppel, R., Remy, S., and Beck, H. (2011). Dendritic integration in hippocampal dentate granule cells. *Neuron*, 71(3):512–528.

Kudrimoti, H. S., Barnes, C. A., and McNaughton, B. L. (1999). Reactivation of hippocampal cell assemblies: effects of behavioral state, experience, and EEG dynamics. *J Neurosci*, 19(10):4090–4101.

Kumaran, D. and Maguire, E. A. (2007). Which computational mechanisms operate in the hippocampus during novelty detection? *Hippocampus*, 17(9):735–748.

Lacaille, J. C., Mueller, A. L., Kunkel, D. D., and Schwartzkroin, P. A. (1987). Local circuit interactions between oriens/alveus interneurons and CA1 pyramidal cells in hippocampal slices: Electrophysiology and morphology. *J Neurosci*, 7(7):1979–1993.

Larkum, M. E., Kaiser, K. M., and Sakmann, B. (1999). Calcium electrogenesis in distal apical dendrites of layer 5 pyramidal cells at a critical frequency of back-propagating action potentials. *Proc Natl Acad Sci U S A*, 96(25):14600–14604.

Larkum, M. E., Nevian, T., Sandler, M., Polsky, A., and Schiller, J. (2009). Synaptic integration in tuft dendrites of layer 5 pyramidal neurons: A new unifying principle. *Science*, 325(5941):756–760.

Lawson, V. H. and Bland, B. H. (1993). The role of the septohippocampal pathway in the regulation of hippocampal field activity and behavior: Analysis by the intraseptal microinfusion of carbachol, atropine, and procaine. *Exp Neurol*, 120(1):132–144.

Lee, A. K. and Wilson, M. A. (2002). Memory of sequential experience in the hippocampus during slow wave sleep. *Neuron*, 36(6):1183–1194.

Lee, I., Hunsaker, M. R., and Kesner, R. P. (2005). The role of hippocampal subregions in detecting spatial novelty. *Behav Neurosci*, 119(1):145–153.

Leung, L. S. and Yu, H. W. (1998). Theta-frequency resonance in hippocampal CA1 neurons in vitro demonstrated by sinusoidal current injection. *J Neurophysiol*, 79(3):1592–1596.

Leung, L. W. and Yim, C. Y. (1991). Intrinsic membrane potential oscillations in hippocampal neurons in vitro. *Brain Res*, 553(2):261–274.

Leutgeb, S., Leutgeb, J. K., Treves, A., Moser, M.-B., and Moser, E. I. (2004). Distinct ensemble codes in hippocampal areas CA3 and CA1. *Science*, 305(5688):1295–1298.

Lipowsky, R., Gillessen, T., and Alzheimer, C. (1996). Dendritic Na^+ channels amplify EPSPs in hippocampal CA1 pyramidal cells. *J Neurophysiol*, 76(4):2181–2191.

Lisman, J. and Spruston, N. (2010). Questions about STDP as a general model of synaptic plasticity. *Front Synaptic Neurosci*, 2:140.

Lorincz, A. and Nusser, Z. (2010). Molecular identity of dendritic voltage-gated sodium channels. *Science*, 328(5980):906–909.

Losonczy, A. and Magee, J. C. (2006). Integrative properties of radial oblique dendrites in hippocampal CA1 pyramidal neurons. *Neuron*, 50(2):291–307.

Losonczy, A., Makara, J. K., and Magee, J. C. (2008). Compartmentalized dendritic plasticity and input feature storage in neurons. *Nature*, 452(7186):436–441.

Maccaferri, G. and McBain, C. J. (1995). Passive propagation of LTD to stratum oriens-alveus inhibitory neurons modulates the temporoammonic input to the hippocampal CA1 region. *Neuron*, 15(1):137–145.

Magee, J. C. (1998). Dendritic hyperpolarization-activated currents modify the integrative properties of hippocampal CA1 pyramidal neurons. *J Neurosci*, 18(19):7613–7624.

Magee, J. C. (2000). Dendritic integration of excitatory synaptic input. *Nat Rev Neurosci*, 1(3):181–190.

Magee, J. C. and Cook, E. P. (2000). Somatic EPSP amplitude is independent of synapse location in hippocampal pyramidal neurons. *Nat Neurosci*, 3(9):895–903.

Maguire, E. A., Gadian, D. G., Johnsrude, I. S., Good, C. D., Ashburner, J., Frackowiak, R. S., and Frith, C. D. (2000). Navigation-related structural change in the hippocampi of taxi drivers. *Proc Natl Acad Sci U S A*, 97(8):4398–4403.

Mainen, Z. F., Malinow, R., and Svoboda, K. (1999). Synaptic calcium transients in single spines indicate that nmda receptors are not saturated. *Nature*, 399(6732):151–155.

Makara, J. K., Losonczy, A., Wen, Q., and Magee, J. C. (2009). Experience-dependent compartmentalized dendritic plasticity in rat hippocampal CA1 pyramidal neurons. *Nat Neurosci*, 12(12):1485–1487.

Malenka, R. C., Kauer, J. A., Zucker, R. S., and Nicoll, R. A. (1988). Postsynaptic calcium is sufficient for potentiation of hippocampal synaptic transmission. *Science*, 242(4875):81–84.

Manns, J. R. and Eichenbaum, H. (2006). Evolution of declarative memory. *Hippocampus*, 16(9):795–808.

Martina, M., Vida, I., and Jonas, P. (2000). Distal initiation and active propagation of action potentials in interneuron dendrites. *Science*, 287(5451):295–300.

McBain, C. J. and Fisahn, A. (2001). Interneurons unbound. *Nat Rev Neurosci*, 2(1):11–23.

McNaughton, B. L., Barnes, C. A., Rao, G., Baldwin, J., and Rasmussen, M. (1986). Long-term enhancement of hippocampal synaptic transmission and the acquisition of spatial information. *J Neurosci*, 6(2):563–571.

Megías, M., Emri, Z., Freund, T. F., and Gulyás, A. I. (2001). Total number and distribution of inhibitory and excitatory synapses on hippocampal CA1 pyramidal cells. *Neuroscience*, 102(3):527–540.

Migliore, M. and Shepherd, G. M. (2002). Emerging rules for the distributions of active dendritic conductances. *Nat Rev Neurosci*, 3(5):362–370.

Miles, R. (1990). Synaptic excitation of inhibitory cells by single CA3 hippocampal pyramidal cells of the guinea-pig in vitro. *J Physiol*, 428:61–77.

Miles, R., Tóth, K., Gulyás, A. I., Hájos, N., and Freund, T. F. (1996). Differences between somatic and dendritic inhibition in the hippocampus. *Neuron*, 16(4):815–823.

Miles, R., Wong, R. K., and Traub, R. D. (1984). Synchronized afterdischarges in the hippocampus: Contribution of local synaptic interactions. *Neuroscience*, 12(4):1179–1189.

Misgeld, U., Bijak, M., and Jarolimek, W. (1995). A physiological role for $GABA_B$ receptors and the effects of baclofen in the mammalian central nervous system. *Prog Neurobiol*, 46(4):423–462.

Morin, F., Beaulieu, C., and Lacaille, J. C. (1998). Selective loss of GABA neurons in area CA1 of the rat hippocampus after intraventricular kainate. *Epilepsy Res*, 32(3):363–369.

Morris, R. G., Davis, S., and Butcher, S. P. (1990). Hippocampal synaptic plasticity and NMDA receptors: A role in information storage? *Philos Trans R Soc Lond B Biol Sci*, 329(1253):187–204.

Morris, R. G., Garrud, P., Rawlins, J. N., and O'Keefe, J. (1982). Place navigation impaired in rats with hippocampal lesions. *Nature*, 297(5868):681–683.

Murnick, J. G., Dubé, G., Krupa, B., and Liu, G. (2002). High-resolution iontophoresis for single-synapse stimulation. *J Neurosci Methods*, 116(1):65–75.

Nakashiba, T., Buhl, D. L., McHugh, T. J., and Tonegawa, S. (2009). Hippocampal CA3 output is crucial for ripple-associated reactivation and consolidation of memory. *Neuron*, 62(6):781–787.

Nádasdy, Z., Hirase, H., Czurkó, A., Csicsvari, J., and Buzsáki, G. (1999). Replay and time compression of recurring spike sequences in the hippocampus. *J Neurosci*, 19(21):9497–9507.

Neves, G., Cooke, S. F., and Bliss, T. V. P. (2008). Synaptic plasticity, memory and the hippocampus: A neural network approach to causality. *Nat Rev Neurosci*, 9(1):65–75.

Newberry, N. R. and Nicoll, R. A. (1984). A bicuculline-resistant inhibitory post-synaptic potential in rat hippocampal pyramidal cells in vitro. *J Physiol*, 348:239–254.

Nicholson, D. A., Trana, R., Katz, Y., Kath, W. L., Spruston, N., and Geinisman, Y. (2006). Distance-dependent differences in synapse number and AMPA receptor expression in hippocampal CA1 pyramidal neurons. *Neuron*, 50(3):431–442.

Nitz, D. and McNaughton, B. (2004). Differential modulation of CA1 and dentate gyrus interneurons during exploration of novel environments. *J Neurophysiol*, 91(2):863–872.

Nurse, S. and Lacaille, J. C. (1997). Do $GABA_A$ and $GABA_B$ inhibitory postsynaptic responses originate from distinct interneurons in the hippocampus? *Can J Physiol Pharmacol*, 75(5):520–525.

Okazaki, M. M., Molnár, P., and Nadler, J. V. (1999). Recurrent mossy fiber pathway in rat dentate gyrus: Synaptic currents evoked in presence and absence of seizure-induced growth. *J Neurophysiol*, 81(4):1645–1660.

O'Keefe, J. (1976). Place units in the hippocampus of the freely moving rat. *Exp Neurol*, 51(1):78–109.

O'Keefe, J. and Dostrovsky, J. (1971). The hippocampus as a spatial map. Preliminary evidence from unit activity in the freely-moving rat. *Brain Res*, 34(1):171–175.

O'Keefe, J. and Nadel, L. (1978). *The Hippocampus as a Cognitive Map*. Oxford University Press.

Oláh, S., Füle, M., Komlósi, G., Varga, C., Báldi, R., Barzó, P., and Tamás, G. (2009). Regulation of cortical microcircuits by unitary GABA-mediated volume transmission. *Nature*, 461(7268):1278–1281.

O'Neill, J., Pleydell-Bouverie, B., Dupret, D., and Csicsvari, J. (2010). Play it again: Reactivation of waking experience and memory. *Trends Neurosci*, 33(5):220–229.

O'Neill, J., Senior, T., and Csicsvari, J. (2006). Place-selective firing of CA1 pyramidal cells during sharp wave/ripple network patterns in exploratory behavior. *Neuron*, 49(1):143–155.

O'Neill, J., Senior, T. J., Allen, K., Huxter, J. R., and Csicsvari, J. (2008). Reactivation of experience-dependent cell assembly patterns in the hippocampus. *Nat Neurosci*, 11(2):209–215.

Otmakhova, N. A., Lewey, J., Asrican, B., and Lisman, J. E. (2005). Inhibition of perforant path input to the CA1 region by serotonin and noradrenaline. *J Neurophysiol*, 94(2):1413–1422.

Otmakhova, N. A. and Lisman, J. E. (1999). Dopamine selectively inhibits the direct cortical pathway to the CA1 hippocampal region. *J Neurosci*, 19(4):1437–1445.

Otmakhova, N. A. and Lisman, J. E. (2000). Dopamine, serotonin, and noradrenaline strongly inhibit the direct perforant path-CA1 synaptic input, but have little effect on the Schaffer collateral input. *Ann N Y Acad Sci*, 911:462–464.

Otmakhova, N. A., Otmakhov, N., and Lisman, J. E. (2002). Pathway-specific properties of AMPA and NMDA-mediated transmission in CA1 hippocampal pyramidal cells. *J Neurosci*, 22(4):1199–1207.

Paré, D. and Gaudreau, H. (1996). Projection cells and interneurons of the lateral and basolateral amygdala: Distinct firing patterns and differential relation to theta and delta rhythms in conscious cats. *J Neurosci*, 16(10):3334–3350.

Pasquier, D. A. and Reinoso-Suarez, F. (1978). The topographic organization of hypothalamic and brain stem projections to the hippocampus. *Brain Res Bull*, 3(4):373–389.

Pearce, R. A. (1993). Physiological evidence for two distinct $GABA_A$ responses in rat hippocampus. *Neuron*, 10(2):189–200.

Penttonen, M. and Buzsáki, G. (2003). Natural logarithmic relationship between brain oscillators. *Thalamus and related systems*, 2:145–152.

Peters, H. C., Hu, H., Pongs, O., Storm, J. F., and Isbrandt, D. (2005). Conditional transgenic suppression of M channels in mouse brain reveals functions in neuronal excitability, resonance and behavior. *Nat Neurosci*, 8(1):51–60.

Poirazi, P. and Mel, B. W. (2001). Impact of active dendrites and structural plasticity on the memory capacity of neural tissue. *Neuron*, 29(3):779–796.

Pouille, F., Marin-Burgin, A., Adesnik, H., Atallah, B. V., and Scanziani, M. (2009). Input normalization by global feedforward inhibition expands cortical dynamic range. *Nat Neurosci*, 12(12):1577–1585.

Pouille, F. and Scanziani, M. (2001). Enforcement of temporal fidelity in pyramidal cells by somatic feed-forward inhibition. *Science*, 293(5532):1159–1163.

Pouille, F. and Scanziani, M. (2004). Routing of spike series by dynamic circuits in the hippocampus. *Nature*, 429(6993):717–723.

Price, C. J., Cauli, B., Kovacs, E. R., Kulik, A., Lambolez, B., Shigemoto, R., and Capogna, M. (2005). Neurogliaform neurons form a novel inhibitory network in the hippocampal CA1 area. *J Neurosci*, 25(29):6775–6786.

Pyapali, G. K., Sik, A., Penttonen, M., Buzsaki, G., and Turner, D. A. (1998). Dendritic properties of hippocampal CA1 pyramidal neurons in the rat: intracellular staining in vivo and in vitro. *J Comp Neurol*, 391(3):335–352.

Raisman, G., Cowan, W. M., and T.B.S., P. (1965). The extrinsic afferent, commissural and association fibres of the hippocampus. *Brain*, 88:963–997.

Rall, W. (1967). Distinguishing theoretical synaptic potentials computed for different soma-dendritic distributions of synaptic input. *J Neurophysiol*, 30(5):1138–1168.

Rall, W. and Rinzel, J. (1973). Branch input resistance and steady attenuation for input to one branch of a dendritic neuron model. *Biophys J*, 13(7):648–687.

Ramón y Cajal, S. (1911). *Histologie du système nerveux de l'homme et des vertébrés*. Paris: A. Maloine. Reprinted (1955) Madrid: Instituto Ramon y Cajal.

Ranck, J. B. (1973). Studies on single neurons in dorsal hippocampal formation and septum in unrestrained rats. I. Behavioral correlates and firing repertoires. *Exp Neurol*, 41(2):461–531.

Rancz, E. A. and Häusser, M. (2006). Dendritic calcium spikes are tunable triggers of cannabinoid release and short-term synaptic plasticity in cerebellar purkinje neurons. *J Neurosci*, 26(20):5428–5437.

Remondes, M. and Schuman, E. M. (2004). Role for a cortical input to hippocampal area CA1 in the consolidation of a long-term memory. *Nature*, 431(7009):699–703.

Remy, S., Csicsvari, J., and Beck, H. (2009). Activity-dependent control of neuronal output by local and global dendritic spike attenuation. *Neuron*, 61(6):906–916.

Remy, S. and Spruston, N. (2007). Dendritic spikes induce single-burst long-term potentiation. *Proc Natl Acad Sci U S A*, 104(43):17192–17197.

Rivas, J., Gaztelu, J. M., and Garcia-Austt, E. (1996). Changes in hippocampal cell discharge patterns and theta rhythm spectral properties as a function of walking velocity in the guinea pig. *Exp Brain Res*, 108(1):113–118.

Robbins, R. J., Brines, M. L., Kim, J. H., Adrian, T., de Lanerolle, N., Welsh, S., and Spencer, D. D. (1991). A selective loss of somatostatin in the hippocampus of patients with temporal lobe epilepsy. *Ann Neurol*, 29(3):325–332.

Sabatini, B. L., Maravall, M., and Svoboda, K. (2001). Ca^{2+} signaling in dendritic spines. *Curr Opin Neurobiol*, 11(3):349–356.

Sainsbury, R. S., Harris, J. L., and Rowland, G. L. (1987a). Sensitization and hippocampal type 2 theta in the rat. *Physiol Behav*, 41(5):489–493.

Sainsbury, R. S., Heynen, A., and Montoya, C. P. (1987b). Behavioral correlates of hippocampal type 2 theta in the rat. *Physiol Behav*, 39(4):513–519.

Sander, J. W. and Shorvon, S. D. (1996). Epidemiology of the epilepsies. *J Neurol Neurosurg Psychiatry*, 61(5):433–443.

Schaffer, K. (1892). Beitrag zur Histologie der Ammon's horn formation. *Archiv für Mikroskopische Anatomie*, 39:611–632.

Schiller, J., Major, G., Koester, H. J., and Schiller, Y. (2000). NMDA spikes in basal dendrites of cortical pyramidal neurons. *Nature*, 404(6775):285–289.

Schiller, J., Schiller, Y., Stuart, G., and Sakmann, B. (1997). Calcium action potentials restricted to distal apical dendrites of rat neocortical pyramidal neurons. *J Physiol*, 505 (Pt 3):605–616.

Scoville, W. B. and Milner, B. (1957). Loss of recent memory after bilateral hippocampal lesions. *J Neurol Neurosurg Psychiatry*, 20(1):11–21.

Seidenbecher, T., Laxmi, T. R., Stork, O., and Pape, H.-C. (2003). Amygdalar and hippocampal theta rhythm synchronization during fear memory retrieval. *Science*, 301(5634):846–850.

Siapas, A. G., Lubenov, E. V., and Wilson, M. A. (2005). Prefrontal phase locking to hippocampal theta oscillations. *Neuron*, 46(1):141–151.

Skaggs, W. E. and McNaughton, B. L. (1996). Replay of neuronal firing sequences in rat hippocampus during sleep following spatial experience. *Science*, 271(5257):1870–1873.

Slawinska, U. and Kasicki, S. (1998). The frequency of rat's hippocampal theta rhythm is related to the speed of locomotion. *Brain Res*, 796(1-2):327–331.

Sloviter, R. S. (1987). Decreased hippocampal inhibition and a selective loss of interneurons in experimental epilepsy. *Science*, 235(4784):73–76.

Softky, W. (1994). Sub-millisecond coincidence detection in active dendritic trees. *Neuroscience*, 58(1):13–41.

Somogyi, P. and Klausberger, T. (2005). Defined types of cortical interneurone structure space and spike timing in the hippocampus. *J Physiol*, 562(Pt 1):9–26.

Spencer, W. A. and Kandel, E. R. (1961). Electrophysiology of hippocampal neurons IV. fast prepotentials. *Journal of Neurophysiology*, 24:272–285.

Spruston, N. (2008). Pyramidal neurons: Dendritic structure and synaptic integration. *Nat Rev Neurosci*, 9(3):206–221.

Spruston, N. and Johnston, D. (1992). Perforated patch-clamp analysis of the passive membrane properties of three classes of hippocampal neurons. *J Neurophysiol*, 67(3):508–529.

Spruston, N., Schiller, Y., Stuart, G., and Sakmann, B. (1995). Activity-dependent action potential invasion and calcium influx into hippocampal CA1 dendrites. *Science*, 268(5208):297–300.

Staley, K. J. and Mody, I. (1992). Shunting of excitatory input to dentate gyrus granule cells by a depolarizing gabaa receptor-mediated postsynaptic conductance. *J Neurophysiol*, 68(1):197–212.

Steward, O. (1976). Topographic organization of the projections from the entorhinal area to the hippocampal formation of the rat. *J Comp Neurol*, 167(3):285–314.

Stokes, C. C. A. and Isaacson, J. S. (2010). From dendrite to soma: Dynamic routing of inhibition by complementary interneuron microcircuits in olfactory cortex. *Neuron*, 67(3):452–465.

Stuart, G., Schiller, J., and Sakmann, B. (1997). Action potential initiation and propagation in rat neocortical pyramidal neurons. *J Physiol*, 505 (Pt 3):617–632.

Stuart, G., Spruston, N., and Häusser, M., editors (2008). *Dendrites*. Oxford University Press.

Stuart, G. J. and Häusser, M. (2001). Dendritic coincidence detection of EPSPs and action potentials. *Nat Neurosci*, 4(1):63–71.

Thompson, L. T. and Best, P. J. (1989). Place cells and silent cells in the hippocampus of freely-behaving rats. *J Neurosci*, 9(7):2382–2390.

Thomson, A. M. (2000). Facilitation, augmentation and potentiation at central synapses. *Trends Neurosci*, 23(7):305–312.

Tolman, E. C. (1948). Cognitive maps in rats and men. *Psychol Rev*, 55(4):189–208.

Traub, R. D. and Miles, R. (1995). Pyramidal cell-to-inhibitory cell spike transduction explicable by active dendritic conductances in inhibitory cell. *J Comput Neurosci*, 2(4):291–298.

Tricoire, L., Pelkey, K. A., Daw, M. I., Sousa, V. H., Miyoshi, G., Jeffries, B., Cauli, B., Fishell, G., and McBain, C. J. (2010). Common origins of hippocampal ivy and nitric oxide synthase expressing neurogliaform cells. *J Neurosci*, 30(6):2165–2176.

Vanderwolf, C. H. (1969). Hippocampal electrical activity and voluntary movement in the rat. *Electroencephalogr Clin Neurophysiol*, 26(4):407–418.

Vinogradova, O. S. (2001). Hippocampus as comparator: Role of the two input and two output systems of the hippocampus in selection and registration of information. *Hippocampus*, 11(5):578–598.

Wang, S.-H. and Morris, R. G. M. (2010). Hippocampal-neocortical interactions in memory formation, consolidation, and reconsolidation. *Annu Rev Psychol*, 61:49–79, C1–4.

West, M. J. (1990). Stereological studies of the hippocampus: A comparison of the hippocampal subdivisions of diverse species including hedgehogs, laboratory rodents, wild mice and men. *Prog Brain Res*, 83:13–36.

Whitlock, J. R., Heynen, A. J., Shuler, M. G., and Bear, M. F. (2006). Learning induces long-term potentiation in the hippocampus. *Science*, 313(5790):1093–1097.

Wigström, H., Gustafsson, B., Huang, Y. Y., and Abraham, W. C. (1986). Hippocampal long-term potentiation is induced by pairing single afferent volleys with intracellularly injected depolarizing current pulses. *Acta Physiol Scand*, 126(2):317–319.

Williams, S. and Lacaille, J. C. (1992). $GABA_B$ receptor-mediated inhibitory postsynaptic potentials evoked by electrical stimulation and by glutamate stimulation of interneurons in stratum lacunosum-moleculare in hippocampal CA1 pyramidal cells in vitro. *Synapse*, 11(3):249–258.

Williams, S. R. and Stuart, G. J. (2000). Site independence of EPSP time course is mediated by dendritic I_h in neocortical pyramidal neurons. *J Neurophysiol*, 83(5):3177–3182.

Wilson, M. A. and McNaughton, B. L. (1993). Dynamics of the hippocampal ensemble code for space. *Science*, 261(5124):1055–1058.

Wittenberg, G. M. and Wang, S. S.-H. (2006). Malleability of spike-timing-dependent plasticity at the CA3-CA1 synapse. *J Neurosci*, 26(24):6610–6617.

Wong, R. K., Prince, D. A., and Basbaum, A. I. (1979). Intradendritic recordings from hippocampal neurons. *Proc Natl Acad Sci U S A*, 76(2):986–990.

Wuarin, J. P. and Dudek, F. E. (1996). Electrographic seizures and new recurrent excitatory circuits in the dentate gyrus of hippocampal slices from kainate-treated epileptic rats. *J Neurosci*, 16(14):4438–4448.

Ylinen, A., Bragin, A., Nádasdy, Z., Jandó, G., Szabó, I., Sik, A., and Buzsáki, G. (1995). Sharp wave-associated high-frequency oscillation (200 Hz) in the intact hippocampus: Network and intracellular mechanisms. *J Neurosci*, 15(1 Pt 1):30–46.

Zucker, R. S. (1999). Calcium- and activity-dependent synaptic plasticity. *Curr Opin Neurobiol*, 9(3):305–313.

Zucker, R. S. and Regehr, W. G. (2002). Short-term synaptic plasticity. *Annu Rev Physiol*, 64:355–405.